Erasmus MC
Universitair Medisch Centrum Rotterdam

ICIN

Thoraxcentre

# The Twelfth European Symposium on Ultrasound Contrast Imaging

Folkert J. Ten Cate, MD
Nico de Jong, PhD
Thomas Albrecht, MD

# Abstract book

January 25-26, 2007, Rotterdam, The Netherlands

# 12th EUROPEAN SYMPOSIUM ON ULTRASOUND CONTRAST IMAGING
## 25-26 JANUARY 2007, Rotterdam, The Netherlands

WEDNESDAY, 24 January 2007



THURSDAY, 25 January 2007



*ICIN = The Interuniversity Cardiology Institute of the Netherlands

FRIDAY, 26 January 2007

FRIDAY, 26 January 2007



*Announcement of the winners of the Martin Blomley poster prize and the technical poster-prize.*

**Real Time 3D Myocardial Perfusion-Is it Feasible?**

**Amit Bhan , Stam Kapetanakis, Bushra S Rana, Emily Ho, Karen Wilson, Mark J Monaghan.**

**Background**
2D low mechanical index (LMI), contrast specific, myocardial perfusion imaging is now an accepted technique. We evaluated the first real time 3D echo (RT3DE) LMI implementation to establish it's feasibility, in unselected patients..
**Methods**
22 consecutive patients (10 m) referred for contrast enhanced echo were imaged using a Philips iE33 3D scanner, with novel 3D LMI power modulation software. All patients underwent 2D contrast echo and a RT3DE apical full volume acquisition, during contrast infusion (Sonovue 0.7 ml/min). Datasets were taken in left ventricular opacification (LVO), and LMI perfusion modes.
These were then evaluated segmentally, for wall motion and myocardial contrast enhancement, relative to the LVO mode.
**Results**
A total of 352 left ventricular segments were evaluated. Wall motion and perfusion could be assessed in 98.8% and 98% respectively of the 2D segments, and in 97.4% and 96% of the 3D segments.
318 segments had normal wall motion and thickening. In these, normal 3D myocardial opacification was seen in, 97.5% of apical, 96.5% of mid and 94.3 % of basal segments (p=NS for all comparisons).
21 segments were akinetic with no 2D evidence of perfusion and of these RT3DE successfully demonstrated a perfusion defect in 19 (90.5%). (p=NS)

**Cropped 3D** - LVO setting -LMI perfusion setting

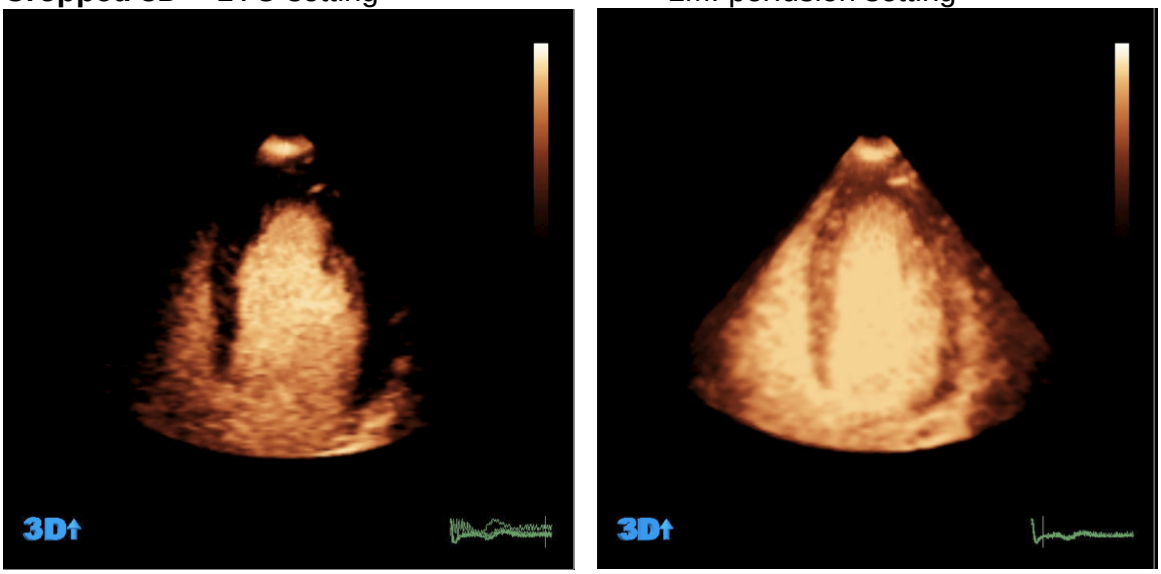

In conclusion, evaluation of myocardial perfusion using LMI RT3DE appears to be feasible in most segments. In the future it should be useful, not only for specifying accurate location, but also quantifying volume of perfusion defects.

# The Measurement of Myocardial Blood Flow by MCE

Rolf Vogel MD, PhD, MSEE

Cardiology, University Hospital Bern, Switzerland

**Background:** Perfusion disturbances, as an early consequence of coronary atherosclerosis, can be studied by quantitative myocardial contrast echocardiography (MCE). The diverse techniques in use, however, produce protocol- and equipment-dependent parameters that more or less suitably represent myocardial perfusion. As promising way out, we recently advanced MCE to measure myocardial blood flow (MBF, ml/min/g), which is the reference to quantitatively assess the myocardial blood supply.

**Objective:** Validation and clinical application of MBF measurements by MCE

**Methods and Results:** MBF was derived from the spatial form of the continuity equation describing ultrasound contrast agent (UCA) kinetics at the level of the microcirculation: $MBF = rBV \cdot \beta / \rho_T$, where *rBV* is the relative blood volume (ml blood per ml myocardium), $\beta$ reflects the exchange rate (1/min) of this blood volume and $\rho_T$ equals tissue density. *rBV* and $\beta$ were derived from UCA destruction refill sequences acquired by real-time by comparing myocardial with left ventricular contrast signals before UCA destruction and by fitting the UCA refill to the kinetic model, respectively.

*Validation*: (1) In vitro experiments using haemodialysis filters, confirmed the kinetic model and the reliable determination of *rBV*, $\beta$ and *MBF* for physiologic flow velocities. (2) Healthy volunteers underwent MCE and positron emission tomography (PET) at rest (group I: n=15; group II: n=5) and during adenosine-induced hyperaemia (group II). In group I, 187 of 240 segments were analyzable by MCE and a linear relation was found between MCE and PET MBF data (y=0.899x+0.079; $r^2$=0.88). In group II, resting and hyperaemic MBF data showed good agreement between MCE and PET (y=1.011x+0.124; $r^2$=0.92). (3) Fifteen patients with coronary artery disease (CAD) underwent simultaneous MCE and intracoronary Doppler measurements before and during intracoronary adenosine injection. Coronary stenosis varied between 0-89% and myocardial perfusion reserve (MPR) , i.e. the rate of hyperaemic to baseline MBF, was in good agreement with coronary flow velocity reserve (y=0.92x+0.14; $r^2$=0.73). (4) 30 patients with stable coronary artery disease underwent MCE of the collateral receiving territory during (i.e. reduced perfusion) and after (i.e. normal perfusion) elective coronary angioplasty. MBF during and after angioplasty varied between 0.060–0.876ml/min/g and 0.676–1.773ml/min/g, respectively. The collateral perfusion index defined as the rate of MBF during and after angioplasty varied between 0.05–0.67 and demonstrated

excellent agreement with the pressure derived collateral flow index ($y$=0.88$x$+0.01; $r^2$=0.92, $P$<0.0001).

Clinical Application: 48 patients underwent stress testing by MCE and subsequent quantitative coronary angiography. Baseline and adenosine-induced (140μg/min/kg) hyperaemic MBF were analyzed according to a 3 coronary artery territory model. Coronary stenosis severity was assessed as percent diameter reduction. Complete perfusion data were obtained in 128 (89%) territories. Mean±SD baseline $\beta$ and MBF were 9.714±4.288/min and 1.073±0.395ml/min/g, respectively, and did not differ between territories supplied by coronary arteries with mild (<50% stenosis), severe (50%-74% stenosis) or very severe (≥75% stenosis) disease. Mean±SD hyperaemic $\beta$ and MBF were 18.762±7.996 and 2.509±1.078ml/min/g and decreased linearly ($r^2$=0.22 and $r^2$=0.21) with stenosis severity. Mean±SD $\beta$-reserve and MPR were 2.16±1.02 and 2.54±1.03 and decreased linearly ($r^2$=0.34 and $r^2$=0.39) with stenosis severity. ROC analysis demonstrated superior diagnostic performance of MPR (area under the curve 0.928) versus $\beta$-reserve (AUC 0.899), whereas a territorial MPR < 1.937 detected significant disease of the respective coronary artery defined as ≥50% stenosis with 89% sensitivity and 92% specificity.

**Conclusion:** MBF is the biophysical gold standard, i.e. a platform-independent parameter, to quantitatively assess the myocardial blood supply. In humans, MCE provides accurate estimates of MBF at rest, during hyperaemia as well as during ischemia, and can be used for the non-invasive and reliable assessment of coronary artery disease.

# Quantitative assessment of myocardial perfusion by MCE

Dr R Senior, MD, DM, FRCP, FESC, FACC

Address for correspondence:
Dr R Senior MD DM, FRCP, FESC, FACC
Consultant Cardiologist and Director of Cardiac Research,
Department of Cardiovascular Medicine,
Northwick Park Hospital,
Watford Road, Harrow
Middlesex, HA1 3UJ
United Kingdom.
Tel: +44 (0)208 869 2547
Fax: +44 (0)208 864 0075
E-mail: roxysenior@cardiac-research.org

Myocardial contrast echocardiography (MCE) is an ideal imaging tool for the assessment of the myocardial microcirculation. The microcirculation is generally defined as vessels. <200 um in diameter, which are not visualised on coronary arteriography. At baseline, approximately 8% of left ventricular mass is constituted by blood present in the microcirculation termed myocardial blood volume (MBV), 90% of which is comprised of blood in the capillaries. MCE is ideal for measuring microcirculatory flow because it utilises gas filled microbubbles that are inert, remain entirely within the vascular space and possess an intravascular rheology similar to that of red blood cells. Furthermore, MCE has good spatial and temporal resolution. When microbubbles are administered as a constant infusion and once a steady state is achieved (approximately 1-2 minutes), the acoustic intensity measured from the myocardium after background substraction (to eliminate native backscatter from myocardial tissue), provides a measure of MBV fraction. Because 90% of MBV fraction comprises capillary blood, a single MCE image provides an assessment of capillary density in the different myocardial regions. An excellent correlation was observed between signal intensity obtained from a region of interest in the myocardium of patients with capillary density obtained from the biopsied myocardium of the same region.[1] At steady state, when microbubbles within the myocardium are destroyed with high-energy ultrasound pulses, the rate of microbubble reappearance reflects RBC velocity or blood velocity. Because myocardial blood flow (MBF) constitutes a volume of blood moving at a certain mean velocity, the product of MBV fraction and myocardial blood velocity reflects myocardial microvascular flow.

Therefore, unlike other clinical methods that measure myocardial blood flow (MBF), this approach provides an assessment of 2 individual components of capillary (tissue) perfusion, i.e. MBV and myocardial blood velocity. This method of assessment of MBF can also be

represented by per gram of tissue by knowing the sample volume size and specific gravity of the myocardium. MBF by MCE has been validated using radio-labelled microsphere experimental models and clinically using the standard technique of positron-emission-tomography over a wide range of MBF. Coronary flow reserve assessed by MCE followinga vasodilator not only detects flow-limiting CAD but can accurately grade severity of CAD in various clinical conditions.

# Quantification OF Myocardial Perfusion Abnormalities in Hypertrophic Cardiomyopathy by Myocardial Contrast Echocardiography

Osama I.I. Soliman MD, Paul Knaapen MD[*], Marcel L. Geleijnse MD PhD,
Ashraf M. Anwar MD, Attila Nemes MD PhD[1], Michelle Michels MD,
Wim B. Vletter MSc, Adriaan A. Lammertsma PhD[*], and Folkert J. Ten Cate MD PhD

**From The Thoraxcenter, Erasmus MC, Rotterdam, and [*]VUMC, Amsterdam, The Netherlands**

**Objectives.** We sought to assess mechanisms of myocardial perfusion impairment in patients with hypertrophic cardiomyopathy (HCM) by real-time myocardial contrast echocardiography (MCE) and positron emission tomography (PET).

**Methods.** Fourteen patients with obstructive HCM (mean age 53 ± 10 years, 11 men) underwent intravenous adenosine MCE using (continuous infusion of SonoVu), PET and cardiac catheterization. Contrast time-volume curves were generated from manually drawn-ROIs over myocardial segments and over corresponding left ventricular (LV) cavity using the QLAB® ROIs software program. Additional ROIs were drawn over sub-endocardial and sub-epicardial areas from septal and lateral walls in apical 4CH-view. Values of peak contrast intensity (A) and its flow velocity (ß) were measured. The relative myocardial blood volume (rBV) calculated as ($A_{myocardial}/A_{LV}$), absolute myocardial blood flow in $ml.min^{-1}.g^{-1}$(MBF) calculated as (rBV x ß / myocardial density), its reserve (MFR) and endo-to-epi MBF ratio were measured.

**Results.** MBF increased from rest to hyperaemia (0.92 ± 0.12 vs. 2.56 ± 0.49 $ml.min^{-1}.g^{-1}$, P <0.01). At rest, mean rBV tended to be lower in HCM patients (0.094 ± 0.016 vs. 0.138 ± 0.014 $ml.ml^{-1}$), and during hyperaemia (0.104 ± 0.018 $ml.ml^{-1}$ vs. 0.185 ± 0.024 $ml.ml^{-1}$, P <0.001) as compared to controls. β tended to be higher in HCM at rest (9.4 ± 4.6 vs. 7.7 ± 4.2

ml.min$^{-1}$, P =NS) and hyperaemia (25.8 ± 6.4 vs. 23.1 ± 6.2 ml.min$^{-1}$) as compared to controls. MCE-MBF correlated well with PET at rest (R = 0.84, P <0.001) and hyperaemia (R = 0.87, P <0.001). MFR was lower in HCM compared to controls with MCE (2.80 ± 0.62 vs. 3.22 ± 0.46, P <0.01), and in the septum compared to lateral wall (2.88 ± 0.82 vs. 3.36 ± 0.80, P <0.05). MBF endo-to-epi decreased during hyperaemia (0.86 ± 0.15 to 0.64 ± 0.18, P <0.01) in the septum and (0.92 ± 0.19 to 0.77 ± 0.23, P <0.01) in the lateral wall. The rBV was inversely correlated to LV mass index (LVMI) (P <0.05). Hyperaemic and endo-to-epi MBF were inversely correlated to LVEDP, LVMI, and LV outflow tract peak gradient LVOTG (all P <0.05).

**Conclusions.** In HCM patients, the blunted hyperemic perfusion is due to exhausted autoregulation of myocardial microcirculation (failure to increase rBV) as well extravascular compression forces. LV-EDP, LVOTG, and LVMI are independent predictors of hyperaemic perfusion and endo-to-epi myocardial blood flow. These findings may have important practical implications for the understanding and follow-up of patients with HCM and can be measured accurately with MCE.

# Technology for Bubble Imaging: Current State of the Art

Peter N Burns PhD
Professor of Medical Biophysics
University of Toronto

While the technology used for contrast imaging has to a large extent stabilised around a class of amplitude and phase modulated techniques used at low MI, some considerable challenges remain. For example, the newer generation of ultrasound scanners have not offered any striking improvement in image quality or signal to clutter ratio (CTR), and this may reflect the difficulty in producing the precision transmit characteristics required for these imaging methods in an increasingly cost-driven industry: perhaps the market for contrast has not proved itself to be worthy of the expense of better hardware. Thus, efforts in new signal processing approaches that improve performance at little cost are receiving more attention. For example, the MI limitation imposed by real time bubble imaging invites longer pulses and compression techniques that enable more energy to be deposited into tissue while keeping the bubbles intact. Coded and chirp excitations have been combined with nonlinear modulation schemes with success that is perhaps surprising, considering the reluctance of bubbles to yield echoes that mimic the phase modulation of their exciting pressure. Codes may help to produce better CTR and hence more robust contrast imaging modes, an oft-repeated request from clinical users.

The natural way to move to higher frequency – and hence higher resolution - bubble imaging would be to scale the bubble radius with decreasing wavelength of the ultrasound, but it is unlikely to be worth waiting for such bubbles to be made for us. More promising is a method that can decouple the imaging frequency from the resonant frequency of the bubble, and still suppress tissue echoes. Radial modulation imaging is a particularly attractive candidate as it places no requirements on the imaging transmitter to modulate the phase of the bubble oscillation, but instead relies on a second sound source at lower frequency. The effect is that a normal imaging or Doppler device at high frequency can easily be converted to a nonlinear imager by modulating the bubble size using a separate sound source. Whether such a method will work in the 20-50MHz range – or indeed the 1-4MHz range - remains to be demonstrated. In the meantime, contrast shares with the rest of ultrasound imaging a conundrum over 3-dimensional imaging, the solution that is still seeking a problem. While slow, mechanically scanned 3D systems can still produce very attractive contrast images, yet it is clear that temporal resolution is important for our applications. Thus a longer term solution must exploit 2D array technology, which at present does not seem capable of such high quality nonlinear low MI images. Improvement in this filed is very rapid, however, and it will probably not be long before real time 3D perfusion imaging becomes possible. It is important, however, that target clinical applications are defined now so that technology development can be carried out with realistic goals in view.

One area where 3D imaging – or at least 3D acquisition – may have a clear role is in quantification of perfusion. Quantitative measures of response to anti- and pro-angiogenic therapies (some of which might be delivered or potentiated with bubbles and ultrasound) remains one of the most pressing unmet needs in our field. No-one has yet demonstrated the ability of

ultrasound to make reproducible, validated measurement of perfusion parameters in a tumour, in spite of many optimistic studies and claims. The problem will almost certainly require both 3D approaches and better, more physical models of perfusion and contrast kinetics. Modelling may also help in another, perhaps less considered problem encountered in liver imaging: that there are two circulations and once the portal phase has begun, these two are shown indistinguishably on the image. Yet the information that shows the distribution of the arterial phase is available in the first seconds of enhancement by the agent. This can be used for subsequent segmentation of the portal phase image with the help of simple algorithms developed for other tracer kinetic applications.

Finally, an update will be given of progress in the approval and adoption of contrast, with recent decisions creating pessimism that the FDA will ever approve an agent for myocardial perfusion being mitigated by good news from the Japan, where the authorities have allowed the first perfluorocarbon agent into clinical use.

Title: High-contrast high-speed imaging using a copper vapor laser to resolve contrast agents in tissue

Presenter: Paul A. Dayton

Co-authors: Charles F. Caskey, Susanne. M. Stieger, Katherine.W. Ferrara

High-speed imaging of microbubble oscillations plays a crucial role in exploring the use of contrast ultrasound for harmonic imaging and drug delivery. In recent years, researchers used systems capable of imaging at millions of frames per second to capture images of a single microbubble as it oscillates in a transparent tube. Although these high-speed systems help researchers optimize theoretical models describing microbubble oscillations, this *in vitro* scenario is an idealized approximation to a microbubble in the vascular system. To date, no one has produced high-speed images of microbubble oscillations within the microvasculature, presumably due to contrast limitations with available ultra-high speed cameras when imaging through thick tissue. We demonstrate that a pulsed copper vapor laser can be used to capture images of microbubble oscillations with excellent dynamic range for use in these low contrast situations. Here, a copper vapor laser is used in conjunction with a digital high-speed camera, where both are adapted to a microscope whose objective is aligned with a 1 MHz, cylindrically focused ultrasound transducer. The ultrasonic pulse is triggered upon opening of the camera‘s shutter, and the laser is triggered after a time delay, T, relative to the propagation time of the ultrasonic pulse from the transducer to the visible area, producing an effective exposure time of 50 nsec. Although the kiloHertz frame rate is too slow to continuously image microbubble oscillations, the system can produce a single 2D image of a microbubble during a specific time point during its oscillatory cycle. Repeated ultrasonic pulses and increasing values of T can produce a series of images for video viewing of microbubble oscillation, from which microbubble symmetry and expansion are measured. Results are demonstrated for contrast agents oscillating within the microvasculature, where the dynamic range of the laser-based system allows fine detail, such as microvessel walls, to be resolved. The relative expansion of a microbubble, as well as the asymmetries resulting from constrained oscillation will be summarized as a function of the vessel diameter.

# MICROBUBBLE CONTRAST AGENT DETECTION USING PULSE ENCODED SEQUENCES

Robert J. Eckersley[1], Mengxing Tang[2], Kevin Chetty[1], Claudia Leavens[3], Joseph V Hajnal[1].

[1]*Imaging Sciences Department, Imperial College, London, U.K.*
[2]*Department of Bioengineering, Imperial College, London, U.K.*
[3]*Department of Medical Biophysics, University of Toronto, Canada*

Real-time visualisation of microbubbles in the microvasculature of deep tissues remains a challenge for existing non-linear microbubble imaging techniques. Although the microvasculature makes up a large part of the overall blood pool the individual vessels are minute and the flow within them is extremely slow. To detect these signals using microbubble contrast agents, a technique with high sensitivity to non-linear signals is required, furthermore the insonating pressures which the microbubbles are exposed to must be kept as low as possible to prevent the destruction of the agents before they arrive in the region of interest. The use of coded pulses in ultrasound imaging is well established as means of improving the signal-to-noise ratio (SNR) within B-mode ultrasound imaging [1, 2]. In previous work we have shown that the combination of multi-pulse sequences modulated in both phase and amplitude (PIAM) combined with chirp encoding can enhance the sensitivity for microbubble imaging in such applications [3, 4]. In this work we investigated the potential advantages of combing binary pulse encoding, such as Barker or Golay coding, with the PIAM sequence. A series of simulation experiments were conducted using a modified Rayleigh-Plesset model to demonstrate: i) The ability of binary encode PIAM to detect non-linear signals; ii) The effect of reduced signal to noise ratio (SNR) on the detection process; iii) The sensitivity of different pulse encoding approaches; iv) The effects of bubble resonance behaviour on the detection process. The results show that the non-linear scattering from the microbubbles degrades the sensitivity of the binary encoded approach such that at high SNR there is no advantage in using these pulses over existing short pulse PIAM. However, in deeper tissues where the SNR of the received signals is lower due to the attenuation of the overlying tissues the coded approach provides increased sensitivity without significant reduction in spatial resolution, under conditions in which existing approaches cannot be used.

References:

[1] T. Misaridis and J. A. Jensen, "Use of modulated excitation signals in medical ultrasound. Part I: basic concepts and expected benefits," *Ultrasonics, Ferroelectrics and Frequency Control, IEEE Transactions on*, vol. 52, pp. 177-191, 2005.

[2] R. Y. Chiao and X. Hao, "Coded excitation for diagnostic ultrasound: a system developer's perspective," *IEEE transactions on ultrasonics, ferroelectrics, and frequency control*, vol. 52, pp. 160-70, 2005.

[3] R. J. Eckersley and K. Chetty, "Combining multipulse sequences with coded excitation for enhanced sensitivity to microbubbles.," presented at 10th European Symposium on Ultrasound Contrast Imaging, Rotterdam, Netherlands, 2005.

[4] K. Chetty, J. V. Hajnal, and R. J. Eckersley, "Investigating the nonlinear microbubble response to chirp encoded, multipulse sequences.," *Ultrasound in Medicine & Biology*, vol. in press, 2007.

# MICROBUBBLE SPECTROSCOPY OF ULTRASOUND CONTRAST AGENTS: INFLUENCE OF THE SHELL AND OF A CONFINING WALL

Benjamin Dollet[1], Sander van der Meer[1], Marlies Overvelde[1], Valeria Garbin[1], Nico de Jong[2], Michel Versluis[1], Detlef Lohse[1]

[1] Physics of Fluids, University of Twente, Enschede, The Netherlands.
[2] Experimental Echocardiography, Erasmus Medical Center, Rotterdam, The Netherlands.

We present a new optical characterization of the behavior of single ultrasound contrast bubbles. The method, termed microbubble spectroscopy, consists of insonifying individual bubbles several times successively sweeping the applied frequency, and to record movies of the bubble response up to 25 million frames per second with the ultra-high speed camera Brandaris [1] operated in a segmented mode. Extracting the oscillation amplitude for each frequency, we reconstruct a resonance curve in a single run. We analyze the data through a linearized model for bubbles with a monolayer coating [2].

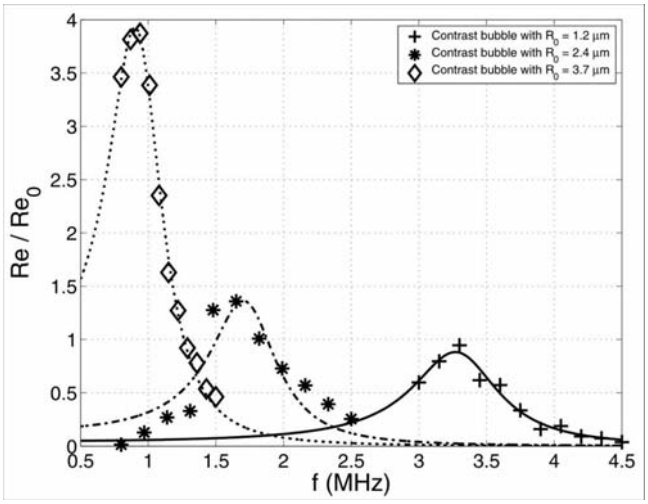


**Figure 1 - Examples of resonance curves obtained by microbubble spectroscopy**

We first use this method to characterize the effect of the bubble shell. The results confirm the significant influence of the shell on the bubble dynamics: the shell elasticity increases the resonance frequency by about 50%, and the shell viscosity is responsible for about 70% of the total damping. The obtained values for shell elasticity and viscosity are in quantitative agreement with previously reported values. Furthermore, we show that the shell viscosity significantly increases with increasing bubble radius, which possibly reveals a surface rheothinning effect.

These experiments were done for bubbles floating against a top wall. As a second step, we probe the effect of the wall by using optical tweezers specially designed for bubble 3D micromanipulation. This allows us to displace bubbles at an arbitrary distance from the wall. We then use the microbubble spectroscopy method to compare the resonance behavior of a given bubble against a wall and far from it. We show that the presence of a wall induces a decrease of both the resonance frequency and the oscillation amplitude.

[1] C. T. Chin *et al.*, *Rev. Sci. Instr.* **74**, 5026 (2003).
[2] P. Marmottant *et al.*, *J. Acoust. Soc. Am.* **118**, 3499 (2005).

# Improving contrast agent detection with SURF imaging

R. Hansen[1,2], S.-E. Måsøy[1], Ø. Standal[1], P. Nasholm[1], T. Johansen[1], B. Angelsen[1]
1) Dept of Circulation and Medical Imaging, Norwegian University of Science and Technology, 2) Dept of Medical Technology at SINTEF Health Research, Trondheim, Norway

**Abstract - We present a contrast agent detection technique for improved contrast imaging and discuss some important fundamental theoretical aspects and report *in vitro* and initial *in vivo* results obtained with the new technique.**

## INTRODUCTION

Current contrast agent detection methods have some fundamental limitations reducing the applicability of ultrasound contrast imaging in many clinical situations. First, available methods rely on driving the contrast bubbles into strong nonlinear oscillations by the imaging pulse. Contrast bubbles that are available and practical for clinical use generally have resonance frequencies in the range 2-4 MHz forcing the transmit frequency below 4 MHz and thus limiting spatial image resolution in many clinical applications. Second, nonlinear scattering from tissue (and contrast bubbles) will accumulate in the forward propagating transmit pulse, something which is utilized in the second harmonic tissue imaging method with good results. This forward propagation effect will produce the same signal characteristics in the strong linear back-scattering from tissue as for the local nonlinear back-scattering from contrast agents thus limiting the specificity. As an example, this phenomenon affects imaging of contrast agents in the myocardium where transmit pulses pass the ventricle with a high concentration of contrast agents before entering the myocardium which has a much lower concentration of contrast agents. Since such accumulative nonlinear forward propagation effects are not taken into account with current contrast agent detection techniques, quantitative contrast agent imaging is difficult to achieve. And third, current methods utilize only a fraction of the scattered contrast agent signal where the received linear part of the signal is thrown away to suppress tissue hence limiting the sensitivity. Our group has for several years been working with improved methods for nonlinear acoustic imaging and contrast agent imaging has been an important part of this work. The resulting nonlinear methods are given the name Second order UltRasound Field imaging, abbreviated SURF imaging.

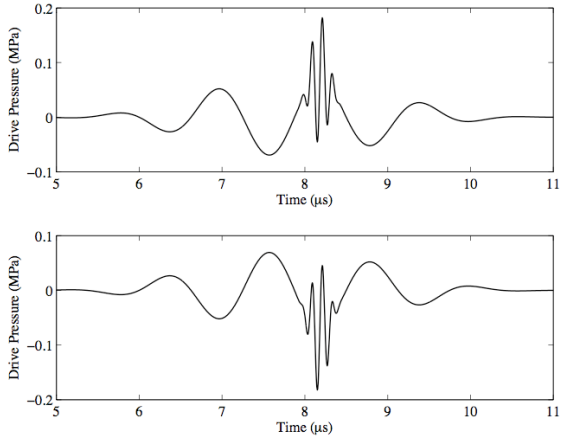


Figure 1. Example of transmitted pulse complexes used with SURF imaging.

## METHOD

The SURF contrast imaging method is achieved by processing of the received echoes from transmitted dual frequency band pulse complexes, as depicted in Figure 1, with overlapping high and low frequency pulses. The transmitted high frequency pulses are used for image reconstruction whereas the transmitted low frequency pulses are used to manipulate the nonlinear scattering and propagation properties of the high frequency pulses. Several groups have during the last few

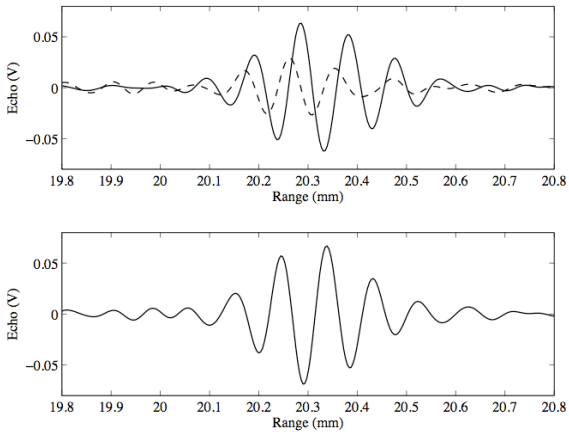


Figure 2. Upper panel: *In vitro* contrast agent echo obtained with pulse complex in upper and lower panel of Fig. 1, solid and dashed line, respectively. Lower panel: Detection signal.

years been working with pulses similar to the ones depicted in Figure 1 for contrast agent imaging, *e.g.* Deng and Lizzi in New York, de Jong in Rotterdam, and Burns in Toronto, in addition to our group in Trondheim. Our group has gained significant and comprehensive knowledge regarding the use of such pulse complexes for nonlinear acoustic imaging in general and for contrast agent imaging in particular.

With drive pulses such as displayed in Figure 1 the imaging pulse can be decoupled from the resonance properties of the contrast bubble. When imaged well above their resonance frequency contrast bubbles approach linear scatterers with a scattering cross section proportional to the cross sectional area of the bubble. If a manipulation pulse with frequency below or around the bubble equilibrium resonance frequency is applied to manipulate the size of a 3 μm bubble, so that the bubble is interrogated by the high frequency imaging pulse at peak manipulation rarefactional and compressional phase, the bubble diameter is for example 5 μm and 2 μm, respectively. The scattering cross section is then 6.25 timers larger for the expanded bubble relative to the compressed bubble whether imaged at 15 MHz or at 50 MHz, assuming the bubble to be small relative to the wavelength. If the high frequency imaging pulse approaches the resonance frequency of the compressed bubble the situation may be significantly altered as shown in Figure 2. The high frequency imaging pulse is centered around 8 MHz and nonlinear and resonant properties thus become important. Here, the scattering cross section for the small compressed bubble (solid line) is increased relative to the large expanded bubble (dashed line). In addition to variations in scattered pressure amplitude we notice a significant time delay in the scattered pressure from the compressed bubble relative to the expanded bubble.

From nonlinear acoustics it is known that the high frequency pulse in the upper panel of Figure 1 will propagate at a slightly higher speed of sound than the high frequency pulse in the lower panel of Figure 1. Two such consecutively received high frequency tissue echoes will thus be time delayed relative to each other. For example, with high frequency pulses placed at peak positive and peak negative manipulation pressure of 100 kPa, this corresponds to a delay of 2.6 ns/cm if the linear propagation velocity is assumed to be 1540 m/s. A simple subtraction of two 10 MHz tissue echoes that have propagated 1 cm on the crest and trough of a 100 kPa manipulation pressure will result in a suppression of linearly back-scattered tissue signal of only -15 dB due to the effect of nonlinear accumulative propagation delay, significantly limiting specificity. This limited specificity is similar to what seen with harmonic contrast agent detection techniques, such as Pulse Inversion, where the transmitted pulse is distorted in the forward wave propagation. The second harmonic component of this distortion is then linearly back-scattered from tissue scatterers. With SURF imaging, the resulting nonlinear propagation effects can be estimated along radial image lines and applied to significantly improve the differentiation of local nonlinear scattering from contrast agents and accumulative nonlinear effects in the forward wave propagation, hence increasing specificity. Figure 3 shows examples of obtained detection envelopes from a tissue mimicking flow phantom using high frequency imaging pulses around 8 MHz and manipulation pulses around 900 kHz. Solid lines corresponds to detection signals where additional signal processing is performed to suppress accumulative nonlinear forward effects whereas dashes lines are obtained simply subtracting two consecutively received echoes obtained from transmit pulses as indicated in Figure 1. The signal beyond approximately 30 mm corresponds to the noise floor of the imaging system in this particular setup.

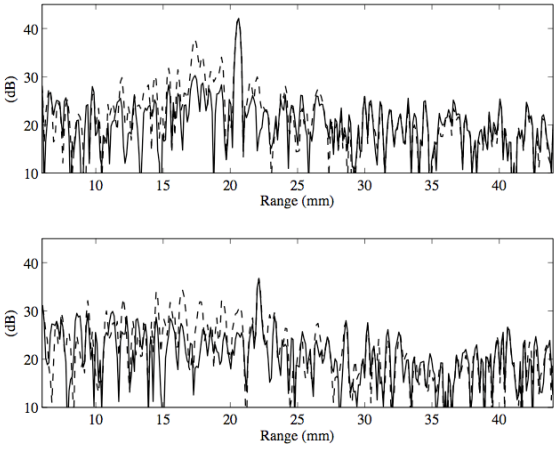


Figure 3. *In vitro* detection signal envelope from tissue mimicking flow phantom. With and without signal processing to suppress tissue, solid and dashed line, respectively. Upper panel: Contrast flow around 20.5 mm. Lower panel: Contrast flow around 22 mm.

*In vivo* results using SURF contrast imaging at 8 MHz will also be shown.

# Ultrasound molecular imaging in fast-flow conditions in murine models: targeted microbubbles carrying polymeric sialyl Lewis$^x$

A.L. Klibanov, Y.K. Cho, J.J. Rychak, W.C.Yang, S. Alikhani, J. Hossack, K. Ley.

Cardiovascular Division, Cardiovascular Research Center, Department of Biomedical Engineering, University of Virginia, Charlottesville VA 22908-0158 USA

Targeted ultrasound contrast imaging of inflammatory conditions is often performed with antibody-coated microbubbles (such as anti-P-selectin antibody RB40.34). Antibodies may offer high overall binding affinity, but mostly they are not designed to attach to the target rapidly, and cannot always mediate efficient and firm targeting of microbubbles to the vessel wall receptors in the conditions of high shear flow. Nature has evolved specialized ligands, such as P-selectin Glycoprotein Ligand-1 (PSGL-1) to achieve slow rolling targeting of leukocytes on activated endothelium expressing P-selectin. We apply a simplified variant of that ligand, polymeric sialyl Lewis$^x$ (PSLEX), attached to the microbubble surface, to achieve successful ultrasound contrast targeting to inflamed vasculature.

Microbubbles were prepared from decafluorobutane gas, stabilized with a distearoyl phosphatidylcholine monolayer with embedded PEG stearate and biotin-PEG-DSPE; trace amount of a lipid fluorescent dye (DiO, DiI) was added when necessary. Biotinylated antibodies (anti-P-selectin or anti-VCAM-1) and biotinylated polyacrylamide sialyl Lewis$^x$ were attached to the microbubble surface via a streptavidin bridge. Control microbubbles were lacking targeting ligands. Excess of free ligands was removed by centrifugal flotation of microbubble preparations. Intravital microscopy and ultrasound imaging were performed with intravenous RB40.34- or PSLEX-microbubbles in a murine hindlimb inflammation model 2-3 hours after footpad administration of TNF-$\alpha$. Targeting of atherosclerosis-related inflammation was tested in apoE -/- mice on high-cholesterol diet. Contrast microbubbles for this study were carrying a combination of two ligands: anti-mouse VCAM-1 antibody and PSLEX. Ultrasound contrast imaging was performed with a 15L8 probe on a Sequoia imaging system; Contrast Pulse Sequences mode was used for nondestructive imaging of microbubble contrast at 8 MHz and MI 0.2.

Intravital fluorescence microscopy in the murine hindlimb model showed that anti-P-selectin antibody (RB40.34) and PSLEX provided similar binding efficacy of targeted microbubbles in the inflamed femoral vein setting; PSLEX-microbubbles were superior to RB40.34-bubbles in targeting femoral artery. Control microbubbles (or microbubbles in the non-inflamed tissues) cleared the bloodstream and tissues of interest 10-15 min following intravenous bolus administration of contrast agent, as evaluated by ultrasound imaging. Statistically significant selective accumulation of PSLEX-targeted bubbles in the inflamed hindlimb vasculature was observed.

In the high cholesterol-diet apoE -/- mice, dual-targeted anti-VCAM-1 and PSLEX-carrying microbubbles selectively accumulated in the inflamed arterial vasculature. Preinjection of the cocktail containing excess amounts of anti-P- and E-selectin and anti-VCAM-1 antibody blocked targeting of microbubbles.

# Molecular Imaging

**Flordeliza S. Villanueva, MD**
**University of Pittsburgh, Pittsburgh, PA**

Myocardial contrast echocardiography utilizes gas-filled acoustically active microspheres as intravascular red blood cell tracers that transit unimpeded through the coronary microcirculation, permitting ultrasound imaging of myocardial perfusion. Molecular imaging with ultrasound utilizes microbubbles which are surface modified and targeted such that they bear a ligand on their surface which causes adherence to molecules of interest, such as markers of disease present on vascular endothelial cells. Targeted microbubble adhesion to vascular epitopes renders the molecules ultrasonically visible, which manifests as persistent tissue contrast enhancement during ultrasound imaging.

Ultrasound molecular imaging has the potential to uniquely address unmet clinical needs in the post-genomic era, when advanced imaging strategies will be required to evaluate new therapies targeted at the molecular basis of disease. Molecular imaging with ultrasound may permit earlier diagnosis of a variety of cardiovascular diseases by virtue of identifying molecular pre-cursors of clinical symptoms. Furthermore, targeted imaging with ultrasound can prove useful in the pre-clinical arena, particularly in the interrogation of molecular events in specialized rodent models which are vital to investigations of disease mechanisms and to the design and testing of novel treatments.

Targeted ultrasound contrast agents have been developed for a variety of cardiovascular and non-cardiovascular clinical applications, which will be discussed. These include agents targeted to bind to endothelial markers of angiogenesis and inflammation, and to thrombus-specific epitopes. Such agents have been ultrasonically imaged in vivo in animal models of myocardial ischemia-reperfusion (ischemic memory imaging), acute heart transplant rejection, atherosclerosis, and angiogenesis associated with ischemia and tumors.

Clinical translation of this technology requires a multidisciplinary approach that combines knowledge in key areas such as microbubble chemistry and microbubble surface modifications, advanced biological knowledge for selection of appropriate markers and ligands, acoustic approaches to microbubble detection, as well as fundamental knowledge of the underlying disease pathways. Ongoing work in these various arenas will be discussed, and the current state of the art for ultrasound molecular imaging will be reviewed.

## Non-invasive Cardiovascular Imaging:
## Steven B. Feinstein, M.D., FACC, Professor of Medicine

With approximately 1.2 million heart attacks and 750,000 strokes afflicting an aging USA population each year, cardiovascular disease remains our country's number one cause of death. Unfortunately, this grim statistic is likely to worsen in the years ahead due to the prevalence of obesity, metabolic syndrome and clinical diabetes in the burgeoning Baby Boomer population. Therefore, it is critical that we develop non-invasive screening methods that safely and reliably identify surrogate markers of atherosclerosis, indicating the presence of unstable plaques and an increased risk of cardiovascular events. Once "vulnerable patients" are identified, it may be possible to institute timely preventive therapy, monitor its effectiveness, and potentially reverse the course of these disease processes.

New data suggest that contrast-enhanced ultrasound (CU) imaging of the carotid arteries may provide a clinically relevant and cost-effective means of identifying patients who are at increased risk of cardiovascular diseases. CU is currently used for imaging of the heart structures, and current ultrasound contrast agents are not yet approved by the FDA for vascular imaging; however, with institutional research approval, physicians can perform CU carotid imaging in the office or hospital setting. These direct carotid images can provide an enhanced assessment of the arterial lumen and plaque morphology, improved resolution of carotid intima-media-thickness (c-IMT), and, importantly, direct visualization of the adventitial vasa vasorum and plaque neovascularization. The latter is particularly significant because neovascularization of the atherosclerotic plaque has been described as a predictor of vulnerable lesions in patients.

Real-time CU images of neovascularization within the carotid atherosclerotic plaque appear to indicate the presence of systemic atherosclerosis. Therefore, with continued investigation, CU imaging of the carotid vasa vasorum promises to become a routine non-invasive means of identifying an atherosclerotic plaque in its earliest stages. These observations may lead to early interventions with medical therapies (statins, anti-inflammatory medications, ACE or calcium channel medications, etc.) or mechanical interventions (stents, carotid endarterectomy surgery), potentially reducing the incidence of heart attack and stroke.

**Update on high frequency contrast imaging in the mouse**

**FS Foster**

Research on microbubble ultrasound contrast has largely and justifiably focused on the development and translation of these agents for clinical applications. One of the continuing challenges for the exploitation of microbubble contrast has been the development of methods suitable for high resolution imaging at high ultrasound frequencies. This is particularly true for preclinical imaging or intravascular ultrasound where frequencies exceed 20 MHz and imaging targets are correspondingly smaller. The recent introduction of high frequency micro-ultrasound imaging for mice has created a significant appetite for contrast specific imaging modes for the examination of functional and targeted imaging in disease models and interventional studies. In this presentation, the current state of the art in high frequency contrast for functional and molecular imaging of the mouse will be reviewed. Examples of functional imaging of inflammation, cardiovascular disease, and tumour microcirculation will be used to illustrate the potential and limitations of the current implementations. Potential for molecular imaging will be explored in a melanoma xenograft model in which the expression pattern of VEGFR-2 is studied. The current signal processing approaches rely on simple linear subtraction schemes. While simple and practical, these algorithms may not be optimal for quantitative interpretation. Performance improvements will require optimization of the microbubbles themselves, a better understanding of microbubble interactions at high frequencies in both the bound and unbound state, and improved capabilities in nonlinear excitation and signal processing that are easily translated to commercial instrumentation. These challenges will be discussed and the future of high frequency contrast imaging will be examined.

# Assessment of tumour developmental using molecular ultrasound contrast imaging

Annemieke van Wamel[1], Muzaffer Celebi[2], Joseph Backer[3], Marina Backer [3], John Hossack[4], Klaus Ley[5], Nico de Jong[1], Alexander Klibanov[2].

1 Biomedical Engineering, Erasmus MC Rotterdam , The Netherlands.
2 Cardiovascular Division, University of Virginia, Charlottesville, VA, USA.
3 Sibtech Inc., Newington, CT, USA
4 Biomedical Engineering, University of Virginia Charlottesville, VA, USA.
5 Cardiovascular Research Center, University of Virginia, Charlottesville, VA, USA.

*Background:* Human tumour progression stages include benign, malignant and metastatic lesions, each having their own treatment strategy. Direct assessment of these marker molecules requires tissue biopsy, which is not always possible and not feasible for serial monitoring of patients. Therefore, new non-invasive monitoring techniques for tumour assessment is a major need in tumour diagnosis and treatment. Next to size, several marker molecules such as selectins and VEGF-R (vascular endothelial growth factor receptor) can be used for tumour stage assessment. In this study, changes in P/E selectin and VEGF-R expression during MC38 (murine colon carcinoma) tumour development were assessed using targeting contrast agents, a tumour bearing mouse model, and the Vevo 770.

*Methods:* Microbubbles were prepared from decafluorobutane gas and stabilized with a monolayer of phosphatidylcholine, PEG stearate and biotin-PEG-lipid. Biotinylated Sulfo-Le$^x$-PAA (Sulfo Lewis$^x$ polyacrylamide, Glycotech) or biotinylated $VEGF_{121}$ (Sibtech Inc) was attached to microbubbles via a streptavidin bridge. A bolus of 0.05 ml of microbubbles ($10^8$/ml) was manually injected retro-orbital for 1-2 seconds using a hypodermic needle. To confirm microbubble injection, inflow of bubbles into the MC38 tumour vasculature was recorded with the Vevo 770 micro-imaging system (VisualSonics, Toronto, Canada) using the RMV 704 scanhead at a center frequency of 40 MHz. After the contrast was allowed to circulate and bind to the tumour vasculature for 3 minutes, the tumour was imaged in a destruction image sequence mode. During this mode first the attached and free circulating contrast was imaged for 20 seconds at 50% power after which a 1 second high power ultrasound destroyed all the contrast. After destruction the free circulating contrast agent was recorded. Levels of echo-intensity levels were compared between the different targeted contrast agents and in tumours sizing from 4 to 11 mm and in TNF-α-induced tumours.

*Results:* Contrast enhanced ultrasound recordings were obtained. Figure 1 shows two frames from a recording obtained after 3 minutes of targeted microbubbles incubation.

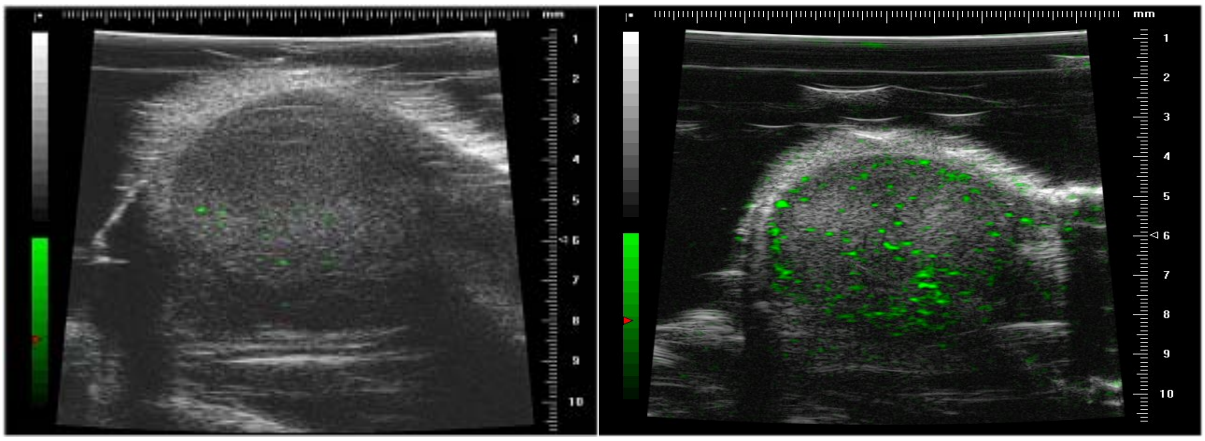

Figure 1. Contrast enhanced ultrasound in MC38 ~5mm tumours. Microbubbles (obtained by reference-substracted pixel amplitude post-processing) are shown in green and overlaid on greyscale images 3 min after contrast agent injection. Left image depicts accumulation of PSlex microbubbles and right image accumulation of $VEGF_{121}$ microbubbles.

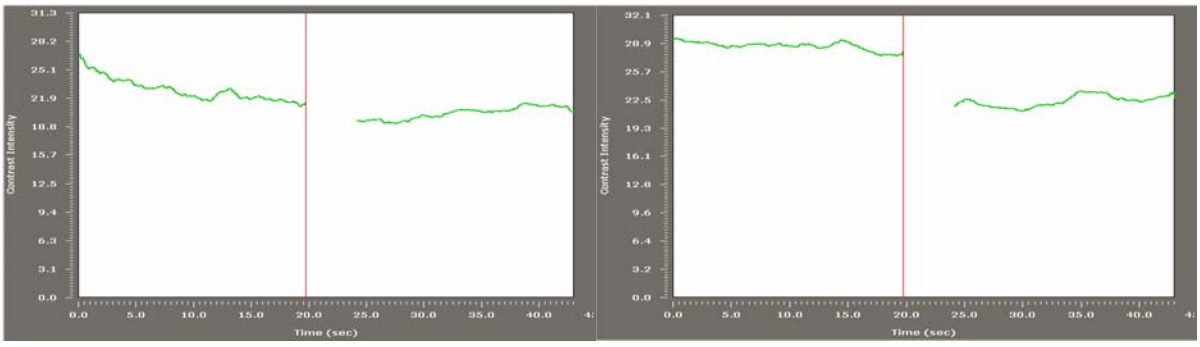


Figure 2. Destruction sequence mode contrast intensity measurements of PSLex-microbubbles (left) and $VEGF_{121}$-microbubbles (right) in 5 mm tumours. Red lines indicate the onsets of destruction periods.

Corresponding contrast intensity measurements are plotted in figure 2. Figure 3 shows the results of the tumour sizes studied. VEGF-R targeted contrast agent accumulated in all tumours. The attached contrast echo-intensity level reaches up to 45% of the circulating contrast agent intensity levels. The intensity levels generated by the attached contrast agent are more than sufficient to be distinguished from the free circulating contrast agent. P/E-selectin targeted contrast agent accumulated in tumours bigger than 10 mm. The attached contrast echo-intensity level reaches up to 50% of the circulating contrast agent intensity levels. When small tumours were induced with TNFα, P/E-selectin targeted contrast agent accumulated with contrast echo-intensity levels reaching up to 100% of the circulating contrast agent intensity levels. This means that the intensity levels of the adhered together with the free circulating contrast were twice as high as the intensity levels of the free circulation contrast alone.

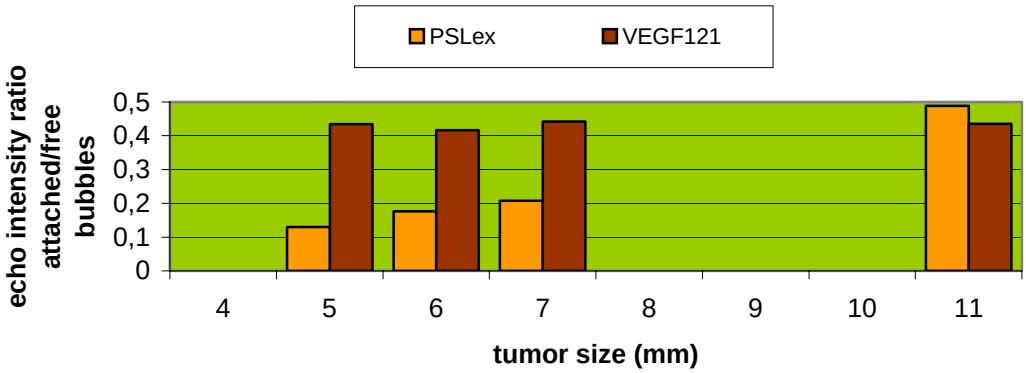


Figure 3. Echo intensity ratio of attached PSLex and $VEGF_{121}$ microbubbles versus free circulating microbubbles.

*Conclusion:* Mature tumours can be distinguished from of tumours in an earlier developmental stage by using a sequence of P/E-selectin and VEGF-R targeted contrast agents. However, using a wider variety of marker molecules would make the diagnosis more informative. Because every tumour type has its own expression patterns during development, we can expect that using a sequence of ultrasound contrast agents visualizing several molecular markers will contribute to a more personalized and successful cancer treatment.

**Cadence CPS Capture Vascular Imaging**

Cadence CPS Capture creates a single image from many frames to provide an increase in signal-to-noise ratio (SNR) and an increase in contrast resolution. The temporal persistence provides increased SNR due to averaging of front-end generated thermal noise; furthermore, contrast resolution is increased by a form of steered spatial compounding due to the motion of contrast agents in sequential frames. The two keys to this mode are excellent rejection of tissue signal and low total bulk tissue motion. Tissue rejection is provided by the Cadence CPS non-linear fundamental imaging, which provides 15 dB-35 dB greater specificity to tissue than phase inversion imaging [1]. Bulk tissue motion is a significant challenge and is application specific. Breath holding is a necessity and often challenging in sick patients; therefore, high sensitivity and frame rate are required to create a vascular image within seconds. Cadence CPS Capture imaging examples in the kidney and liver show greatly improved contrast resolution and increased SNR for tumor characterization and imaging tumor response to treatment. Examples of liver tumor response to RF ablation show greatly enhanced contrast resolution of the treated area versus the untreated area, and provide guidance for clinical treatment planning.

Other applications benefit from the CPS Capture technology, including tumor imaging in the breast and thyroid and vascular imaging with a newly developed 9L4 1.25D transducer. Early studies suggest imaging vaso-vasorum perfusion to carotid plaques with CPS Capture can provide a more sensitive view of plaque vasculature.

[1] Phillips, P.J., Contrast pulse sequences (CPS): Imaging nonlinear microbubbles, 2001
IEEE Ultrasonics Symp Proc 1739-1741.

Jim Chomas - Siemens

# Up-date on transit time analysis of the liver

Thomas Albrecht, MD, FRCR
Joachim Hohmann, MD, PhD
Dept. of Radiology
Campus Benjamin Franklin
Charité – Universitätsmedizin Berlin
Berlin, Germany
thomas.albrecht@charite.de

Hepatic transit time analysis of microbubble contrast agents was first proposed in the late 1990ies as a method of showing arterialisation of the liver in patients with diffuse liver disease (cirrhosis) or liver metastases.
Early approaches used spectral Doppler of a hepatic vein with Doppler intensitometry to assess the first passage of a bolus of Levovist through the liver. The time difference between peripheral venous injection of a contrast medium bolus and the first appearance of the bubbles in the hepatic vein was defined as the arrival time. It was shown, that the arrival time was significantly shorter in patients with cirrhosis or metastases than in normal volunteers. A limitation of this method was the dependence of the results on extra-hepatic factors such as cardiac out-put and peripheral vascular resistance.
This limitation was overcome by the use of newer "low MI" agents such as Optison or SonoVue and 2D contrast specific imaging modes. With this approach, the hepatic artery, portal vein and a major hepatic vein can be imaged simultaneously, so that the liver transit time (arterial to hepatic venous and portal to hepatic venous) can be assessed more independently of extra-hepatic factors. Several commercial analysis tools are now available for quantitative analysis of the US sequences using regions of interest placed in the relevant vessels.
The choice of contrast agent for liver transit time analysis is important. Several studies have shown that arterio-venous transit time in normal subject is longest with Levovist (approximately 20s), followed by Optison (approximately 16s) and SonoVue (approximately 11 s). Transit times in arterialised livers (cirrhosis or metastases) is $\leq$ 10 s irrespective of the agent used. This indicates a larger differEnce and therefore probably a better separation of normal liver and arterialised livers with Levoivst and, to a lesser degree, with Optison than with SonoVue.
For diffuse liver disease and especially cirhosis, the underlying mechanisms for shorting of the hepatic transit time are well recognised: arterialisation of the liver and formation of intrahepatic arterio-venous shunt. Transit time analysis has shown its potential for non-invasive diagnosis of cirrhosis as well as for grading the severity of o viral hepatitis.
For liver metastases, the underlying changes of hepatic perfusion are less well understood. Previous work by Leen et al. using the Doppler perfusion index (DPI) has demonstrated hat measurements of hepatic arterialisation can in principle be used to diagnose metastases at a very early stage, where they are undetectable with conventional imaging. However, other groups have been unable to reproduce these results. The rationale for using hepatic transit time analysis in patients with metastases is that this may be a more reproducible method than the DPI for achieving the goal of detection of occult metastases. Experimental studies have shown that liver arterialistion occurs at an early microscopic stage of metastatic seeding, even before vascular supply of the metastatic cell nests is established. The haemodynamic changes occur at the general splanchnic circulation mainly by reducing portal venous flow with a reactive increase in arterial flow. Furthermore, local intrahepatic perfusion changes have been

observed. A vaso-active humoral factor such as cytokine has been proposed to cause these changes.
We studied changes in hepatic transit time in 22 patients with liver metastases from colorectal cancer and compared them with 22 healthy volunteers. We used 2D phase inversion imaging and a bolus injection of SonoVue. Quantitative analysis confirmed that there was significant shortening of arterio – hepatic venous transit time in patients (7.27 ± 1.92) compared to controls (10.73 ± 2.58 s). Furthermore we also observed significant shortening of portal – hepatic venous transit time from 7.83 ± 2.72 s in controls to 3.99 ± 2.44 s in patients. ROC analysis showed an area under the curve A = 0.86 for arterio – hepatic venous transit time and A = 0.85 for portal – hepatic venous transit time. ROC analysis of subjective transit time analysis by two independent blinded readers showed only slightly inferior results (blinded reader 1: A = 0.80 and 0.78 respectively; blinded reader 2: A = 0.78 and 0.84 respectively), fig 1 and 2. Sensitivities and specificities are shown in table 1.
Transit time measurements in patients were independent of the number of liver segments involved (range 1 – 8) or volume of total metastasis load (range: 1 – 393 ml), indicting that shortening of transit time occurs at an early stage of disease.

**Table 1:**

| **Transit time** | **Sensitivity** | **Specificity** | **Cut-off** |
|---|---|---|---|
| Arterio - hepatic venous quanti | 82 % | 81 % | 9 s |
| Arterio - hepatic venous reader 1 | 86 % | 71% | 11.6 s |
| Arterio - hepatic venous reader 2 | 77 % | 71 % | 11.6 s |
| Portal - hepatic venous quanti | 77 % | 77 % | 6.07 s |
| Portal - hepatic venous reader 1 | 73 % | 73 % | 5.5 s |
| Portal - hepatic venous reader 2 | 73 % | 77% | 5.5 s |

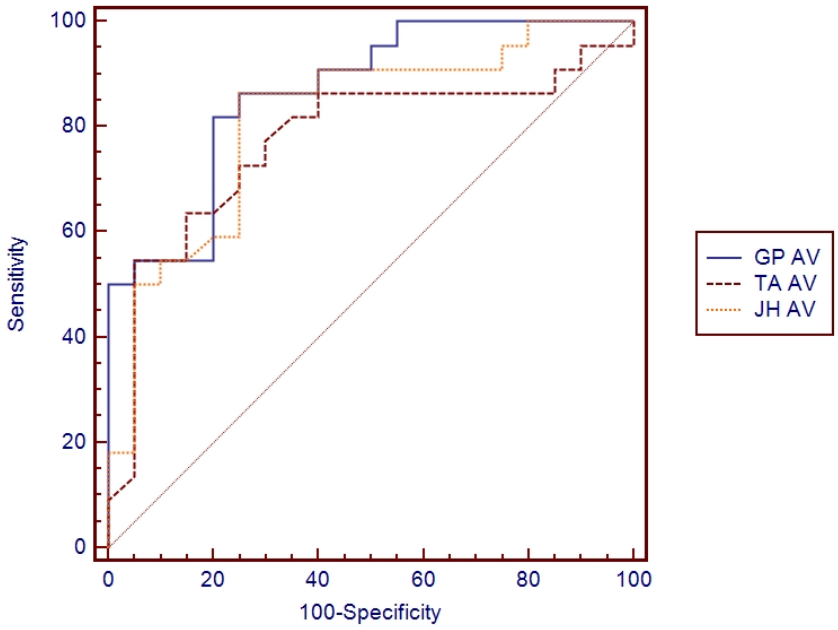


**Fig. 1**: ROC analysis for separation of normal volunteers and patients with metastases based on arterio – hepatic venous transit time. GB = quantitative analysis, JH = blinded reader 1, TA = blinded reader 2

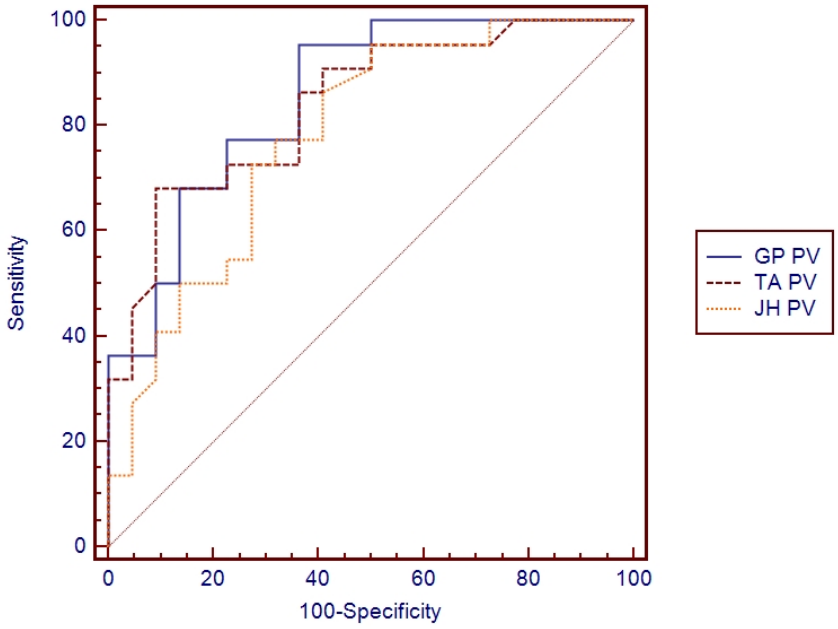


**Fig. 2**: ROC analysis for separation of normal volunteers and patients with metastases based on protal – hepatic venous transit time. GB = quantitative analysis, JH = blinded reader 1, TA = blinded reader

# New applications of contrast ultrasound imaging to diagnosis of tumorous and diffuse liver diseases

Fuminori Moriyasu, M.D.
Chairman and Professor
The Department of Gastroenterology and Hepatology
Tokyo Medical University
moriyasu@tokyo-med.ac.jp

Recent years several ultrasound contrast agents such as Definity™ and SonoVue™ have been developed and become commercially available in various countries. Ultrasound contrast agents are applied to diagnosis not only for cardiology but also radiology. However, the market size of ultrasound contrast agents in radiology field has not been increased as expected and it is much smaller than that of CT contrast agents.

In the applications for liver diseases, especially tumor diseases, CT has diagnostic ability of both detection and characterization. On the other hand, ultrasound contrast imaging has been used only for characterization of known lesions.

Sonazoid™ has been approved by Japanese Authorities and commercially available since January 10, 2007. Sonazoid has made Kupffer cell targeted imaging possible and the utility for liver disease diagnosis will be widened.

At the present time, applications of ultrasound contrast agents in the liver can be divided into three categories; 1) vascular enhancement, 2) Kupffer imaging, 3) therapy assisting imaging. Newly developed technique for vascular imaging such as Micro Flow Imaging (MFI), which employs flash replenishment imaging and maximum intensity holding technique has made it possible to visualize small sized vascular structure down to 200μ at minimum in diameter. This technique is useful to visualize neovascularization of the tumorous disease but also evaluation of recanalization of ischemic lesions such as organ transplantation and sclerotic plaque.

Kupffer imaging, which is obtained from resonating microbubbles phagocytosed by hepatic macrophages, has been used for detection of liver lesions lacking Kupffer cells. Levovist™, Sonazoid™ and Optison™ are phagocytosed by Kupffer cells, while SonoVue™, Definity™ and Imagent™ are not. Among the former agents, Sonazoid™ is the most suitable for Kupffer imaging because the effect of Kupffer imaging lasts longer than the others. This is because 1) lifespan of Sonazoid™ in the Kupffer cells is so long that imaging lasts for one hour or more and, 2) Sonazoid™ microbubbles emit harmonic signals continuously since they resonance under low to middle MI (0.1-0.3) ultrasound

exposure.

Real time ultrasound contrast imaging using low MI contrast agents such as SonoVue™ has been used for guidance and therapeutic evaluation of local ablation therapy for liver cancers. Recently contrast 3D and real time contrast 3D (4D) imaging are expected to be useful for the therapeutic guidance. Delineation of the tumor border and ablation area can be estimated correctly using these techniques.

Sentinel lymph node can be enhanced using ultrasound contrast agents. Sonazoid™ is the most promising agent for lymph node enhancement. Sentinel node navigation surgery using ultrasound contrast agent is expected to be applied not only to breast cancer but also to other organs such as esophagus, gastrointestinal and colorectal cancers, in which endoscopic ultrasound approach is possible.

Various applications and new technologies of ultrasound contrast imaging will be reviewed in this session.

**Challenges of quantitative tumor response imaging with microbubbles**

Mike Averkiou[1], Dina Kyriakopoulou[2], Matt Bruce[3], Jeff Powers[3], and Peter Burns[4]
[1]University of Cyprus, [2]Henry Dynan Hospital Athens, [3]Philips Medical Systems,
[4]University of Toronto

Microbubble contrast agents allow the imaging of blood in the microcirculation. Diagnostic imaging of tumors and differential classification based on their blood flow in the microcirculation is the first and most obvious application. Another perhaps more important use of microbubbles is the quantification of the perfusion characteristics, including that of the tumor angiogenic circulation, in an effort to create a quantitative measure of tumor response to therapy.

Over the last ten years nonlinear imaging techniques for microbubble contrast agents have been developed and refined. Today, low Mechanical Index (MI) imaging is widely accepted and when combined with the appropriate nonlinear pulsing scheme blood flow in the tumor microvasculature is reliably observed. Low MI ensures the preservation of microbubbles (avoids disruption), and nonlinear imaging enables the rejection of tissue and thus, a lasting real-time bubble specific image is produced. The most significant aspect of the development of instrumentation to date is that blood flow in the capillary bed is observed routinely. Angiogenesis, the formation of new blood vessels and the remodeling of existing vasculature, now may be imaged and quantified. Most cancer therapies today target tumor angiogenesis and a quantitative assessment of tumor response is badly needed.

A first step towards perfusion quantification is the formation of time-intensity curves from a region of interest. This may be calculated with either digitized video data, or native logarithmically compressed data (in dB), or native linear (absolute scale with all logarithmic compression removed) data. Even though the first 2 categories are more readily available, the latter is perhaps the one with the greatest potential for reproducible quantification.

In the present work we consider quantitative tumor response for various liver tumors. The dual blood supply of liver (arterial and portal venous supply) further complicates the issue. Some aspects of liver tumor quantification may be borrowed from myocardial perfusion but it is not certain yet how similar the two approaches may be. For example, the use of destruction replenishment technique may not be easily adopted or even suitable at all for the liver. A form of parametric quantification similar to the one for cardiology may be formulated but at the present a suitable parameter that will act as a surrogate for tumor response has not been proposed. Currently, time intensity curves of liver tumors indicate in a quantitative manner their specific blood flow behavior. For example, often malignancies show a quick wash-in and a quicker than normal tissue wash-out. This differential response can be transformed in a form of parametric imaging, as explained later on.

The greatest challenge today in tumor response quantification is tissue motion.

This is mainly due to breathing but other sources of motion exist as well. Typically, loops over 60 seconds are required and thus breath holding is not feasible. In order to quantify blood flow in the microcirculation we must ensure that the same 2D plane is maintained over the period of the loop. And even more challenging will be to find the plane of interest at a later time after the course of therapy. One option is to require the patient to perform shallow controlled breathing. In addition, motion compensation algorithms are applied to correct for all *in-plane* movements. However, motion compensation can not be used in *out-of-plane* movements and 2D imaging. Three dimensional (3D) imaging can solve many of tissue motion problems and the same plane may be found repeatedly in a volume of data. With 3D imaging, and an appropriate lesion segmentation scheme, the blood volume of the whole tumor may be quantified.

Until 3D contrast enhanced imaging and quantification is fully developed and refined, a lot of ground on angiogenesis quantification may be covered. Current efforts on automatic lesion segmentation and motion compensation have addressed some of the issues described above. Results are shown from a recent release of Philips' QLAB quantification software for user assisted border detection in Fig. 1. In addition to easy measurements and observation of the lesion filling characteristics, the potential to automatically track the lesion in order to quantify it exists.

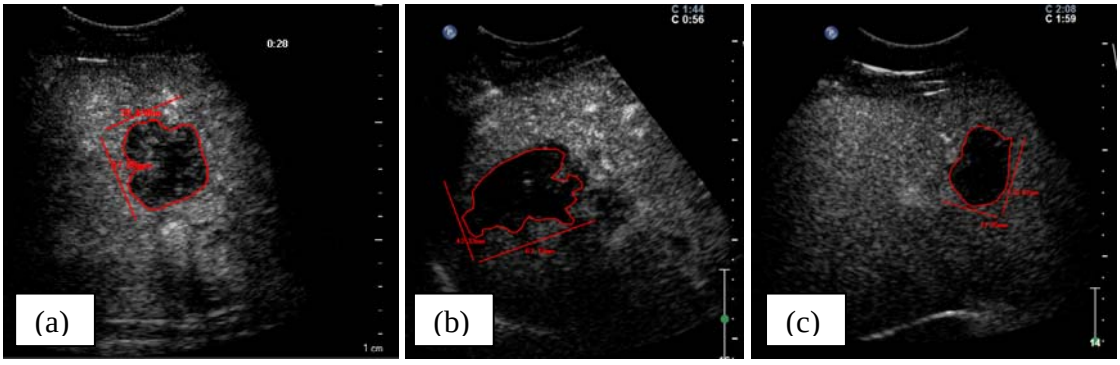


***Figure 1.*** *Examples of user assisted border detection for lesion segmentation*

With the use of QLAB software, patient data with liver lesions imaged with SonoVue (Bracco) and Definity (BMS) have been analyzed. As a first step, native logarithmic data (in dB) were used, but in later stage the software will also be capable to unmap the system compression and display linear (echo amplitude) data. A simple algorithm is described here for liver lesions. Malignant liver lesions (HCC's and metastases) have increased flow in the arterial phase and reduced or no flow during the portal venous phase, as shown in Fig. 2.

As a first step, the zero (or background) level of every region of interest is found and subtracted from the data. Next, a smoothing filter (running average) is applied. Finally, the curves from the various regions are normalized so that they all begin at 0 and peak at 1. Preliminary results show curves from malignant ROIs to plateau and decrease whereas the curves from normal liver ROIs are still increasing. Application of the above algorithm over the whole image suggests a simple model for parametric imaging. In addition, the crossing point between a malignant ROI and a normal ROI may be

indicative of the start of the portal phase. A similar approach is also applied to linear scale intensity, though in the case of this particular algorithm the results can be expected to be similar.

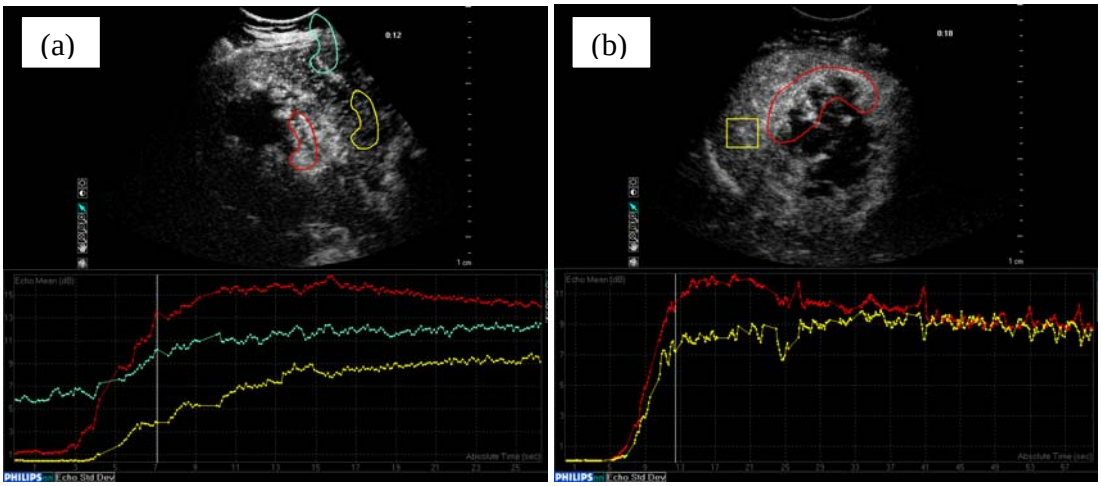


***Figure 2.*** *Time-intensity curves (in dB) for HCC recurrence ROI (red) and normal liver ROI (yellow and blue)*

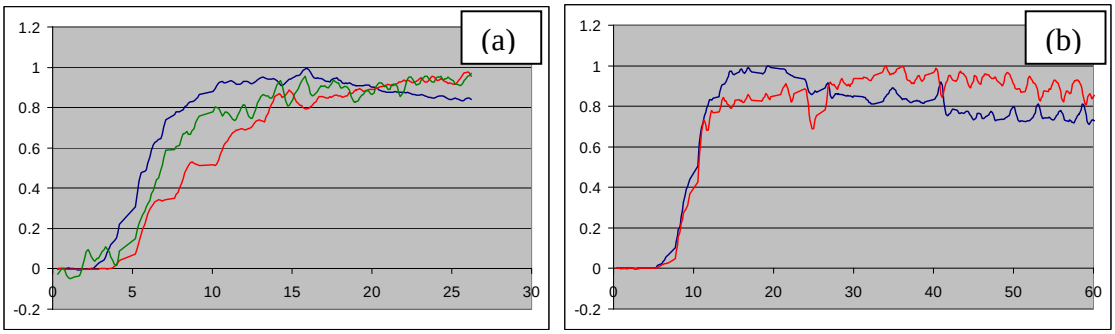


***Figure 3.*** *Processed time intensity curves for the data shown in Fig. 2. The processing includes subtraction of the individual background level, smoothing, and normalization.*

# Contrast Enhanced Ultrasound (CEUS) in ICA stenosis in patients with predominantly soft plaques: First Results

Weskott HP, Kossow K

Department of Internal Medicine, Siloah Hospital, Klinikum Region Hannover, Hannover Germany

**Objective:** Evaluation of plaque vascularization in predominantly soft plaques of the CCA and ICA in pts with different degrees of stenosis

**Methods and Materials:** In 38 patients the morphological and hemodynamical characteristics of 43 soft plaques exceeding 0.2cm thickness leading to various degrees of stenosis were characterized using basic US techniques and contrast enhanced US (CEUS). Mean age: 67.1±11.2yrs, 83% males, 26/38 were on statin and/or 22/38 on ACE medication, 35/38 pts had a history of hypertension. 6 had ICA occlusions, 18 pts ICA stenosis <50% and 19 pts ICA stenosis >50%. 15/38 had ipsilateral neurological symptoms. CEUS was performed in a low MI coded phase inversion mode (7MHz probe, LOGIQ 9, GE Healthcare, USA). Contrast agent: Optison™ (Amersham, GE Healthcare). 1mL bolus was injected i.v. followed by a 10mL saline flash. Time intensity curves (TIC) were calculated from lumen side and within the plaque. Time to peak (TTP), slope gradient (SG), enhancement level (EL), and enhancement difference (ΔEL) were evaluated prior and during CEUS. Additionally a visual grading system for the presence of neovascularization was applied (1=minimal, 2=moderate, 3=extensive plaque enhancement).

**Results:** Soft plaques had a mean Gray-Whale score of 0.35±0.48. 34/43 plaques showed various degrees of enhancement with a mean visual enhancement grade of 1.8±0.9. TTP (CCA), SG and mean increase of enhancement level within the lumen and plaque: 7.9±4.1s and 10.1±5.8s, SG: 1.5±1.2 and 4.3±1.7, 27.7±12.5 and 11.3±5.4dB. No correlation was found between Gray Whale score and ΔEL (r=0.06) SG and ΔEL (r=0.44 in pts with stenosis >50%) or TTP and ΔEL. No correlation was found between hsCRP levels and the presence of plaque vascularization (mean CRP: 1.53±2.7).All occluded vessels had a grade 3 neovascularization. Intralesional vessels were fed by vasa vasorum, its branches showed an up and downstream course. In 5 cases contrast bubbles ran through tiny, sometimes bizarrely shaped channels within the plaque arising from the patent lumen side and not from the vessel wall. All circumscript thickend CCA walls were diffuse hypervascularized.

**Conclusions:** CEUS proved a great variability of neovascularization in soft ICA plaques and occluded ICA which could be explained by the high number of patients under statin medication. Gray scale appearance and CRP levels did not correlate to plaques vascularity. All circumscript thickened arterial walls were hypervascularized, probably due to an active remodelling process. Thin channels filling up from the lumen side suggest open fissures in cracked plaques, probably indicating highly vulnerable plaques. Further long term studies are needed to evaluate clinical impact and effects of medication on plaque vascularity.

# USE OF CONTRAST-ENHANCED ULTRASOUND IN GYNECOLOGY

F. Tranquart[1], H. Marret [2], S. Sauget [2], A. Bouakaz[1] and A. Bleuzen[1]

[1]- INSERMU619, Technical Innovation Center. CHRU Tours. France

2- Department of Obstetrics and Gynaecology. CHRU Tours. France

Worldwide, ultrasound is the primary imaging modality for the detection and characterization of female pelvis lesions during screening, or for any pelvic symptom. It has been proven that the association of supra-pelvic way and transginal way gives a complete view of the female pelvis and provides some specific indicators for a high level confidence diagnosis. As it was demonstrated that Doppler ultrasound plays a role in this diagnosis assessment, some research has been conducted to better detect vessels within or surrounding a lesion. The recent introduction of ultrasound contrast agents (UCA) has totally changed the depiction of specific vascular signs for a definite diagnosis by a marked increase in signal from the vessels, especially with modern non linear imaging techniques. The recent availability of these imaging techniques for transvaginal applications has allowed physicians to use UCA in ovarian or uterine lesions for a better assessment of vascular patterns which could play a role in diagnosis management.

## I- Ovarian lesions

Ovarian carcinoma represents the second most frequent gynecological cancer observed in women, with a poor long term outcome largely related to a late diagnosis and the frequency of malignant lesions of around 15%. This is due to the absence of any alarm signal for initiating an ultrasound exam to detect any ovarian abnormalities. It has been proven for a long time that ultrasound is the most powerful technique for detecting ovarian cancer, with a sensitivity of 80-85%. One of the most common hypotheses for an early diagnosis of ovarian cancer is to detect the neovessels which allow the tumor to grow. Vessel changes within the ovary may be visualized before tumor detection itself. Color Doppler has been assessed as one of the ultrasound (US) techniques that can be used to describe specific characteristics of ovarian vascularization[1-4]. Power Doppler is useful to map ovarian vessels, including those associated with malignancy (in septa, papillarities and tissular parts of the lesion) while Pulsed Doppler is used to measure blood flow velocity. Doppler imaging and the subjective evaluation of the grey-scale image improves our ability to make a correct diagnosis prior to surgery, which will improve patient outcome if a malignancy is present.

Levovist® (Schering, Berlin Germany), from the first UCA generation, has been used in few studies for gynecological purposes. The studies have validated the feasibility of the technique in ovaries and proposed that AUC and wash-out time were the two discriminant parameters for benign-malignant differentiation [5,6].

To date only a small number of studies has been carried out in woman ovaries using new generation of contrast microbubbles such as Sonovue® or Definity®. Very recently, Testa et al.[7] have described some vascular patterns in the female pelvis. Following Sonovue® injection, wash-out time and AUC were the most stable parameters derived from the time intensity curve between ovaries and between the follicular and luteal phases in an ewe model [8]. Uptake time and total time of enhancement were also constant. Enhancement ratio and wash-in period were modified with the corpus luteum formation. In our preliminary experience using both drugs, we

were able to describe with high accuracy the microbubble distribution inside the tumor vessels resulting in an improvement in the diagnostic confidence for the discrimination of benign from malignant ovarian tumors. For example, the absence of enhancement inside solid tissue or intracystic papillarities can confirm a diagnosis of clots or solid component included within a dermoïd cyst. Absence of Doppler signal and detection of microbubbles is always associated with a benign lesion when presence of both is associated with malignant characteristics. In contrast absence of Doppler signal with detection of bubbles needs careful attention as this category includes both types of lesions for which quantification will be helpful.

The results of all these preliminary studies are in favor of the use of contrast ultrasound to be applied prospectively in non invasive studies of ovarian angiogenic function, first for the diagnosis of malignancy but also including response to drug treatment, fertility research, ovarian hyperstimulation syndrome, and early assessment of response to antiangiogenic chemotherapy.

**II- Uterine lesions**

Study of the uterine vascularity using power Doppler is nowadays one of the most important tools to describe and discriminate uterine tumors. Macroscopic vascularization of myomas, polyps, endometrium cancer, adenomyosis, or cervical cancer is well known but encountered some limitations for therapeutic monitoring of these tumors. Microbubble enhancement affords the direct depiction of tumor neoangiogenesis and may help us to establish a more precise vascular map of the tumor and normal surrounding myometrium.

**II-a Myomas evaluation.**

Leiomyomas are the most common benign tumors of the uterus in women between 20 and 50 years old. A successful and safe alternative treatment to hysterectomy is uterine artery embolization (UAE) [9-11]. We successfully used contrast-enhanced sonography with SonoVue® during UAE procedure in a patient with multiple large leiomyomas to demonstrate that injected micro-particles of size between 350 and 900 µm were targeted uniquely to leiomyomas [12]. It is remarkable that this indication could be reached by the use of transvaginal way for tiny fibroids (with injection of 4.8 ml of SonoVue®) but also by the use of supra-pubic way for large fibroids (with injection of 2.4 ml of SonoVue® only). Injection of Sonovue could provide a very precise description of the uterine vascularization in an easier way compared to angiography and using a cheaper tool compared to MRI. Enhancement patterns vary markedly among the patients from an absence of enhancement for the whole tumor to a complete and rapid enhancement after injection. Washout was typically complete after 3 minutes giving a black hole corresponding to the whole lesion. This washout helps us to identify some tiny fibroids which are not visible on conventional sonography for a perfect matching with MRI detection. Secondly it is remarkable that most of the endometrium parts clearly demonstrate an early washout after contrast injection, and in some cases exceeding the size of endometrium. By using contrast-enhanced ultrasound, we could quickly assess the efficacy of UAE and evaluate local consequences on normal myometrium and ovaries whereas both uterine arteries were totally occluded. This ultrasound method could play a major role in the assessment of early technical failure rate and in the identification of vascular risk factors for clinical failure and late recurrences.

**II-b Cancer of the cervix**

Cancer of the cervix is frequent and is accompanied by local extension or lymph node extension which guides the treatment planning i.e. surgery first or radio-chemotherapy. An intense enhancement is reported for these lesions before specific treatment with an improvement in the definition of limits but with some limitations

in the positive diagnosis as reported by Testa et al [7]. Local assessment of angiogenesis will be of value to follow local changes under chemotherapy or radiotherapy and to better schedule surgery. This method could replace of MRI to assess treatment efficacy and in conjunction with TEP for treatment planning.

## III- Conclusion

CEUS is a well adapted method in gynaecological disease by improving the detection of fibroids and the discrimination of benign from malignant adnexal lesions, guiding the treatment and allowing an adapted follow up of patients under specific therapy.

## IV- References


1. Valentin L. Prospective cross-validation of Doppler ultrasound examination and gray-scale ultrasound imaging for discrimination of benign and malignant pelvic masses. Ultrasound Obstet Gynecol. 1999; 14: 273-283.
2. Timmerman D, Valentin L, Bourne TH, Collins WP, Verrelst H, Vergote I. Terms, definitions and measurements to describe the sonographic features of adnexal tumors: a consensus opinion from the International Ovarian Tumor Analysis (IOTA) Group. Ultrasound Obstet Gynecol 2000;16:500-5. Review.
3. Marret H, Ecochard R, Giraudeau B, Golfier F, Raudrant D, Lansac J. Color Doppler energy prediction of malignancy in adnexal masses using logistic regression models. Ultrasound Obstet Gynecol. 2002; 20: 597-604.
4. Marret H, Sauget S, Giraudeau B, Body G, Tranquart F. Power Doppler vascularity index for predicting malignancy of adnexal masses. Ultrasound Obstet Gynecol. 2005; 25: 508-13
5. Orden MR, Jurvelin JS, Kirkinen PP. Kinetics of a US contrast agent in benign and malignant adnexal tumors. Radiology 2003; 226: 405-410.
6. Marret H, Sauget S, Giraudeau B, Brewer M, Ranger-Moore J, Body G, Tranquart F. Contrast-enhanced sonography helps in discrimination of benign from malignant adnexal masses. J Ultrasound Med 2004 ; 23: 1629-1639.
7. Testa A, Ferrandina G, Fruscella E, Van Holsbeke C, Ferrazzi E, Leone FPG, Arduini D, Exacoustos C, Bokor D, Scambia G, Timmerman D. The use of contrasted transvaginal sonography in the diagnosis of gynecologic diseases. J Ultrasound Med 2005; 24: 1261-6.
8. Marret H, Brewer M, Giraudeau B, Tranquart F, Voelker K, Satterfield W. Ovine model to evaluate ovarian vascularization using contrast enhanced sonography. Comparative Medicine 2005; 55: 150-5.
9. Brunereau L, Herbreteau D, Gallas S, Cottier JP, Lebrun JL, Tranquart F, Fauchier F, Body G, Rouleau P. Uterine artery embolization in the primary treatment of uterine leiomyomas: technical features and prospective follow-up with clinical and sonographic examinations in 58 patients. Am J Roentgenol 2000;175:1267-1272.
10. Pelage JP, Ledref O, Soyer P, Kardache M, Dahan H, Abitbol M. Fibroid related metrorrhagia: treatment with superselective embolization of the uterine arteries and midterm follow-up. Radiology 2000;215:428-431.
11. Tranquart F, Brunereau L, Cottier JP, Marret H, Gallas S, Lebrun JL, Body G, Herbreteau D, Pourcelot L. Prospective sonographic assessment of uterine artery embolization for the treatment of fibroids. Ultrasound Obstet Gynecol 2002;19:81-87.
12. Marret H, Tranquart F, Sauget S., Alonso AM, Cottier JP, Herbreteau D, Contrast enhanced sonography during myomas embolization Ultrasound Obstet Gynecol. 2004; 23: 77-79.

# Influence of Coronary Pressure on Myocardial Blood Volume: First Measurements in Humans

Andrea Grêt, Andreas Indermühle, Christian Seiler, Rolf Vogel
Swiss Cardiovascular Center Bern, University Hospital Bern, Switzerland

***Background*** – Clinically used hemodynamic indices such as fractional flow reserve, coronary flow reserve and collateral flow index are based on simplified models of the coronary circulation. In particular, myocardial resistance is assumed to be independent of the perfusion pressure. Objective of this study was to quantify the influence of perfusion pressure on myocardial blood volumes (MBV) that the reflect microcirculatory resistance.

***Method and Results*** – 30 patients with coronary artery disease underwent measurement of intracoronary perfusion pressures and MBV of 32 coronary arteries and their territories during and after angioplasty. MBV was measured in ml blood per 100g tissue by quantitative myocardial contrast echocardiography as recently validated by our group. During angioplasty, perfusion pressures, i.e. the distal occlusive pressure, and MBV varied between 9-57mmHg (27±12mmHg) and 1.2-15.2ml/100g (6.8±3.9ml/100g). After successful angioplasty, perfusion pressures and MBV varied between 64-118mmHg (94±12mmHg) and 3.9-18.2ml/100g (10.3±3.5ml/100g). MBV and perfusion pressures correlated positively (Figure, dotted lines) in 25 cases and negatively (Figure, solid lines) in 7 cases, suggesting periprocedural microembolisation of the latter. In agreement with animal data, mean MBV variation was 0.04ml/100g per 1mmHg. Thus, a coronary pressure drop of 60mmHg reduces MBV by approximately 30%.

***Conclusions*** – The human coronary microcirculation is distensible, the fact of which may challenge the use of coronary hemodynamic indices for clinical decision making.

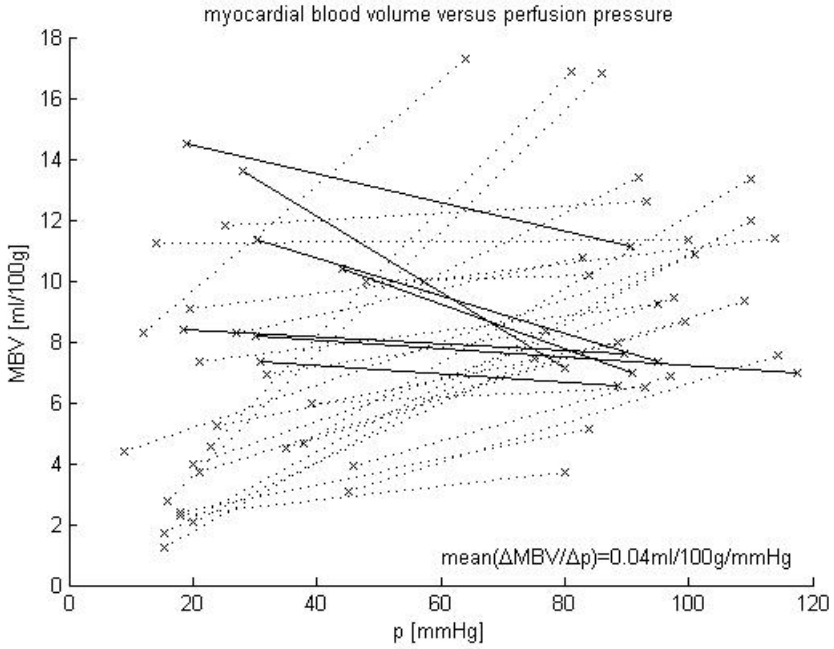

# Role of Parasternal Data Acquisition During Contrast Enhanced Real-Time Three-Dimensional Echocardiography

Attila Nemes, Marcel L. Geleijnse, Wim B. Vletter, Boudewijn J. Krenning, Osama I.I. Soliman, Folkert J. ten Cate

*Department of Cardiology, Thoraxcentre, Erasmus MC, Rotterdam, The Netherlands*

**Background.** Recent technical developments have resulted in high-resolution real-time three-dimensional echocardiography (RT3DE). The purpose of this study was to investigate the beneficial role of parasternal-acquired images in addition to apical-acquired images during contrast stress RT3DE.

**Methods.** The study comprised 30 consecutive patients (52 ± 11 years, 18 males) with chest pain referred for routine stress testing. The contrast RT3DE images were acquired from the apical and parasternal window with a Sonos 7500 echo system (Philips Medical Systems, Best, The Netherlands) attached to a X4 matrix array transducer.

**Results.** From the apical and parasternal acquisition, 464 segments (91%) and 267 segments (52%) could be analysed, respectively ($P < 0.001$). From the apical window, more basal segments were not analysable (22 of 180, 12% vs. 24 of 330, 7%; $P = 0.06$). From the parasternal window, more apical segments were not analysable (117 of 150, 78% vs. 126 of 360, 35%; $P < 0.01$). The mean image quality index of the 464 analysable segments from the apical-acquired images was 2.43. Fourteen out of 180 basal segments (8%), 12 out of 180 mid-ventricular segments (7%) and 2 out of 150 apical segment (1%) were only available with parasternal data acquisition. In addition to these 28 segments, 79 segments (17%) already visualised from the apical window improved in quality. The overall mean image quality index, now assessed from 292 (96%) of all segments, using both the apical and parasternal acquired data, improved to 2.74 ($P < 0.05$).

**Conclusions.** Addition of parasternal to apical acquisition of contrast RT3DE data can decrease the number of non-visualised segments and improve mean image quality.

# Ultrasound targeted microbubble destruction increases capillary permeability in hepatomas

Richard D. Kroll[1], Steliyan Tinkov[2], Conrad Coester[2], Gerhard Winter[2], Raffi Bekeredjian[1]

[1] Internal Medicine III, University of Heidelberg, Heidelberg, Germany
[2] Department of Pharmaceutical Technology and Biopharmaceutics, Ludwig-Maximilians University, Munich, Germany

**Introduction:** Ultrasound targeted microbubble destruction (UTMD) has evolved as a promising tool for organ specific gene and drug delivery. Taking advantage of high local concentrations of therapeutic substances and transiently increased capillary permeability, UTMD could be used for the treatment of ultrasound accessible tumors. The aim of this study was to evaluate if ultrasound targeted microbubble destruction can locally increase capillary leakage in a hepatoma model of the rat.
**Methods:** Subcutaneous Morris hepatomas were induced in both hindlimbs of ACI rats by cell injection. A total of 18 rats were divided into three groups. Only one tumor per rat was treated by ultrasound. The first group received injection of Evans Blue, followed by UTMD. The second group received a PBS infusion and ultrasound to the target tumor after Evans Blue injection. The third group received UTMD first, followed by Evans Blue injection. Tumors and control organs were harvested, and Evans Blue extravasation was quantified.
**Results:** Evans Blue injection followed by UTMD showed about 5-fold higher Evans Blue amount in the target tumors compared to the control tumors. In contrast, no difference in Evans Blue content was detected between target and control tumors when ultrasound was applied without microbubbles or when UTMD was performed before Evans Blue injection.
**Conclusion:** Ultrasound targeted microbubble destruction is able to transiently increase capillary permeability in hepatomas. Combined with a therapeutic substance, this effect could be used to deliver large amounts of chemotherapy drugs into solid tumors.

# Markedly increased signal enhancement after the second injection of SonoVue® compared to the first – a quantitative normal volunteer study

Jan Skrok

Abteilung für Radiologie und Nuklearmedizin
Charité - Universitätsmedizin Berlin - Germany

Purpose:
During a contrast enhanced ultrasound (CEUS) examination, multiple contrast injections may be required. We noted during routine CEUS with SonoVue® that the enhancement from a second injection seemed higher than that from the first injection, even after complete disappearance of contrast from the first. This study was performed to verify this effect quantitatively under standardized conditions.

Methods:
Liver and aorta of 7 normal volunteers were studied using an Acuson Sequia (Siemens, CPS, MI 0.08, 1 frame/s) over 5min after injection of 1ml of SonoVue® and 10ml saline. A second injection (same dose, identical scan parameters) was performed 12 min after the first and after complete disappearance of enhancement. Digital videos were analyzed quantitatively using AXIUS software (Siemens).

Results:
Peak enhancement increased by 5 +- 1.5 dB after the second injection in aorta and liver ($p<0.05$). Enhancement after the second injection remained >3db above that of the first throughout the experiment. The area under the curve (linear data reflecting microbubble concentration) increased by a factor of 3.5, indicating a dramatic increase of bubble load in the circulation by a similar factor. A possible explanation is saturation of pulmonary macrophages by the first injection, allowing more microbubbles to pass the lung into the left circulation after the second injection.

Conclusion:
A second injection of SonoVue® provided significantly stronger enhancement than the first. This has two clinical implications: (1) The dose of a second injection can be reduced by a factor of three if the first provided sufficient enhancement. (2) If enhancement from the first injection is suboptimal, a second identical dose will provide better enhancement.

# DELIVERY OF ANTISENSE OLIGONUCLEOTIDES TO MDX MYOCARDIUM USING ULTRASOUND AND MICROBUBBLES

***[1]Julia Alter, [1]Charles A Sennoga, [1]Robert J Eckersley and [2]Dominic J Wells***

*[1]Ultrasound Group, Imaging Sciences Department*
*MRC Clinical Sciences Centre, Imperial College London, London W12 0HS U.K.*
*[2]Gene Targeting Group, Department of Cellular and Molecular Neuroscience,*
*Division of Neuroscience and Mental Health, Imperial College London, W6 8RP U.K.*

**Purpose:** Duchenne Muscular Dystrophy (DMD) is a genetic muscle degenerative disorder caused by mutations in the dystrophin gene leading to a lack of functional dystrophin protein. Antisense Oligonucleotides have the potential to restore functional levels of dystrophin by mediating skipping of specific exon(s) and restoring the open reading frame. A previous study, [Alter, J., *et al.* (2006) *Nat Med*. **12**, 175–177], showed that when injected intravenously (IV), Phosphorodiamidate Morpholino Oligomers (PMOs) effectively mediated exon skipping in body-wide muscles in the dystrophic *mdx* mouse, but failed to induce dystrophin expression in the heart. Since heart failure is a major cause of death in DMD, achieving dystrophin expression in heart is of great importance for a successful treatment. Here, we investigate the use of diagnostic ultrasound in conjunction with microbubbles as a safe, physical enhancer for the delivery of PMOs into the heart.

**Method:** 2mg PMOs together with Optison® (approximately $10^8$ bubbles) were injected IV into the tails veins of *mdx* mice, while ultrasound was applied to the heart. Ultrasound was applied for 2 minutes with a 15L8-S probe on a Siemens Sequoia scanner. In these experiments the transmitted ultrasound frequency was fixed at 7 MHz. The amplitude of the transmitted pulses was set to a mechanical index (MI) of 1.9.

**Results:** 7 days after microbubble ultrasound (MBUS) treatment, expression of dystrophin was detected in the *mdx* heart. Immunohistochemical analysis showed large numbers of dystrophin-positive cardiomyocytes throughout the heart (see Figure). RT-PCR confirmed the presence of dystrophin mRNA of the size expected for deletion of

exon 23. No pathology was noted in treated hearts at either 24 hours or 7 days after treatment. Importantly the addition of Optison® to the morpholino did not reduce the efficiency of PMO delivery to skeletal muscles.

**Conclusion:** Our data demonstrate that microbubble ultrasound treatment of the heart is a valuable addition to complete the systemic treatment of DMD by PMO-mediated exon skipping.

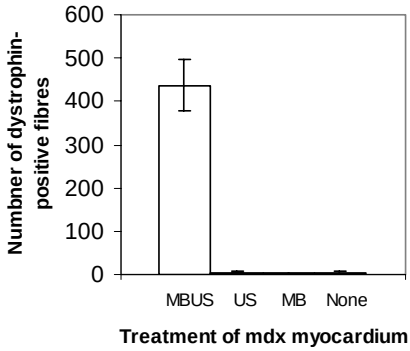


**Figure:** Number of dystrophin-positive fibres expressed in one cross-section of *mdx* myocardium after a single injection of PMOs with different treatments to the heart.

**Acknowledgment:** This project was originally the idea of Prof Martin Blomley of the Imaging Sciences Department, Imperial College London who died in April 2006.

**Visualizing Chemotherapy: Contrast Driven Drug delivery**

Margaret A. Wheatley†, John Eisenbrey†, Odelia Mualem-Burstein†, Michael Soulen*

*School of Biomedical Engineering, Drexel University, Philadelphia, PA 19104 USA†*
*Division of Interventional Radiology, Hospital of the University of Pennsylvania, Philadelphia, PA 19104, USA†*

About 80% of cancers involve solid tumors. Local treatments involve radiation and surgery, and systemic chemotherapy uses high drug doses, which often result in devastating side effects, and are frequently toxic to organs such as heart and kidney. Drug delivery directly to the tumor would have the advantage of reducing these undesirable side effect. Problems to overcome at the tumor site include high interstitial pressures, and a tortuous, aberrant vasculature with uneven, slow and multi-directional blood flow. We are developing an injectable microbubble-based drug delivery platform that enables minimally invasive delivery of chemotherapy directly to the tumors. Treatment is envisioned to be performed in conjunction with ultrasound (US) imaging. Delivery will be both activated and controlled by the US wave, allowing the physician to simultaneously monitor and deliver metered, localized doses of chemotherapy. We have investigated methods of loading drug into a highly echogenic contrast agent developed in our laboratory. The agent is composed of the biodegradable polymer poly (lactic-*co*-glycolic) acid. The effects of drug (Doxorubicin, a commonly used chemotherapeutic in liver cancer) loading method, polymer composition and insonation frequency on the payload and release characteristics are discussed.

When loading drug by surface adsorption longer loading times resulted in lowering of the echogenicity or the resulting drug-loaded capsules compared to the unloaded capsules. PLGA (50:50 poly(DL-lactide-co-glycolide)) was more sensitive to loss in echogenicity during loading than capsules prepared from PLA (poly(DL-lactic acid)). Loading time did not have a direct affect on the amount of drug attached to each capsule. PLGA showed more drug adsorption than PLA. Incorporation of drug during the capsule manufacturing process had little effect on the echogenicity of the capsules. Drug release was highly dependent on both loading method and polymer composition.

# LIPOPLEX LOADED MICROBUBBLES FOR ULTRASOUND TARGETED GENE DELIVERY

Lentacker I., De Smedt S.C., Demeester J., Sanders N.N.

Laboratorium voor Algemene Biochemie en Fysische Farmacie, UGent, Faculteit Farmaceutische Wetenschappen, Harelbekestraat 72, 9000 Gent.

**Purpose.** The aim of this work was to attach lipoplexes to microbubbles and to evaluate the ultrasound-assisted gene transfer of these lipoplex loaded microbubbles. **Methods.** The physicochemical properties of the lipoplexes were evaluated with dynamic light scattering, zeta-potential measurements and gel electrophoresis. Coupling of the lipoplexes to the microbubbles, via the avidin-biotin interaction, was confirmed using Confocal Laser Scanning Microscopy (CLSM). Finally, the capacity of the lipoplex loaded microbubbles to transfect melanoma cells was analysed using luciferase as reporter gene. **Results.** Lipid microbubbles containing 95mol% DPPC and 5mol% DSPE-PEG-biotin were prepared. Cationic liposomes containing increasing amounts of DSPE-PEG-biotin (2, 5 or 15mol%) were prepared. Ultrasound radiation of the lipoplex loaded microbubbles caused a release of the lipoplexes, with properties similar to the lipoplexes before attachment to the microbubbles.
The transfection efficiency of the lipoplexes alone decreases with increasing pegylation degrees and was almost zero for lipoplexes containing 15mol% DSPE-PEG-biotin. The application of ultrasound had a limited and variable effect on the transfection efficiency of the lipoplexes. However, attaching of the lipoplexes on microbubbles, drastically enhanced the gene transfer efficiency in the presence of ultrasounds, whereas no gene transfer was observed in the absence of ultrasounds. Where the lipoplexes with 15mol% DSPE-PEG-biotin had almost no effect on the BLM-cells when applied without microbubbles, we found out that they had a superior transfection efficiency after coupling to the microbubbles
**Conclusions.** Attaching lipoplexes to lipid stabilized microbubbles drastically increases the ultrasound-assisted transfection efficiency of highly pegylated lipoplexes. Furthermore, this new gene carrier offers a solution to achieve a targeted gene delivery by the local application of ultrasound.

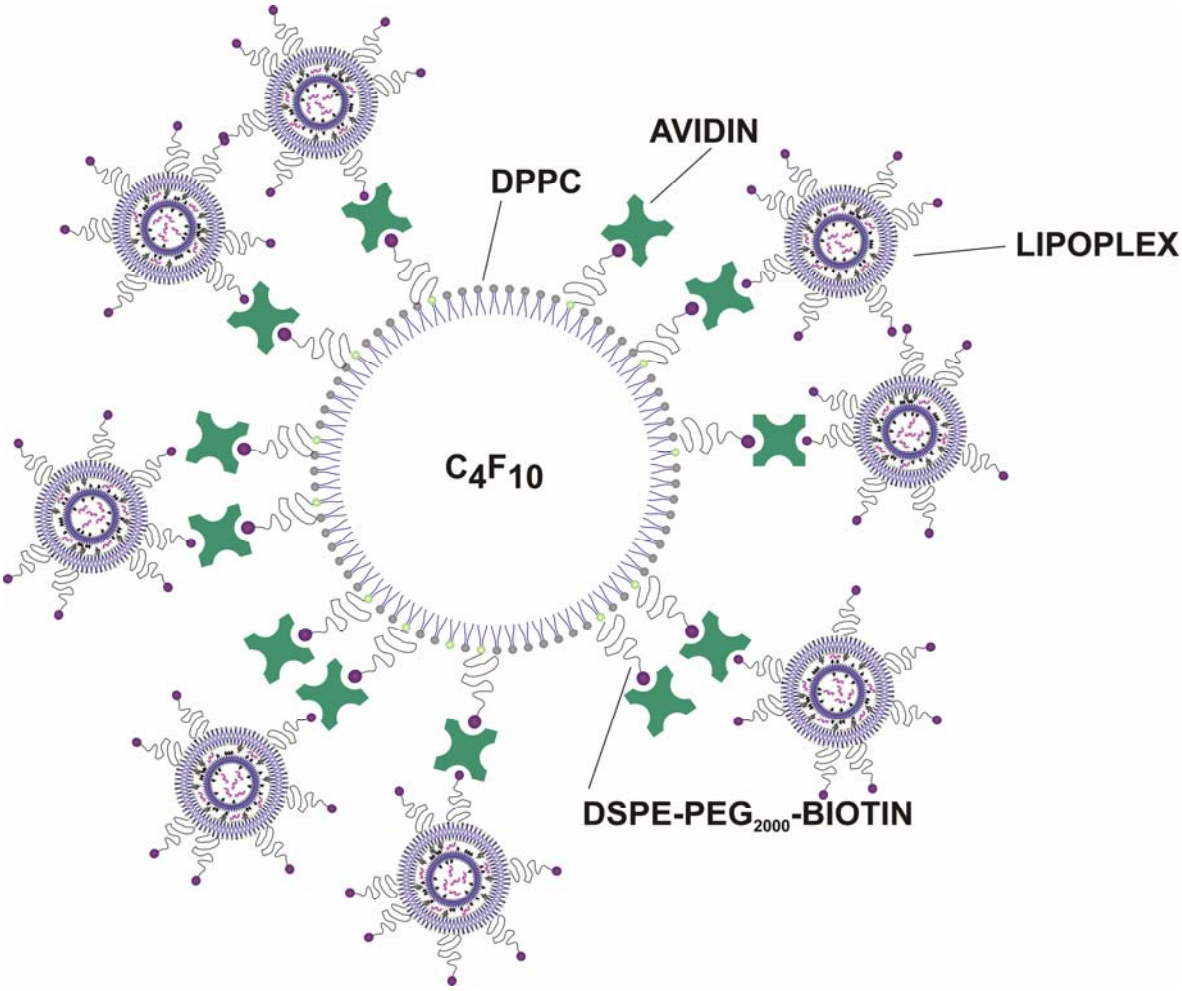
AVIDIN
DPPC
LIPOPLEX
$C_4F_{10}$
$DSPE\text{-}PEG_{2000}\text{-}BIOTIN$

**Unraveling the mechanisms of ultrasound microbubble targeted gene delivery.**

B. Meijering[1,4], L. Juffermans[2,4], K. Kooiman[3], L. Deelman[1,4], W. van Gilst[1,4], R. Musters[2], O. Kamp[2,4], C. Visser[2,4], N. de Jong[3,4] and A. van Wamel[3,4].

[1] Department of Clinical Pharmacology, University Medical Center Groningen, University of Groningen, Groningen , The Netherlands; [2]Department of Fysiology and Cardiology, VU University Medical Center, Amsterdam, the Netherlands; [3]Dept. of Biomedical Engineering, Thoraxcenter, Erasmus MC, Rotterdam, The Netherlands; [4]Interuniversity Cardiology Institute of the Netherlands, Utrecht, the Netherlands.

Several papers have demonstrated, *in vitro* as well as *in vivo*, that ultrasound and microbubble targeted gene delivery (UMTGD) is a promising non-viral vector for local gene delivery. However, the main drawback of non-viral vectors over viral vectors is their limited transfection efficiency, limiting their clinical usefulness. Beside the knowledge of the manner UMTGD parameters influence gene delivery efficiency, a better understanding of the mechanism(s) of UMTGD may further improve UMTGD efficiency and thereby its potential for gene therapeutic use. The exact mechanism(s) behind the uptake of DNA by UMTGD are still not fully understood. Until now, uptake of DNA has been attributed to transient cavitation, causing transient holes in the cell membrane. In this study we propose an alternative mechanism, namely endocytosis. Endocytosis refers to the cellular uptake of macromolecules and solutes into membrane-bound vesicles derived by the invagination and pinching off of pieces of the plasma membrane, which is an energy dependent process. The main endocytotic routes are caveolin and clatherin mediated endocytosis and macropinocytosis. Preliminary results show that UMTGD efficiency is decreased with 60% when cells are deprived of energy (ATP) by 30 min pretreatment with 650 µM oligomycin before UMTGD. Furthermore immunofluorescent detection of clatherin and caveolin-1 indicated changes in intracellular distribution after ultrasound and microbubbles. These results indicate that both clatherin as well as caveolin mediated endocytosis are affected by UMTGD. We think that endocytosis may be a mechanism in which DNA is brought into the cells by UMTGD. Further study has to elucidate if DNA mediated delivery to cells by UMTGD is indeed through endocytosis.

# Non-linear oscillations and collapse of encapsulated microbubbles subject to ultrasound

**K. Tsiglifis & N. Pelekasis**
**Dept. of Mechanical and Industrial Engineering, University of Thessaly, Volos 38334, Greece**

The nonlinear radial oscillations of contrast agents are investigated numerically subject to three different constitutive laws describing the viscoelastic properties of the shell: the Mooney-Rivlin (MR), the Skalak (SK) and the Kelvin-Voigt (KV) models are used in order to describe strain-softening, strain-hardening and small displacement (Hookean) behavior of the shell material, respectively. The equations governing liquid motion coupled with the radial micro-bubble pulsations in response to an ultrasonic beam are obtained based on the Keller – Miksis model, which also takes into consideration the compressibility of the external liquid far from the micro-bubble. The resonance frequency and scattering cross section of the fundamental and higher harmonics depend strongly upon the nonlinear material behavior as well as the shell and liquid parameters. When the membrane is strain-softening (MR) the resonance frequency decreases with increasing sound amplitude whereas the apposite happens when the membrane is strain-hardening (SK). These are quite measurable variations that, for an isotropic load such as is the case for spherosymmetric pulsations, are determined by the area dilatation modulus. In addition, as the amplitude of the acoustic disturbance increases the total scattering cross section of a microbubble with an SK membrane tends to decrease whereas, that of a KV or an MR membrane tends to increase. The importance of this effect in the interpretation of certain features of experimental observations [1,2] of oscillating micro-bubbles subject to large peak negative pressures is discussed [3].

Controlling the cohesion of contrast agents is important in optimizing perfusion imaging but also drug delivery techniques. In order to gain understanding regarding its cohesion range, the large-amplitude axisymmetric oscillations and collapse of an encapsulated mibrobubble is examined theoretically and numerically. Thus, the stability of spherosymmetric pulsations to infinitesimal axisymmetric shape deformations is examined, in a manner similar to that previously employed for free bubbles [4]. The elastic stresses that develop on the membrane due to the bending moments are accounted for, based on the shell stability theory [5], and are determined by the scalar bending modulus, $k_B'$. This is a measure of the shell resistance to bending and is introduced as an additional parameter, due to the anisotropy of the membrane elasticity along the interface and perpendicular to it [6]. Once this parameter is known the resonance frequencies for shape oscillations of the microbubble are predicted as well as conditions for break-up. The two constitutive laws that were employed in the spherosymmetric model are implemented here also.

Conditions for buckling are recovered using static considerations and are seen to be relevant only for slow compression studies or when the forcing frequency is much smaller than the eigenfrequency for volume pulsations of the micro-bubble. Dynamic considerations reveal two major instabilities in a manner analogous to the case with free bubbles. For given equilibrium radius the parametric instability is first obtained as the amplitude of acoustic disturbance crosses a certain threshold. It corresponds to subharmonic resonance between the forcing frequency and the resonance frequencies of shape harmonics. As the amplitude of sound is further increased dynamic buckling occurs, evolving in a much shorter time scale. It can be viewed as the equivalent of Rayleigh-Taylor instability for the case of encapsulated microbubbles. In this fashion it is possible to construct phase diagrams for an encapsulated microbubble, figure 1 shows preliminary results in this direction, that define the regions marking the onset of instability.

A numerical model was also developed, implementing a hybrid boundary-finite element method, in order to solve for the velocity potential and shape deformation of an axisymmetric encapsulated microbubble. Thus, the above instability modes were verified and interesting dynamic phenomena such as jet formation and break-up were captured.

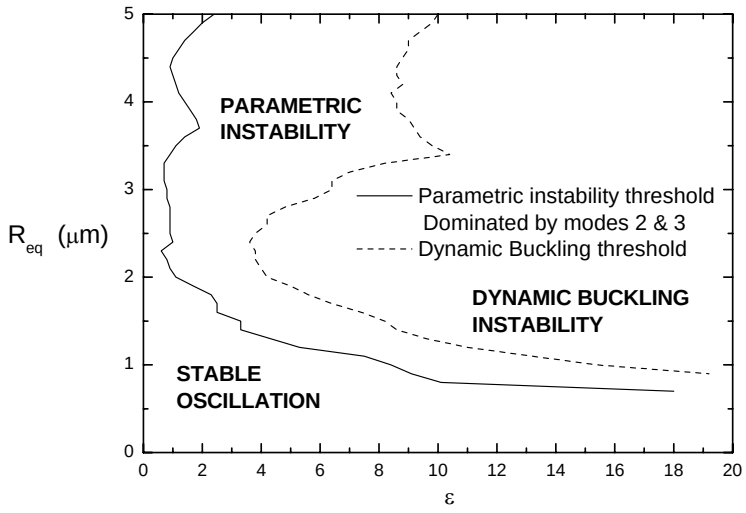


**Figure 1**: Phase diagram for an encapsulated microbubble (contrast agent MP1950). The surface and bending elasticity $G_s = 165\ MPa$ and $k_B' = 5.0 \cdot 10^{-14}\ Nm$, have been fitted to the experimental results provided in [7]; the forcing frequency is set to $v_f = 2.4\ MHz$ and the far field pressure disturbance to $P_\infty' = P_{st}' \left[ 1 + \varepsilon \cos\left( 2\pi v_f \right) \right]$

**References**


1. Sarkar, K. Shi, W.T. Chatterjee, D. & Forsberg, F. “Characterization of ultrasound contrast microbubbles using in vitro experiments and viscous and viscoelastic interface models for encapsulation.” J. Acoust. Soc. Am. **118**(1), 539-550, 2005.
2. Sboros, V., MacDonald, C. A., Pye, S. D., Moran, C. M., Gomatam, J., McDicken, W. N. “The dependence of ultrasound contrast agents backscatter on acoustic pressure: theory versus experiment”. *Ultrasonics,* 40: 579 – 583, 2002.
3. Tsiglifis K. & Pelekasis N. ‘Radial oscillations of insonated contrast agents – Effect of the membrane constitutive law’, submitted to the JFM.
4. Hilgenfeldt, S. Lohse, D. & Brenner M. P. “Phase diagrams for sonoluminescing bubbles”, Phys. Fluids, Vol. **8,** No. **11**, 1996.
5. Timoshenko, S. and Woinowsky-Krieger, S. Theory of Plates and Shells. *McGraw-Hill* Companies,1964
6. Zarda, P. R., Chien, S. & Skalak, R. 1997 “Elastic deformations of red blood cells.” J. Biomechanics **10**, 211-221.
7. Chomas J. E., Dayton P. A., May D. & Allen J. “Optical observation of contrast agent destruction.” Appl. Phys. Lett., Vol. **77**, No. **7**, 14 August 2000.



**Acknowledgement**

Mr. Kostas Tsiglifis wishes to acknowledge scholarship “HRAKLEITOS” from the Greek Ministry of education, for financial support.

# A NEW METHOD FOR ENHANCING DYNAMIC VASCULAR PATTERNS OF FOCAL LIVER LESIONS IN CONTRAST ULTRASOUND

***Nicolas Rognin[1], Peter Frinking[1], Tristan Messager[1], Marcel Arditi[1]***
***Geneviève Perrenoud[2], Jean-Yves Meuwly[2]***

[1] Bracco Research S.A. – Geneva / Switzerland
[2] University Hospital, Lausanne, Switzerland

***Introduction:*** Dynamic Vascular Patterns (DVP) of Focal Liver Lesions (FLL), obtained during a contrast ultrasound examination after a bolus injection, allow clinicians to accurately characterize suspicious lesions, and to better differentiate among benign and malignant lesion types. Typically, a FLL is characterized by examining its DVP and comparing it with the perfusion kinetics of normal liver parenchyma. The purpose of this work was to develop a software package called SonoLiver™, which can be used as a tool for enhancing the differences in perfusion kinetics between FLL and normal liver parenchyma. Such a tool could help the physician to orient or confirm his/her diagnosis.

***Method:*** The SonoLiver software generates a processed sequence by subtracting the mean pixel-value obtained in a reference region from the original pixel values, an operation called DVP processing. All values considered are derived from curve-fitting of echo-power functions with a parametric model function for bolus kinetics. The echo-power values are estimated from a linearization of the (log-compressed) video images. The result is represented as a composite image sequence comprising an overlay of the processed sequence on the original sequence. Figure 1(a) shows a simulation of the kinetics of normal liver parenchyma (blue solid line), of a hypervascular metastasis (red dash-dot line) and of a hemangioma (green dashed line). Figure 1(b) shows the result after DVP processing, with the normal liver parenchyma taken as reference. Figure 1(c) depicts a bipolar colormap, coding in warm and cold colors the positive and negative amplitudes resulting from subtraction, respectively. Warm colors indicate hyper-echoic and cold colors indicate hypo-echoic areas with respect to the reference region. In this particular case, normal parenchyma appears as black, representing perfect cancellation.

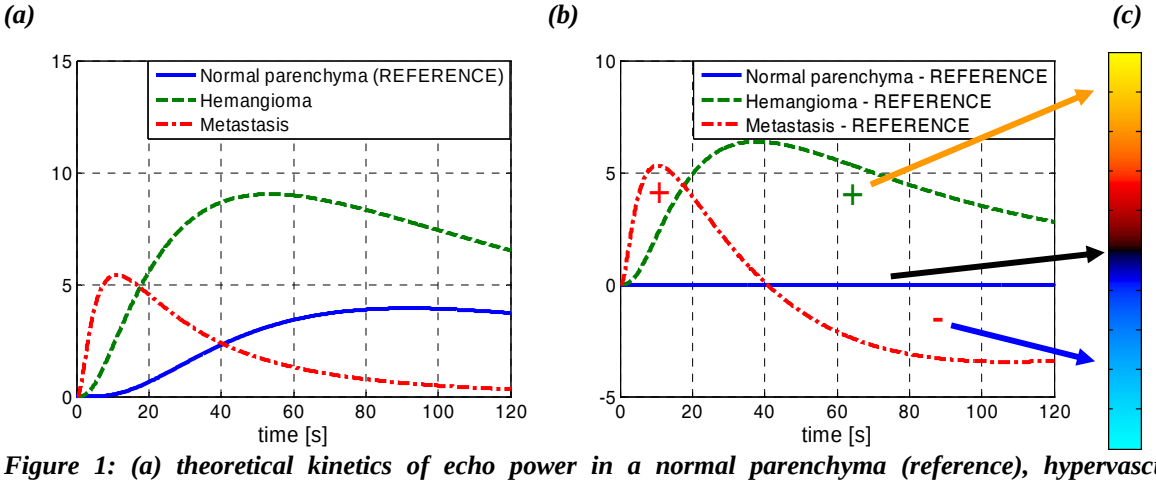


***Figure 1: (a) theoretical kinetics of echo power in a normal parenchyma (reference), hypervascular metastasis and hemangioma, (b) relative kinetics with respect to the reference, (c) bipolar colormap.***

Figure 2 shows a screen copy of the graphical user interface of SonoLiver. It comprises four panels (a-d). Panel (a) shows the original sequence of contrast images and panel (b) the processed sequence. Three regions of interest (ROI) were drawn in panel (a): a delimitation ROI (blue), a reference ROI (yellow), and an analysis ROI (green). The delimitation ROI delimits the global area to be analysed; the reference ROI delimits the reference (normal liver parenchyma in this case) and the analysis ROI delimits the region where DVP processing is to be applied. The analysis ROI typically includes the suspected lesion. Panels (c) and (d) display two output time-intensity curves. Panel (c) shows the reference signal (as a best-fit model-function representing the normal liver kinetics in yellow); panel (d) shows two curves: the best-fit model-function (in red) representing the contrast agent dynamics in the lesion (red ROI in panel (b) ), and the DVP signal (orange) at the same location.

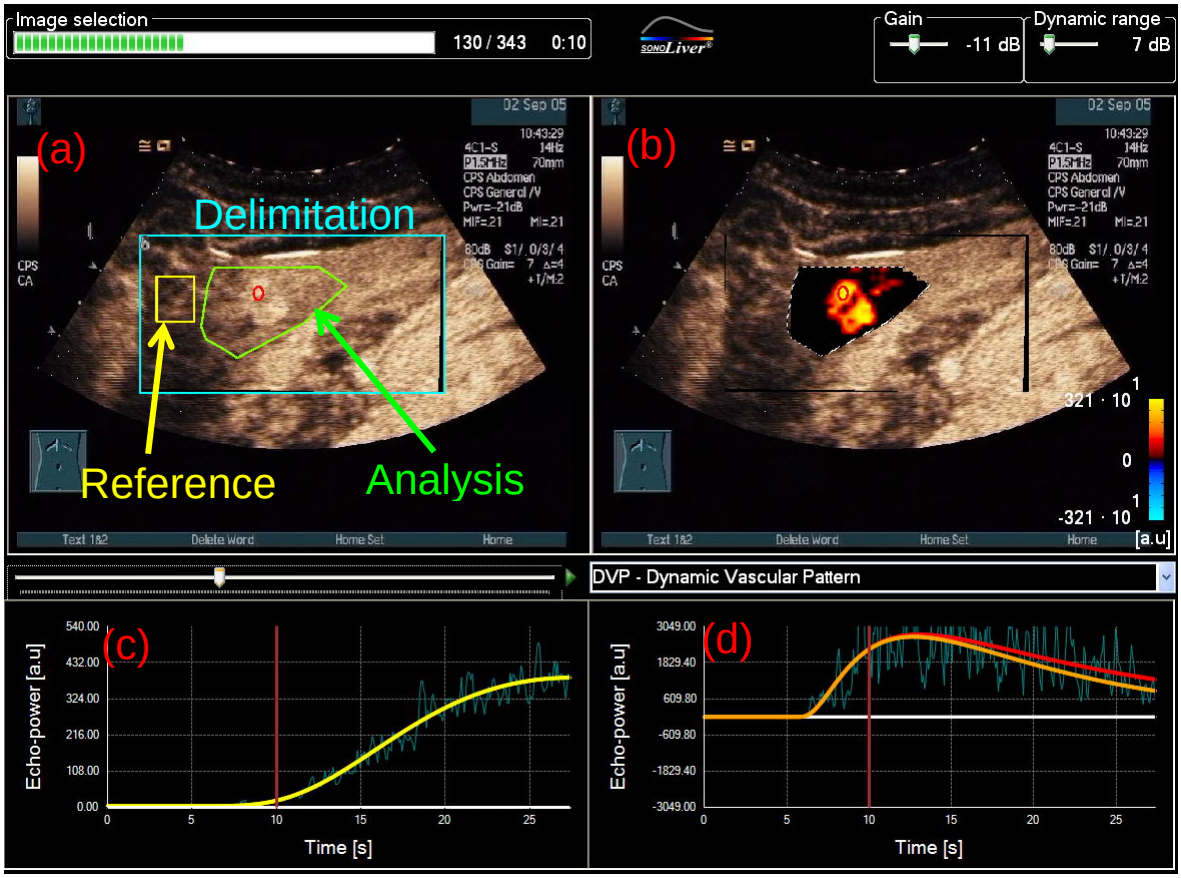


***Figure 2: Screenshot of the SonoLiver software. (a) Native sequence of contrast images. (b) Processed sequence. (c) Reference signal. (d) Best-fit model function (red) and DVP signal (orange) in the lesion (Hemangioma).***

***Results:*** SonoLiver DVP processing was applied on two clinical cases, representative of a benign lesion and a malignant lesion. Each sequence of contrast images were first compensated for the possible presence of motion with the image registration tool. Figure 2 shows a hemangioma (benign lesion) where the DVP signal remains positive over time and the lesion appears in warm color. Figure 3 shows a hypervascular metastasis (malignant) lesion where the DVP signal is positive in the arterial phase and becomes negative in the portal phase (lesion colorized in cold color).


***Figure 3: Hypervascular metastasis.***

***Conclusions:*** SonoLiver implements DVP processing for enhancing differences in contrast kinetics of various FLL. In its present state of development, SonoLiver already offers an easy-to-use interface, yet implements sophisticated signal linearization, processing and display. One objective of SonoLiver is to help observers without extensive experience in contrast ultrasound achieve correct characterization of FLL. It is presently the object of a test of interest among selected clinicians, to assess its value as an aid for the characterization of FLL. Further clinical evaluation will be needed to quantify the possible improvements in terms of sensitivity and specificity.

**Acoustic characterization of Definity disruption**

Peter D. Bevan, Raffi Karshafian, and Peter N. Burns

Department of Medical Biophysics, University of Toronto, Toronto, Ontario, Canada
Sunnybrook Health Sciences Centre, Toronto, Ontario, Canada

Bubble disruption is an important phenomenon associated with the response of ultrasound contrast agents (UCAs) exposed to high acoustic pressures. At a high enough pressure, the same sound that is used diagnostically to image these microbubbles can be used break their shell, releasing the gas inside. This behaviour is important for bubble detection and imaging techniques as well as possible therapeutic applications and drug delivery schemes.

Previous work in our lab has measured, acoustically, the disruption threshold and post-disruption echo from populations of microbubbles where, after shell disruption, free gas bubbles slowly disappear into the surrounding liquid (Bevan, et al., 2004). Diffusion of gas causes the bubbles to shrink and, consequently, reduces the measured backscattered echo over time. Parts of this physical picture were verified through correlation with optical measurements (Bouakaz, et al., 2005). Simulations of populations of shrinking bubbles have also been developed to help further our understanding of the post-disruption echo (Bevan, et al., 2006). These studies used experimental contrast agents, not yet clinically approved. The work presented here investigates and characterizes the disruption and subsequent echo from a contrast agent (Definity, Bristol-Meyer Squibb) approved for clinical use in North America.

The time-course of the bubble response was assessed in a benchtop pulse-echo ultrasound system. A series of pulses was applied to a diluted suspension of contrast agent. The series consisted of: low amplitude pre-disruption pulses, a high amplitude disruption pulse, and a long sequence of post-disruption detection pulses. Five detection pulses, separated by 5 ms, were transmitted up to 0.5 ms before the disruption pulse, and 41 detection pulses, also separated by 5 ms, were transmitted starting 1 ms after. A single-element, spherically focussed transducer (2.25 MHz, Matec, Northborough, MA, USA) was used to transmit these pulses. The detection pulse used in these experiments was a broadband 2 MHz pulse with a peak negative pressure ($P_{neg}$) of 35 kPa.

One of three transducers (Valpey-Fisher, Hopkinton, MA, USA) was placed confocally and orthogonally to the detection pulse transducer and used to transmit the disruption pulses. The disruption pulse was a narrow-band tone burst at 500 kHz, 1 MHz, or 2 MHz. The temporal length of the disruption pulses was kept constant, so 500 kHz was 4 periods long, 1 MHz was 8 periods long, and 2 MHz was 16 periods long. Four $P_{neg}$, over a broad range, were investigated for each disruption frequency. Measurements were made on Definity drawn directly from the vial, diluted to 50 µl/l in deionised water. Some of the measurements were repeated for Definity filtered through 5 µm and 3 µm filters.

At all disruption frequencies, a significant drop in echo was observed between 1 and 200 ms after disruption. The disruption $P_{neg}$ required for a given drop in echo, however, was much lower

for lower frequency insonation; furthermore, the MI associated with this $P_{neg}$ was also lower for lower frequencies. In experiments on unfiltered bubbles the echo reached a baseline level, significantly above zero, approximately 100 ms after disruption. For bubbles filtered at 3 μm, however, the echo dropped below 25% of the original level after approximately 50 ms and disappeared completely by 200 ms after disruption. This suggests preferential disruption of smaller bubbles in the population. Also, the residual baseline echo measured for unfiltered bubbles is likely due to the largest bubbles in the population.

Our lab has also been investigating ultrasound and microbubble potentiated uptake of drugs into cells (Karshafian, et al., 2005). The mechanism for increased uptake is not completely understood; however, bubble disruption and/or oscillation are important for this therapeutic effect. A two-part sequence was used to investigate this. First, a short high-amplitude pulse sequence disrupted the bubbles and, second, a longer low-amplitude pulse sequence oscillated the resulting free gas bubbles. Based on the measurements of Definity disruption, a high-amplitude pulse was chosen that should disrupt the majority of the bubbles, releasing free gas. The measured time-course of the post-disruption echo suggested that a 50 ms sequence of low-amplitude pulses would be sufficient to interact with the free bubbles, most of which would have disappeared by the end of the sequence. The uptake during this two-part sequence was then compared to the effectiveness of high-amplitude (disruptive) pulses alone. Preliminary results suggest that the low-amplitude oscillation of free gas bubbles is important and can be used to enhance uptake.

Two areas of investigation present themselves for further work. First, simulations of the response from shrinking bubbles can be used to explore differences between unfiltered and filtered bubble populations. Second, we aim to optimize therapeutic pulse sequences that enhance uptake through low-amplitude excitation of released free gas bubbles.

**References**

Bevan PD, Karshafian R, Matsumura M, Tickner G, and Burns PN. An acoustic study of disruption of polymer shelled bubbles. IEEE International Ultrasonics Symposium. Montreal, Quebec, Canada, 2004.

Bevan PD, Karshafian R, and Burns PN. Acoustic response of shrinking bubbles.

Bouakaz A, Versluis M, and de Jong N. High-speed optical observations of contrast agent destruction. Ultrasound in Med. Biol., 31(3)391-399, 2005.

Karshafian R, Bevan PD, Burns PN, Samac S and Banerjee M. Ultrasound-induced uptake of different size markers in mammalian cells. IEEE Ultrasonics Symposium, 2005; 1:13-16.

**Acknowledgement**

This work was supported by the Terry Fox Programme of the National Cancer Institute of Canada and the Canadian Institutes of Health Research.

# A Systematic Study of the Mechanical Behaviour of Microbubbles by Using Atomic Force Microscopy Force-Distance Curves.

E. Glynos[1], V. Koutsos[1], C.M. Moran[2], S. D. Pye[3], M. Butler[2], J. Ross[4], W.N. McDicken[2], V. Sboros[2]

*[1]Institute for Materials and Processes, School of Engineering and Electronics, Centre for Materials Science and Engineering, University of Edinburgh, Edinburgh, UK. [2]Medical Physics, School of Clinical Sciences and Community Health, University of Edinburgh, Edinburgh, UK. [3] Medical Physics, Royal Infirmary of Edinburgh, Edinburgh, UK. [4] Clinical and Surgical Sciences, University of Edinburgh, Edinburgh, UK.*

Measurements on individual microbubble properties are essential for the advancement of microbubble science and have the potential of guiding/aiding both modelling and applications. The measurement of the mechanical properties of microbubbles in particular, provides insight on the shell structure and behaviour. Quantitative knowledge of these parameters remains a significant hurdle in microbubble modelling and experimentally is beyond the resolution of optical microscopy. We have already shown that the atomic force microscope (AFM) is capable of probing structural and mechanical properties of microbubbles at the nanometre and nanonewton scale[1]. We now report on a systematic study of the mechanical properties of the microbubbles using AFM force-distance curves.

We used biSphere® (Point Biomedical Corp, San Carlos, CA, USA) microbubbles attached on poly-L-lysine coated Petri dishes. The mechanical properties of the microbubbles were investigated using the MFP-1D (Asylum Research, Santa Barbara, CA, USA) mounted to a Nikon TE2000U (Nikon UK Limited, Surrey, UK) inverted optical microscope. Our micromechanical test involves an AFM tipless cantilever moved towards an individual microbubble in normal direction while its vertical position and deflection are monitored (force-distance curve or fd curve). After the initial contact between the cantilever and the microbubble, the continuation of the cantilever movement towards the bound microbubble results in a micro-compression test which is recorded and subsequently analysed. We performed a systematic study using several cantilevers with spring constants varying from 0.07 to 2.72 N/m and acquired more than two thousand force-distance curves on more than 200 microbubbles with sizes from 2 to 6 micrometers.

Using *low spring constant cantilevers* (less than 1 $N.m^{-1}$) we found that in most cases at small deformations the compression curve has a non-linear shape which quickly becomes linear. In any case, the behaviour seems to be elastic (i.e. fully reversible and subsequently reproducible). The standard deviation of stiffness of the microbubbles in 6 measurements did not exceed 5%. The effective bubble stiffness associated with the linear part of the compression curve depends on the microbubble size in a non-trivial manner, indicating that very low spring constant cantilevers probe the local mechanical properties of the shell while stiffer cantilevers probe the mechanical response of the whole microbubble. The results display a significant dispersion in the mechanical properties of the microbubbles of the same size, indicating an inherent variation of the microbubbles structure/properties (e.g. shell thickness) within the microbubble population. We found that *cantilevers with high spring constants* (more than about 1 $N.m^{-1}$) induce irreversible behaviour at high deformation which in some cases takes the form of a buckling event in the compression curve. This observed buckling appears systematically but in some cases the necessary applied force threshold for this event changes indicating microbubble damage.

Although, the above measurements are performed in the static regime (i.e. ~1 Hz), their relevance to microbubble science remains high. It is known that biSphere® scattered ultrasound is maximised in what previously has been termed as 'sonic cracking'[2]. The disperse nature of the biSphere shell may therefore affect the probability of the above

phenomenon, which is a significant departure from the current theoretical formalism on microbubble behaviour. The study of buckling and permanent deformation in the static regime also provides significant information on the tolerances of microbubble shells in ultrasonic pressure fields.

Acknowledgement: The work was funded by the EPSRC (UK).

## References

1. Sboros, V.; Glynos, E.; Pye, S. D.; Moran, C. M.; Butler, M.; Ross, J.; Short, R.; McDicken, W. N.; Koutsos, V. *Ultrasound In Medicine And Biology* **2006,** 32, (4), 579-585.
2. Postema, M.; Bouakaz, A.; de Jong, N. *IEEE trans Ultrasonics Ferr Freq Cont* **2005,** 52, 1035-1041.

# High Speed Optical Observations and Simulation Results of SonoVue™ Microbubbles at Low Insonation Pressures

**K. Chetty[1], E.Stride[2], C.A. Sennoga[1], J.V. Hajnal[1] and R.J. Eckersley[1].**

[1] Imaging Sciences Department, Imperial College, London. UK.
[2] Department of Mechanical Engineering, University College London. UK.

**Introduction:** Modified Rayleigh-Plesset models are commonly used to characterise the acoustic response of microbubbles to ultrasound exposure. In most instances these models have been validated and parameterised through experimental acoustic measurements taken from bulk suspensions of microbubbles. These acoustic methods require that the number and size distribution of bubbles are accurately known, ignore multiple scattering effects and assume microbubble attenuation is linear. Existing models also generally assume that the visco-elastic shell parameters are a constant bulk property of the microbubble shell material.

**Objectives:** The aim of this study was to parameterise the Hoff model for SonoVue™ using directly observed optical data from individual microbubble oscillations.

**Method:** Individual SonoVue™ microbubbles were exposed to a 4 cycle pulse with 0.5 MHz centre frequency at peak negative pressures between 30-120 kPa. The resulting radial oscillations were recorded using a high speed camera operating between 2-3 million frames per second. Simulated data was then fitted to the experimental measurements. Based on an initial sensitivity analysis the shell elasticity term was selected as the optimisation variable while the shell viscosity and the shell thickness terms were held constant. Preliminary results suggested a limited ability of the model to predict the microbubble behaviour. In subsequent analysis the recorded responses was probed using a sliding window optimisation to examine how the shell elasticity varies during the insonation.

**Results and Conclusions:** Parameterisation of the Hoff model showed that the shell elasticity model term varies proportionally with the initial microbubble radius. This result implies the shell elasticity term is not a constant property.
In most cases bubbles oscillating near their resonant frequency were more successfully modelled by incorporating an elasticity term that decayed over the course of the insonation, indicating some physical change. For non-resonant bubbles the elasticity term was found to remain constant.

# MICROBUBBLE DETERIORATION MECHANISMS OF A PHOSPHOLIPIDIC CONTRAST AGENT

***Sergio Casciaro[1,2], Francesco Conversano[2], Rosa Palmizio Errico[2], Alessandro Distante[1,2,3]***

***(1)*** *Institute of Clinical Physiology, National Council of Research, Lecce, Italy*
***(2)*** *ISBEM (Euro Mediterranean Scientific Biomedical Institute), Brindisi, Italy*
***(3)*** *Cardio Thoracic Department, Pisa University Medical School, Pisa, Italy*

New advanced applications of contrast microbubbles are currently emerging, such as targeting, drug and gene delivery, opening attracting perspectives for innovative imaging modalities, ranging from diagnosis on tissue function, perfusion and morphology to therapy.

For the development of these applications, a better understanding of the influence of ultrasound parameters on contrast agent behaviour, and in particular on microbubble destruction mechanisms, is required.

Previous studies[1-7] have demonstrated that microbubble destruction mechanisms depend on many factors: exciting pulses, chemical-physical properties of the surrounding medium, microbubble shell and gas content. In this paper, we employed an *in vitro* setup to investigate destruction mechanisms of an experimental phospholipid-based ultrasound contrast agent (BR14, supplied by Bracco Research SA, Geneva, Switzerland) by measuring the attenuation of broadband ultrasound signals at various acoustic pressures (range 50-190 kPa). We used also a Multisizer™ III Coulter Counter® (Beckman Coulter, Inc., Fullerton, CA, USA) to perform granulometric analyses on contrast agent solutions before and after each insonification, in order to measure microbubble size distributions and to properly evaluate insonification effects. The latter measurements were also correlated with acoustic attenuation measured as a function of time.

In each measurement, a custom-designed cylinder was filled with the BR14 solution that had been just analyzed by Multisizer™ III Coulter Counter®. The cylinder was designed considering that it had to be closed at the extremities by the insertion of two 3.5-MHz single-element unfocused transducers (V-382-SU, Panametrics, Waltham, MA, USA) and it had to contain a volume sufficient for granulometric analysis. We performed the experiments preparing all the sample solutions at constant microbubble number per millilitre ($1.5\pm0.3 \times 10^4$ microbubbles/ml, background subtracted).

In a typical experiment, the signal that reached the receiving transducer was recorded before contrast agent was introduced into the diluent (Isoton III, Beckman Coulter, Inc., Fullerton, CA, USA) to obtain a reference signal $V_{ref}$. Then, the measurement was repeated immediately after the injection of microbubbles to find the signal attenuated by the contrast agent $V_{CA}$. For each measurement, a sequence of 60 signals was acquired at a PRF of 1 Hz and transferred to a PC.

In order to assess bubble destruction mechanisms and to take into account possible nonlinear energy redistribution from one frequency to another, we computed normalized attenuation (NA) as a function of time. This was obtained by calculating attenuation $A(t)$ at any time instant and dividing it by its initial value $A(0)$, according to the following formulas[7]:

$$A(t) = \frac{10\log_{10}\left(\dfrac{\sum_{\omega} V_{ref}^2(\omega)}{\sum_{\omega} V_{CA}^2(\omega)}\right)}{d} \qquad (1)$$

$$NA(t) = \frac{A(t)}{A(0)} \qquad (2)$$

where $d$ is the distance between the transmitter and the receiver, $V_{ref}(\omega)$ is the spectrum of the $V_{ref}$ signal at a given acoustic pressure, and $V_{CA}(\omega)$ is the spectrum of the $V_{CA}$ signal received at time $t$ insonifying at the same acoustic pressure; summations in eq. (1) were extended to all the spectrum frequencies, in order to consider the total energy of the spectrum.

Figure 1 shows the obtained normalized attenuation curves over time of BR14 microbubbles under different pressure amplitudes. At the lowest excitation amplitude, attenuation increased during insonification, while, at higher excitation levels, the attenuation decreased over time, indicating microbubble destruction.

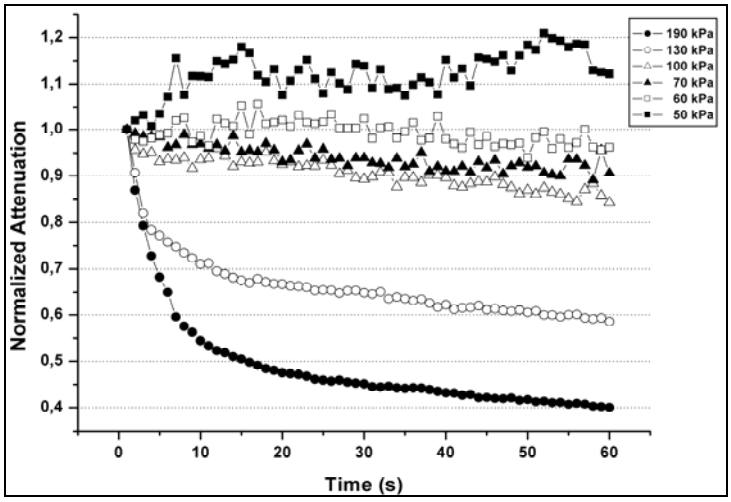


**Fig. 1:** Time variation of normalized attenuation under different acoustic pressure amplitudes.

The observed destruction rate changed with pressure amplitude suggesting different destruction mechanisms, as it was confirmed by granulometric analysis. We in fact analysed the solutions through Multisizer™ III Coulter Counter® before and after insonification in order to check the destruction phenomena and determine, as much as possible, the underlying destruction mechanisms.

Referring to fig. 1, the attenuation decreases slowly with time in the range 60-100 kPa, indicating that there is a moderate microbubble destruction, probably due to a structural deterioration of the shell facilitating gas diffusion. This destruction mechanism is confirmed by size distribution obtained by Multisizer™ III Coulter Counter®. In fact, as one can observe in fig. 2 (corresponding to the 70-kPa insonification), we found a microbubble number reduction distributed all along a wide diameter range (1.5-6 μm).

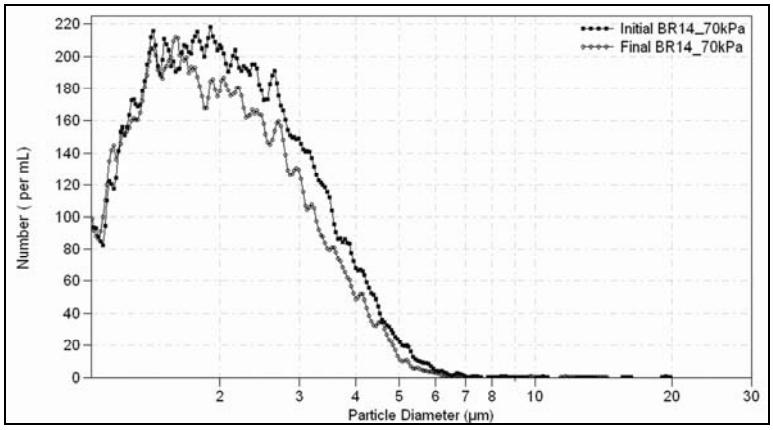


**Fig. 2:** Number size distribution of a BR14 solution before and after insonification at 70 kPa. (The diameter analysis range was from 1.0 to 30 μm, divided into 300 logarithmically spaced channels).

For the highest acoustic pressures the decrease rate of attenuation with time is much higher (fig. 1), as presumably happens for the destruction rate of microbubbles. This suggests that the destruction mechanism is changed compared to the gas diffusion one. In fact, the comparison between initial and final size distributions show that there is fragmentation of bubbles belonging to the diameter range 2-5 μm and generation of bubbles having a smaller diameter. This phenomenon is particularly noticeable for the 190-kPa insonification (fig. 3).

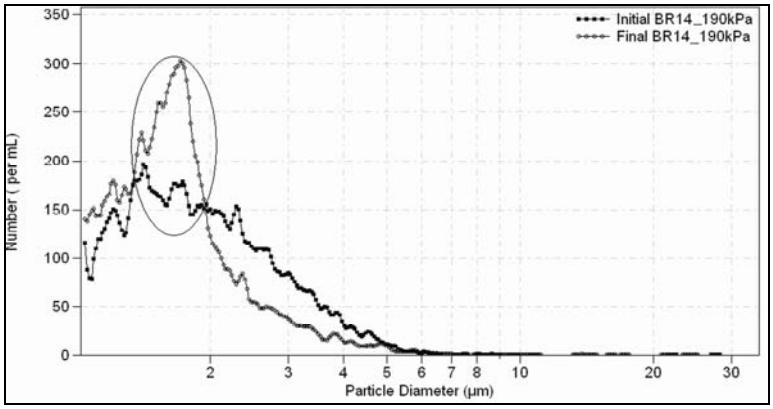


**Fig. 3:** Number size distribution of a BR14 solution before and after insonification at 190 kPa. Circled area emphasizes the fragmentation mechanism: smaller bubbles are originated by the decrease of bubbles of bigger diameters. (The diameter analysis range was from 1.0 to 30 μm, divided into 300 logarithmically spaced channels).

In conclusion, our investigation showed that BR14 microbubbles present two distinct mechanisms of destruction, that sets in for acoustic amplitudes of at least 60 kPa. In fact, in the range 60-100 kPa attenuation decreased with time and a corresponding small bubble number reduction was observed, indicating the gas diffusion mechanism induced by shell deterioration as the main destruction phenomenon. For higher acoustic pressures we observed a faster decrease of attenuation with time, that can be explained with a bubble fragmentation mechanism, evident from the granulometric comparative analysis.

**This work is based on the following paper whose partial reproduction has been kindly authorized by Lippincott Williams & Wilkins:**
S. Casciaro, R. Palmizio Errico, F. Conversano, C. Demitri, A. Distante.
*Experimental Investigations of Nonlinearities and Destruction Mechanisms of an Experimental Phospholipid-Based Ultrasound Contrast Agent*
Investigative Radiology • Volume 42, Number 2, February 2007

## ACKNOWLEDGMENTS

This work was partially funded by the FIRB-US RBNE01E9ZR and CERSUM Laboratory Rif. Min. Decreto Direttoriale 1105/2002 No. 243 granted by the Italian Ministry of Research.
The authors thank Bracco Research SA, Geneva, Switzerland for providing the contrast agent vials.

## REFERENCES

1. Klibanov AL, Hughes MS, Wojdyla JK, et al. Destruction of contrast agent microbubbles in the ultrasound field: the fate of the microbubble shell and the importance of the bubble gas content. Acad Radiol 2002;9:S41-S45.
2. Chomas JE, Dayton P, Allen J, et al. Mechanisms of contrast agent destruction. IEEE Trans Ultrason Ferroelectr Freq Control 2001;48:232-248.

3. Moran CM, Anderson T, Pye D, et al. Quantification of microbubble destruction of three fluorocarbon-filled ultrasonic contrast agents. Ultrasound Med Biol 2000;26:629-639.
4. Kabalnov A, Klein D, Pelura T, et al. Dissolution of multicomponent microbubble in the bloodstream: 1. theory. Ultrasound Med Biol 1998;24(5):739-749.
5. Kabalnov A, Bradley J, Flaim S, et al. Dissolution of Multicomponent microbubbles in the bloodstream: 2.experiment. Ultrasound Med Biol 1998;24(5):751-760.
6. Chen WS, Matula TJ, Brayman A, et al. A comparison of the fragmentation thresholds and inertial cavitation doses of different ultrasound contrast agents. J Acoustic Soc Am 2003;113(1):643-651
7. Chatterjee D, Jain P, Sarkar K. Ultrasound-mediated destruction of contrast microbubbles used for medical imaging and drug delivery. Phys Fluids 2005;17:100603.

Title: High-contrast high-speed imaging using a copper vapor laser to resolve contrast agents in tissue

Presenter: Paul A. Dayton

Co-authors: Charles F. Caskey, Susanne. M. Stieger, Katherine.W. Ferrara

High-speed imaging of microbubble oscillations plays a crucial role in exploring the use of contrast ultrasound for harmonic imaging and drug delivery. In recent years, researchers used systems capable of imaging at millions of frames per second to capture images of a single microbubble as it oscillates in a transparent tube. Although these high-speed systems help researchers optimize theoretical models describing microbubble oscillations, this *in vitro* scenario is an idealized approximation to a microbubble in the vascular system. To date, no one has produced high-speed images of microbubble oscillations within the microvasculature, presumably due to contrast limitations with available ultra-high speed cameras when imaging through thick tissue. We demonstrate that a pulsed copper vapor laser can be used to capture images of microbubble oscillations with excellent dynamic range for use in these low contrast situations. Here, a copper vapor laser is used in conjunction with a digital high-speed camera, where both are adapted to a microscope whose objective is aligned with a 1 MHz, cylindrically focused ultrasound transducer. The ultrasonic pulse is triggered upon opening of the camera‘s shutter, and the laser is triggered after a time delay, T, relative to the propagation time of the ultrasonic pulse from the transducer to the visible area, producing an effective exposure time of 50 nsec. Although the kiloHertz frame rate is too slow to continuously image microbubble oscillations, the system can produce a single 2D image of a microbubble during a specific time point during its oscillatory cycle. Repeated ultrasonic pulses and increasing values of T can produce a series of images for video viewing of microbubble oscillation, from which microbubble symmetry and expansion are measured. Results are demonstrated for contrast agents oscillating within the microvasculature, where the dynamic range of the laser-based system allows fine detail, such as microvessel walls, to be resolved. The relative expansion of a microbubble, as well as the asymmetries resulting from constrained oscillation will be summarized as a function of the vessel diameter.

# 3D Optical Micromanipulation of Ultrasound Contrast Agents: bubble-bubble and bubble-wall interactions

**Marlies Overvelde[1*], Valeria Garbin[2], Benjamin Dollet[1], Dan Cojoc[2], Enrico Ferrari[2], Nico de Jong[1,3], Enzo Di Fabrizio[4], Detlef Lohse[1], and Michel Versluis[1]**

[1]Physics of Fluids, University of Twente, P.O. Box 217, 7500 AE Enschede, The Netherlands
[2]CNR – INFM, TASC National Laboratory, S.S. 14 km 163.5, 34012 Basovizza (TS), Italy
[3]Experimental Echocardiography, Thoraxcentre, Erasmus MC, Rotterdam, The Netherlands
[4]Università 'Magna Græcia', Dipartimento di Medicina Sperimentale e Clinica, Germaneto (CZ), Italy
[*]e-mail: m.l.j.overvelde@utwente.nl

## ABSTRACT

Studies on the dynamics of ultrasound contrast agents are hampered by the presence of neighboring walls, while the influence of the wall on the bubble dynamics is not known. In addition, for molecular imaging applications wall effects may prove to be important in distinguishing targeted bubbles from freely flowing ones. Here we present optical tweezers as a micromanipulation tool for contrast microbubbles. In addition we present how the dynamics of freely oscillating bubbles is changed by bubble-wall and bubble-bubble interactions.

Optical tweezers are generally obtained by focusing a laser beam through a microscope objective, as the high intensity gradient in the focal region causes dielectric microparticles to be attracted in the focus. Microbubbles, however, with a lower refractive index, are pushed away from the region of maximum intensity. Instead, bubbles can be trapped in the dark core of a donut-shaped beam [1,2]. We developed an optical setup where the laser beam shaping is performed by using diffractive optical elements, which are computer-generated through a home-developed algorithm and implemented on a spatial light modulator (SLM). The setup allows for trapping and manipulating even a multiple set of microbubbles, and to dynamically control the distance to interfaces and neighboring bubbles.

The experimental phospholipid encapsulated agent BR-14 (Bracco Research SA, Geneva, Switzerland) was used throughout the experiments. The applied ultrasound center frequency was 2.25 MHz and the pressure amplitude was 150 kPa. The Brandaris camera [3] recorded the bubble oscillations (128 frames) at a frame rate of 15 million frames per second. Single bubbles where studied as a function of the distance to the wall (from zero to 100 μm). In theory the proximity of the wall was modeled by an acoustic image bubble ("method of images"), resulting in a modified Rayleigh-Plesset equation which was numerically solved to predict the bubble dynamics. In experiments these bubble pair interactions were also measured in free space at a distance of 70 μm from the wall.

For bubbles we analysed, the presence of the wall decreased the oscillation amplitude. The bubble oscillation amplitude increases with increasing distance to the wall. We verified that the laser trap did not influence the bubble dynamics, although the microbubble was released from the lasertrap during the experiment.

The optical recordings on the insonated bubble pair show a change in the dynamics of the oscillating bubbles and in addition a secondary Bjerknes force acting on both bubbles, see figure 1. The attractive force originates from the acoustic field radiated by the one oscillating bubble in close proximity to the other.

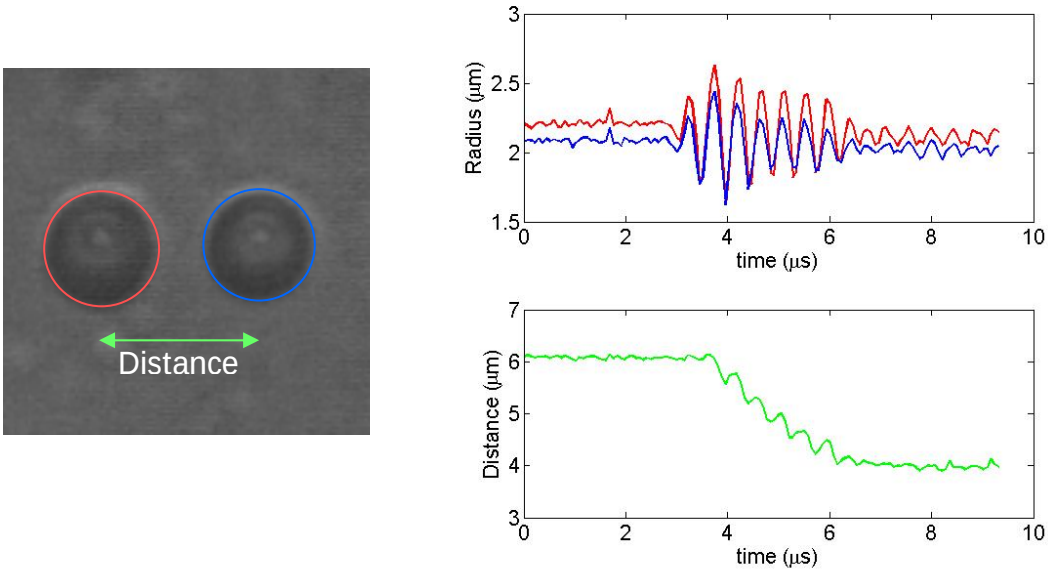


a) b)

Figure 1a shows two bubbles trapped 70 μm away from the wall, the initial distance between the bubble centers is 6.1 μm. Figure 1b shows the radius-time curves of both bubbles (upper graph) and the distance between the bubble centers as a function of the time. The bubbles are oscillating in phase and attracted due to the secondary Bjerknes force. The applied pressure has a frequency of 2.25 MHz and amplitude of 150 kPa.

## REFERENCES

[1] P. Prentice, M. MacDonald, T. Frank, A. Cuschier, G. Spalding, W. Sibbett, P. Campbell, and K. Dholakia, Manipulation and filtration of low index particles with holographic Laguerre-Gaussian optical trap arrays, Optics Express, Vol. 12, No. 4, 2004

[2] Valeria Garbin, Dan Cojoc, Enrico Ferrari, Remo Zaccaria Proietti, Stefano Cabrini and Enzo Di Fabrizio, Optical Micro-Manipulation Using Laguerre-Gaussian Beams, Japanese Journal of Applied Physics, Vol. 44, No 7B, 2005

[3] C. T. Chin, C. Lancee, J. Borsboom, F. Mastik, M. Frijlink, N. de Jong, M. Versluis, D. Lohse, Brandaris 128: A digital 25 million frames per second camera with 128 highly sensitive frames, Review of scientific instruments, Vol. 74, No. 12, 2003

[4] S.M. van der Meer, B. Dollet, M.M. Voormolen, C.T. Chin, A. Bouakez, N. de Jong, M. Versluis, D. Lohse, Journal of the Acoustical Society of America, in press

# Combined optical and acoustical characterization of individual US contrast microbubbles

Jeroen Sijl[1], Rik Vos[2], Nico de Jong[1,2], Detlef Lohse[1] and Michel Versluis[1]

[1] *Physics of Fluids, University of Twente, P.O. Box 217, 7500 AE Enschede, The Netherlands*
[2] *Experimental Echo, Erasmus MC, P.O. Box 1738 ,3000 DR Rotterdam, The Netherlands*

Optical ultra high-speed imaging of ultrasound contrast agents has revealed new detailed information on the dynamics of these microbubbles, e.g. surface modes and "compression-only" behavior[1]. How these non-spherical and non-symmetrical bubble oscillations translate into an acoustic response is unknown. Until recently, acoustic studies were hindered by the ability to isolate a single contrast microbubble and by the transducer calibration and sensitivity. A quantitative study on the acoustical backscatter of individual BR14 bubbles (Bracco Research S.A., Geneva, Switzerland) was presented here last year[2]. Depending on the initial bubble radius, driving pressure amplitude and frequency, acoustical methods can provide an even better sensitivity, while optical methods are limited by the resolving power of the optical system. A combination of the two methods will therefore provide a more complete characterization of ultrasound contrast agents.

Our setup consists of a transmit transducer transmitting a pulsed ultrasound beam, exciting a single BR14 bubble confined in a 200 μm capillary tube positioned at the focal point of the transducer. Another focussed receive transducer collects the echoes of the single bubble. Simultaneously, the time resolved radial oscillation of the very same bubble were recorded optically at a frame rate of 15 million frames per second with the Brandaris camera. The receiving transducer was accurately calibrated, therefore both the optical and acoustical recordings provide quantitative information on the microbubble response, allowing for a direct comparison between the two methods.

Individual bubbles with initial bubble radii below, around and above the resonance radius were insonified with a 2.25 MHz sinusoidal acoustic pulse with peak rarefactional amplitude of 60 kPa or 100 kPa. The acoustic responses and simultaneous optical recordings of the radial oscillations of the very same bubble confirm that the two methods are indeed complementary. Larger bubbles, oscillating off resonance, were more easily detected acoustically, whereas the dynamics of bubbles oscillating close to resonance were better detected optically. Furthermore, for larger bubbles oscillating in the linear regime, the measured acoustic bubble response was in good agreement with the response predicted from the optically recorded radial bubble dynamics.

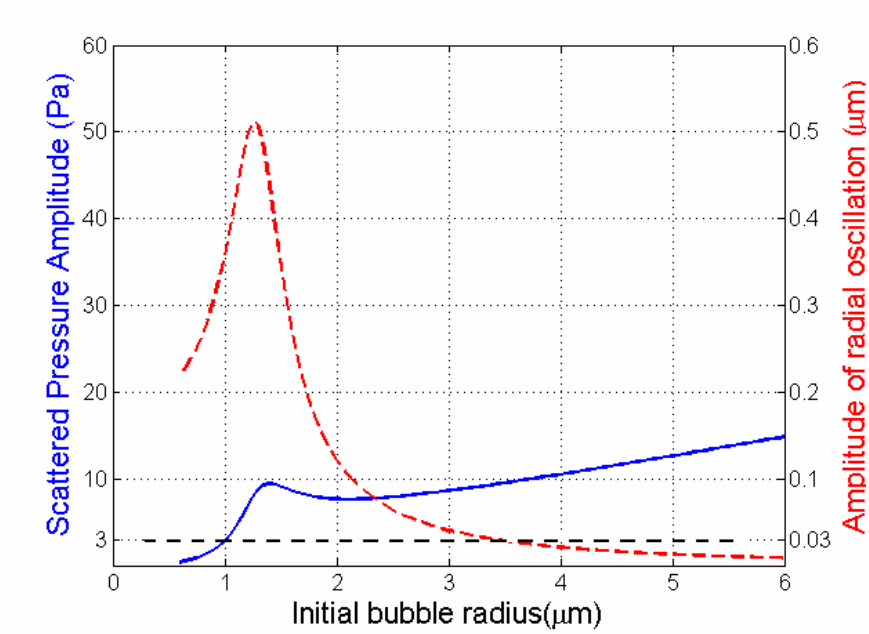


Figure: For bubbles with different initial bubble radii we plot the scattered pressure amplitude (solid line) (at a distance of 2.6 cm from the bubble) and the amplitude of the radial oscillation (dashed line) of a single free bubble (without shell) subjected to a sinusoidal driving pulse with a pressure amplitude of 60 kPa and frequency of 2.25 MHz. Optical methods are capable of detecting radial oscillations as small as 30 nm. This however is not sufficient to detect the small oscillations of the larger bubbles oscillating off resonance. Here, acoustical methods, capable of detecting 3 Pa of pressure amplitude, provide a better way to study the bubble dynamics. On the contrary, for bubbles oscillating close to resonance, optical methods are much more sensitive.

[1] S. M. van der Meer, B. Dollet, M. Voormolen, C.T. Chin, A. Bouakaz, N. de Jong, M. Versluis, and D. Lohse. Microbubble spectroscopy of ultrasound contrast agents. J. Acoust. Soc. Am., 121(1), 2007.

[2] J. Sijl, M. Arditi, P.J.A. Frinking, N. de Jong, M. Versluis and D. Lohse. Acoustical study of the properties of individual phospholipid-based ultrasound contrast agent microbubbles. The Eleventh European Symposium on Ultrasound Contrast Imaging, January 26-27 2006, Rotterdam, The Netherlands.

# Regularized Estimation of Microbubbles Attenuation and Backscatter Coefficients in Contrast-Enhanced Ultrasound Studies

***S. Mulé[1], A. De Cesare[1], O. Lucidarme[1,2], F. Frouin[1], A. Herment[1]***

*1 INSERM UMR_S678, Laboratory of Functional Imaging, Paris, France*
*2 Radiology Department, Pitié-Salpêtrière Hospital, Paris, France*

**Objective:** Accurate quantification of tissue perfusion is prevented by the shadowing effect on the native images. The aim of this study is to provide reliable parametric images of contrast agent (CA) microbubbles attenuation and backscatter, which better reflect CA concentration than native images.

**Methods:** A propagation model of the ultrasound pulse specific to CA studies was proposed [1]. This model considered that the time-intensity variation in a highly echogenic distal area without contrast uptake, thereafter referred to as $R_{dist}$, provided the cumulative attenuation from the transducer to $R_{dist}$. For each A-line (N pixels per line) of an image, the intensity of each pixel was expressed as a function of its associated backscatter coefficient $\beta(k)$ and the attenuation coefficients associated to the pixels situated above the considered pixel ($\alpha(1)$…. $\alpha(k-1)$). Propagation along each A-line is thus modeled by N equations and 2.(N-1) unknowns (i.e., $\alpha(1)$,…, $\alpha(N-1)$, $\beta(1)$,…, $\beta(N-1)$).
To estimate attenuation and backscatter coefficients, a linear relationship between local attenuation $\alpha(k)$ and backscatter $\beta(k)$ was assumed. It was first considered that for each A-line of an image, $\beta(k) = a.\alpha(k)$ with a constant parameter *a* for each A-line. Promising results were obtained. However, large variations from one column to another were observed, due to the spatial variability of the intensity in the $R_{dist}$ area and also to the constraint on parameter *a* which was A-line dependent.
This work proposed an improvement of the method. Parameter *a* was now constrained to be homogeneous in some predefined regions. For each A-line, attenuation and backscatter coefficients $\alpha(k)$ and $\beta(k)$ were obtained by minimization of an error depending on the propagation equations and the additional constraint of homogeneity on parameter *a*. Initial values of parameter *a* were provided by the initial method. The process was then iterated. For each region, the ratio $\beta/\alpha$ was calculated for each pixel and its mean value was used to initialize parameter *a* at the next iteration. The method was applied to murine renal perfusion studies. The mice were imaged after the injection of 0.1 ml of Sonovue®, using a Siemens Sequoia 512 and a linear transducer. Dual images in CPS and fundamental modes were acquired. The skin-table interface at the opposite side of the mice was chosen as $R_{dist}$.

**Results:** Visually, attenuation and backscatter parametric images showed homogeneous coefficients within each cortex. Moreover, these coefficients were similar in both cortices (Fig. 1). Compared with the initial method [1], the new constraint on parameter *a* allowed a spatial regularization of coefficients $\alpha$ and $\beta$ and thus a reduction of variations from one column to another.

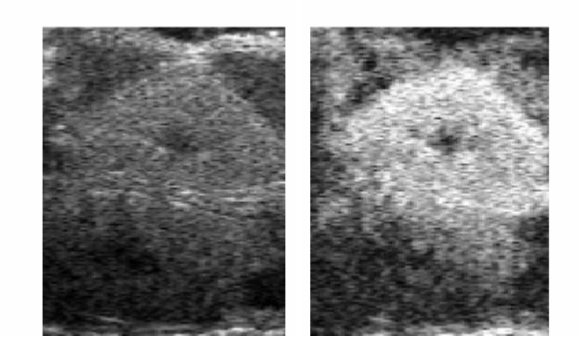

(a)

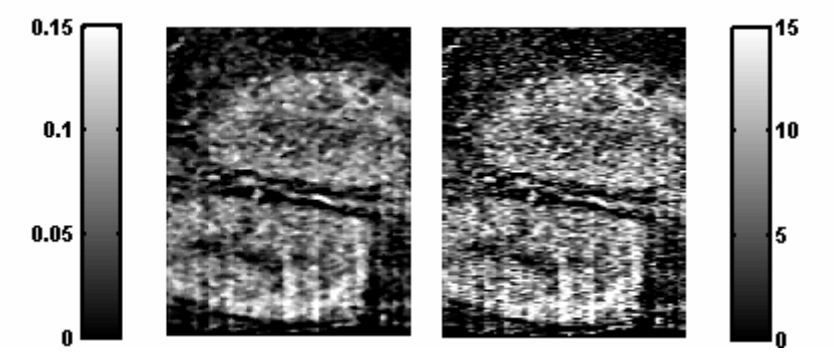


(b)

**Fig. 1**: Estimated parametric images compared with native images acquired 4 seconds after the contrast agent entered into the acquisition plane. (a) Native images acquired in fundamental mode (left) and in CPS mode (right). (b) Estimated attenuation (left) and backscatter (right) images. Coefficients are expressed in dB.

**Conclusion:** A new method for the estimation of CA attenuation and backscatter has been proposed. Parametric images of these two parameters were provided, which better reflected concentration than native images. It seemed therefore to be of potential interest in a subsequent quantification of tissue perfusion. Processing A-lines together and preprocessing the signal in the $R_{dist}$ area could further improve the estimation of these two parameters.

[1] S. Mulé, A. De Cesare, G. Renault, O. Lucidarme, F. Frouin and A. Herment, "*Compensation of Attenuation in Contrast-Enhanced Ultrasound: Application to Small Animal Studies*", Proceedings of the 2006 IEEE International Ultrasonics Symposium (2006), in press.

# Spherical, rectangular and triangular bubble vibrations

Nico de Jong[1,2], Rik Vos[1], Benjamin Dollet[2], Marlies Overvelde[2], Valeria Garbin[2], Annemieke van Wamel[1], Sander van der Meer[2], Marcia Emmer[1], Michel Versluis[2], Detlef Lohse[2], Ayache Bouakaz[3]

1. Biomedical Engineering, Thoraxcentre, Erasmus MC, Rotterdam, The Netherlands
2. Physics of Fluids, University of Twente, Enschede, The Netherlands
3. INSERM U619, and Université François Rabelais, Tours, France

Ultrasound contrast agent (UCA) bubble response to ultrasound (US) is still the subject of several studies, since it determines the power of medical diagnostic imaging modalities. Generally, bubbles are studied using optical or acoustical methods, both having their specific advantages, in an environment that mimic the clinical practice as good as possible (small-diameter capillaries, red blood cells, blood viscosity). Acoustical observations could provide a better insight in the acoustical scattering of bubbles, which determines the final efficacy of contrast-enhanced diagnostic US imaging, and are better suitable to determine the properties of populations of bubbles. Optical observations allow for easier characterization of fewer bubbles and a more detailed characterisation in case where bubbles vibrate non spherically, which is expected for bubbles nearby a wall or red blood cells. In this presentation, we show optical recordings of the various bubble responses with the ultrahigh speed Brandaris-128 camera, and discuss the clinical implications of our findings.

1. Spherical vibration of bubbles

The Rayleigh-Plesset equation predicts that bubbles can show a nonlinear relation between pressure and radial excursion. Using the Brandaris camera, we show that bubbles can indeed show mild and strong nonlinear oscillations. This effect is commonly exploited in power modulation and pulse inversion techniques.

2. Rectangular vibration of bubbles

Non-spherical bubble shapes can be categorized by decomposition of the shape into spherical harmonics. In a study on 20 -100 micron sized free gas bubbles, we observed that bubbles can obtain stable surface modes when irradiated at their resonance frequency. Thus, spherical harmonic orders up to 4 (rectangular) are obtained. The shape oscillation has a frequency of half the exciting frequency (subharmonic), which might be used in subharmonic imaging of bubbles.

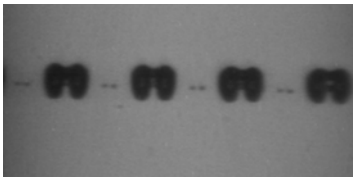

3. Triangular vibration of bubbles

Forty percent of investigated Sonovue (Bracco, Geneva) bubbles showed so-called compression-only behavior; the microbubbles compress in the high pressure phase of the ultrasound wave, yet hardly expand during rarefaction. The radius – time curve shows a triangular shape. It was observed that repetitive irradiation by a sequence of bursts

significantly increased the compression-only behavior, due to enforced dissolution of the gas core into the liquid medium. It was also observed that an increased pressure could enhance the compression-only behavior, due to rupture of the shell coating. Coated microbubbles displaying compression-only behavior can be highly beneficial in non-linear acoustic imaging and bubbles oscillating in this mode are in fact tailor-made for pulse-inversion imaging.

## 4. Onset of the bubble vibration

For individual phospholipid-coated microbubbles with a diameter smaller than 5 μm, camera recordings revealed threshold behaviour in the onset of vibration. Recent studies performed by Tang [1] showed a pressure-dependent attenuation for phospholipid-coated microbubbles, which could be explained by the presence of a threshold. An imaging technique such as power modulation imaging could profit from an acoustic pressure threshold.

## 5. Vibration of bubbles in contact with a wall

Optical studies of the vibrations of bubbles are usually performed in a 2 dimensional image plane. The observations are generally done by positioning the bubble in an acoustically and optically transparent tube, where is float up to the top side. This allows precise focusing of the ultrasound and optical imaging equipment, but the wall might change the dynamic properties of the bubble. In this study, such bubble is imaged orthogonally to obtain a quasi-instantaneous 3D image sequence of a contrast agent microbubble touching a rigid wall. It showed a tendency to vibrate axial-symmetrically around the axis normal to the wall, but asymmetrically in the direction perpendicular to the wall. In the past, the asymmetric oscillation was thought to be much smaller than the radial oscillation for coated bubbles. However, we show that the vibration is strongly asymmetrical in clinically relevant frequencies and pressures (140 kPa at 1 MHz, mechanical index of 0.14).

## 6. Bubble vibration at varying distance to the wall

It has been observed acoustically from a cloud of bubbles that the response is different if the bubbles are attached to the wall compared to freely floating bubbles. In this study we use an optical tweezer (laser trap) to measure the response of single bubbles at different distances to the wall. The optical tweezer controls the position of the single bubble, while the vibration is recorded with the Brandaris camera. We verified that the laser trap did not influence the bubble dynamics, but still the microbubble was temporarily released from the laser trap during the experiment. The study revealed that the amplitude of the bubble oscillation decreased with decreasing distance to the wall at a fixed frequency.

## 7. Response of the vibration to increasing and decreasing chirps

Chirps are generally used to increase the signal-to-noise ratio. If used to irradiate bubbles, resonant behaviour results in a different response to a chirp with increasing frequency compared to a decreasing frequency chirp. This effect is absent in tissue scattering, and could thus provide a mechanism to increase contrast-to-tissue ratio (CTR).

[1] M.-X. Tang and R. J. Eckersley, "Frequency and pressure dependent attenuation and scattering by microbubbles," *Ultrasound in Medicine & Biology,* vol. 33, pp. 164, 2007.

# *Detection of vascular expression of P-Selectin and VEGF-R2 with antibody-targeted microbubbles using a Vevo 770 micro-ultrasound system*

*Thierry Bettinger, Tristan Messager, Philippe Bussat, Alexandre Helbert and Michel Schneider*
*Bracco Research SA, Geneva, Switzerland*

*Background:* The increasing number of studies performed on animal models has stimulated the development of new imaging tools adapted to the particular constraints of *in vivo* studies in small animals. One of the limitations is the need to sacrifice the animals to perform tissue or molecular analyse. This prevents researchers from observing *in vivo* the natural or perturbed evolution of the processes under study. Because of the size of these animals (rat, mouse…) and the size of the biological structure to be imaged, an increase in the resolution of ultrasound imaging systems was necessary. This is the reason why ultrasound bio microscopy has evolved rapidly in the last decade. In relation with this new imaging modality, new contrast agents have been developed for performing perfusion and targeted imaging.

*Materials:*

**Neo-angiogenesis model**: Flk-1 (mouse VEGF-R2) expression was imaged in six Balb/C mice of 12-14 weeks of age. Tumours were inoculated by subcutaneous injection of DA3 cells (mouse mammary carcinoma, $1x10^6$ cells/injection) into the mammary pad. The tumours were imaged at day 8 (average diameter of 2-3 mm).

**Inflammatory model:** P-Selectin expression was imaged in fifteen OF1 mice of 6-10 weeks of age. Inflammation was induced by a 30 µL injection of TNFα in the hind limb (recombinant mouse TNFα, 0.017 µg/µL, Calbiochem) in the hind limb.

MicroMarker™ Target-Ready Contrast Agent (Streptavidin-bearing microbubbles, VisualSonics, Toronto) were functionalised with biotinylated anti-Flk-1 monoclonal antibody (Avas12a1, eBiosciences, San Diego, CA) or biotinylated rat anti mouse P-Selectin (CD62P, RB40.34, BD Pharmingen). A rat isotype control (eBiosciences, San Diego, CA) was used to prepare control microbubbles. Briefly, 15 µg of the antibody were incubated with $1 \times 10^9$ bubbles for 10 min under agitation, and used without washings.

**High frequency ultrasound imaging:** Mice were anesthetized with 1.5% isoflurane. DA3 tumours and inflamed hind limbs were imaged with the Vevo 770 micro-imaging system (VisualSonics, Toronto, Canada). Randomized boluses of $7x10^7$ bubbles of either targeted or

control were administered in jugular vein. Animals were imaged with the RMV 707 scanhead at a center frequency of 35 MHz. Perfusion of the tissues was evaluated with the MicroMarker™ Contrast Enhanced Application (Toronto, VisualSonics) a non targeted contrast agent.

*Results:*

P-Selectin targeted microbubbles gave a high acoustic signal in the inflamed hind limb 24 hours following intramuscular TNFα injection, when compared to control bubbles (comprising an isotype antibody control) (Figure 1). This pattern suggests that retained targeted bubbles interact with P-Selectin receptors expressed by the activated endothelium. No bubble binding was observed after injection of high dose of free anti mouse P-Selectin antibody prior to the administration of targeted microbubbles, thereby showing the specificity of the interaction.

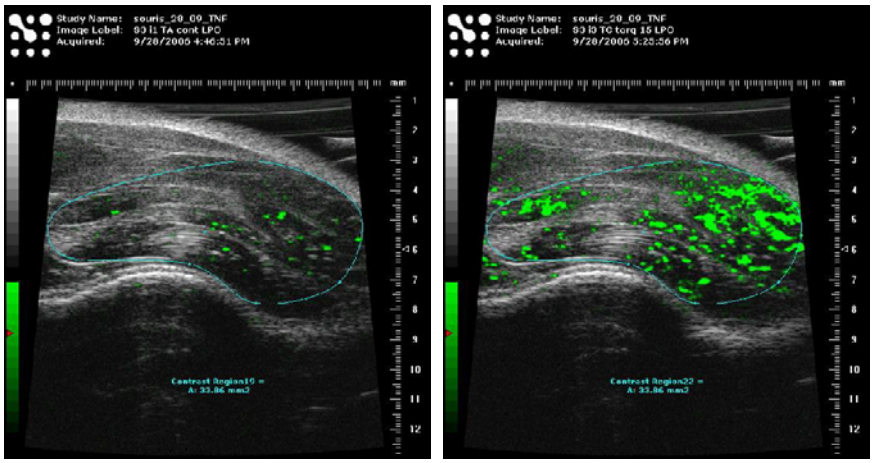

**Figure 1:** Contrast enhanced ultrasound in inflamed hind limb in mouse. Reference-substracted pixel amplitude, shown in green, overlaid on greyscale images 10 min after contrast agent injection. Left image depicts control bubbles, right image P-Selectin-targeted MicroMarker™ Target-Ready Contrast Agent. The ROI is the area encompassed by the blue line.

Flk-1 receptors (mouse VEGF-R2) were probed with anti-Flk-1-MicroMarker™ Target-Ready Contrast Agent, in mouse bearing DA3 tumours (Figure 2). Again control bubbles, gave a relatively low signal when compared to targeted ones.

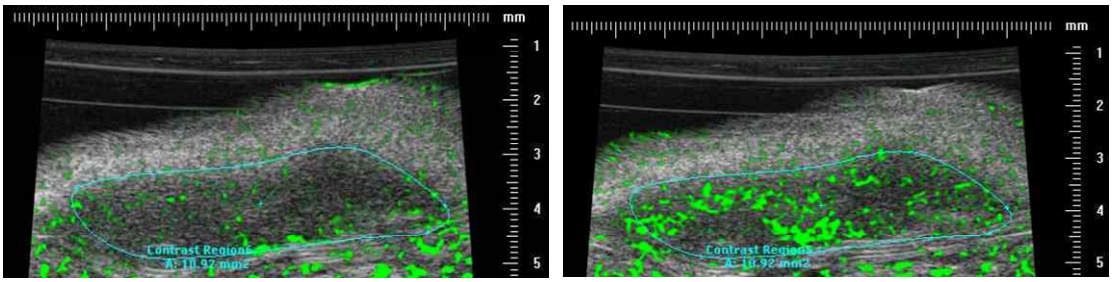


**Figure 2:** Contrast enhanced ultrasound in a DA3 tumour-bearing mouse. Reference-substracted pixel amplitude, shown in green, overlaid on greyscale images 10 min after contrast agent injection. Left image depicts control bubbles, right image Flk-1-targeted MicroMarker™ Target-Ready Contrast Agent. The ROI is the area encompassed by the blue line.

*Conclusion:* New ultrasound imaging tools have been designed for pre-clinical studies in small animals. The specific recognition of the P-Selectin and Flk-1 markers by microbubbles has been demonstrated *in vivo*. The use of these new agents is straightforward, and the preparation relies on mixing of small amount of a biotinylated antibody with MicroMarker™ Target-Ready Contrast Agent (Streptavidin-microbubbles) without further washings of the modified microbubbles. The ease of use and the reproducibility of the results will open new avenues for molecular imaging in small animal, *e.g.* quantification of receptors, follow up studies for new cancer treatments.

# Vibrating microbubbles at low acoustic pressures.

M. Emmer[1], H. J. Vos[1], A. van Wamel[1,2], D. E. Goertz[1,2], M. Versluis[3], and N. de Jong[1-3],

[1]Dept. of Experimental Echocardiography, Thoraxcentre, Erasmus MC, Rotterdam, the Netherlands,
[2]Interuniversity Cardiology Institute of the Netherlands, Utrecht, the Netherlands,
[3]Physics of Fluids, University of Twente, Enschede, the Netherlands.

For individual phospholipid-coated microbubbles with a diameter smaller than 5 µm, optical recordings at a framerate of 13 million frames per second, revealed threshold behaviour in the onset of vibration. Recent studies performed by Tang et al. (2005) showed a pressure-dependent attenuation for phospholipid-coated microbubbles. However, an explanation for pressure-dependent attenuation was not provided. In our study, the hypothesis that it can be explained by microbubble threshold behaviour was investigated. At an acoustic pressure increasing from 5 to 200 kPa, a driving frequency of 1.0 MHz and a concentration of 90 µl/l, the attenuation of the phospholipid-coated microbubbles BR14 increased linearly from 0.45 dB to 0.7 dB/cm. Since BR14 smaller than 3 µm diameter, showed similar pressure-dependent attenuation for acoustic pressures above 50 kPa, we hypothesize that only these smaller bubbles are responsible for the pressure-dependent attenuation. When the acoustic pressure increases above a threshold acoustic pressure, microbubbles smaller than 5 µm start to oscillate and contribute to the attenuation. In contrast to BR14, Levovist did not show pressure-dependent attenuation. Levovist is considered to be a free microbubble, for which threshold behaviour is not expected. An imaging technique such as power modulation imaging could profit from the presence of an acoustic pressure threshold.

Reference

Tang, M. X., Eckersley, R. J., Noble, J. A., *Pressure-dependent attenuation with microbubbles at low mechanical index*, Ultrasound Med Biol, 31(3), pp. 377-384, 2005.

# Initial results of an investigation into single bubble acoustics using amplitude modulation.

DH Thomas[1], V Sboros[1], R Steel[1], MB Butler[1], SD Pye[1], T Brock-Fisher[2], M Poland[2], WN McDicken[1], T Anderson[1]

[1] *Department of Medical Physics and Medical Engineering, University of Edinburgh, Edinburgh, UK*
[2]*Philips Medical Systems, Andover, MA, USA.*

The investigation of single acoustic scattering events from microbubbles has the potential to allow a thorough understanding of the microbubble-ultrasound interaction, and permit optimal processing of microbubble signals. The majority of pulsing regimes available in ultrasound scanners are built on theoretical assumptions of microbubble behaviour and have been tested using microbubble suspensions of large concentrations prior to their introduction in the market. While it is recognised that microbubble theoretical models are of limited predictive value, we have shown that large microbubble concentrations can lead to incomplete understanding of microbubble properties (Sboros et al 2002). The result raises the question whether the properties of microbubbles are fully exploited (Brock-Fisher et al 2005).

A phantom that employs a hydrodynamically focused flow was used to allow the detection of RF backscatter from two types of contrast agents (Sboros et al 2005). The system allows individual microbubbles to be investigated with a range of incident pulses, including pulsing regimes such as pulse-amplitude-modulation. A fine capillary was placed at the centre of the focused flow and single microbubbles were released along a precise vertical path coincident with the axis of the ultrasound beam. RF data were collected using a commercial scanner (Sonos 5500, Philips Medical Systems) and a range of frequencies (1-3MHz). The control of the scanner and data collection were performed using proprietary software written specifically to interface with the scanner. The calibration of transmitted pulses was performed using a membrane hydrophone with active element of diameter 0.2mm, while the calibration of the received pulses was performed using theoretical and experimental data from copper microspheres that range between 20-100μm in diameter (Sboros et al 2005). The frequency range and pulse lengths used allowed increased sample sizes compared to fast optical microscopy.

Results are presented for Definity® (Bristol-Myers Squibb Inc, N Bellarica, MA), a lipid coated agent, containing octafluoropropane gas which is non-soluble in water and biSphere® (Point Biomedical Corp, San Carlos, CA), a biodegradable polymer shell that contains air which is considered water-soluble.
Pulse amplitude modulation employs a sequence of three pulses (275kPa, 550kPa, 275kPa), to enhance the nonlinear signals of received echoes. For this pulse sequence example it was observed that in the majority of scattering events (90%), the initial half amplitude transmit pulse, did not produce a measurable echo from the microbubbles (results shown for 1.62MHz). The full amplitude pulse produces an echo, which is then mirrored by a similar response to the next half amplitude pulse (within 10% RMS

amplitude). This is in contrast to the experimental data from copper spheres, which show the half, full and half amplitude echo pulses as expected. In the case of biSphere, most bubbles give no response to the next set of pulses, confirming the high solubility of the encapsulated gas. Definity shows a steadily decreasing echo over subsequent sets of pulses, showing some resilience to transmitted pulses.
Apart from the solubility of the gas within the respective contrast agents, the results above are evidence for a large shell contribution to the microbubble echoes. The lack of echo from the first half amplitude pulse may be attributed to a lack of shell movement, which is only achieved with the second, full amplitude, pulse.

These results do not bear out the text-book theory of microbubble-pulse sequence interaction and invite a more rigorous assessment of signal processing approaches.

| | Mean RMS echo amplitudes (Pa) | | | |
|---|---|---|---|---|
| Transmit pulse (550kPa peak negative) | Half amplitude | Full amplitude | Half amplitude | |
| **Definity** | **0.1±0.1** | **0.8±0.2** | **0.7±0.2** | (fundamental) |
| | **0.1±0.1** | **1.4±0.6** | **1.4±0.6** | (harmonic) |
| **biSphere** | **0.1±0.1** | **0.3±0.2** | **0.3±0.2** | (fundamental) |
| | **0.1±0.1** | **0.5±0.3** | **0.5±0.3** | (harmonic) |

**Table:** Mean RMS amplitude responses to pulse amplitude modulation, from a sample of 30 bubbles, showing no measurable echo on first transmit pulse. Transmit frequency 1.62MHz, 6-period pulses.

**Acknowledgement:** The work was funded by the EPSRC (UK)

**References:**

Brock-Fisher T, Averkiou M, Bruce M, Jensen S, Rafter P, Powers J. Pulsing schemes for High-MI contrast imaging. 10th European Symposium on Ultrasound Contrast Imaging, January 2005, Rotterdam, the Netherlands

Postema M, Bouakaz A, de Jong N. Ultrasound-induced gas release from contrast agent microbubbles. IEEE trans Ultrasonics Ferr Freq Cont 2005; 52: 1035-1041.

Sboros V, Ramnarine KV, Moran CM, Pye SD, McDicken WN. Understanding The Limitations Of Ultrasonic Backscatter Measurements From Microbubble Populations. Phys Med Biol 2002; 47: 4287-4299.

Sboros V, Pye SD, MacDonald CA, Gomatam J, Moran CM, McDicken WN. Absolute measurement of ultrasonic backscatter from single microbubbles. Ultrasound Med Biol 2005; 31: 1063-1072.

# Nonlinear Golay-Encoded Contrast Agent Imaging

R. Williams[1], C. Leavens[2], M. D. Sherar[2,3], P. N. Burns[1,2]

[1] Sunnybrook Health Sciences Center, Toronto, Canada
[2] Department of Medical Biophysics, University of Toronto, Toronto, Canada
[3] Cancer Care Ontario, Toronto, Canada.

Microbubble ultrasound contrast agents (UCAs) scatter ultrasound nonlinearly and are used to isolate and enhance the blood signal from that of tissue. Techniques such as pulse inversion (PI) (Simpson et al. 1999) and amplitude modulation (AM) (Haider and Chiao 1999), as well as their combination (Eckersley et al. 2005) have been developed to detect the nonlinear UCA response. Coded excitation methods have also been exploited in UCA imaging to increase the SNR and penetration depth by increasing the time-bandwidth product of the incident pulse, while maintaining low peak negative pressures in order to avoid UCA disruption (Borsboom et al. 2005).

We present a method for coded nonlinear imaging of UCAs called Golay Pulse Inversion and Amplitude Modulation (GPIAM). This technique combines the principles of Golay coded excitation, pulse inversion and amplitude modulation, to detect the nonlinear UCA response at the fundamental harmonic. The nonlinear UCA response is modeled as a polynomial expansion of a basis waveform. Pulse inversion and amplitude modulation are used to cancel the linear signals emanating from tissue. The 3$^{rd}$ order nonlinear terms are Golay-encoded, and have a spectral component at the fundamental frequency. Upon reception, the signal is passed through a matched filter in order to compress the Golay-encoded signal components in time, providing the SNR enhancement.

We evaluated GPIAM imaging for 2-, 4-, and 8-chip Golay code lengths using Definity (Bristol-Myers Squibb, Boston, MA), at a concentration of 0.1 mL/L in a flow-cell immersed in water. The experiments were performed with a transmit centre frequency of 2.5 MHz. The peak negative pressure at the focus was measured with a hydrophone to be 158 kPa (MI=0.1). Experiments were repeated using a tissue-mimicking phantom as a

linear scatterer. Results using GPIAM sequences were also compared with PI and AM sequences and conventional excitations.

The contrast-to-tissue ratio (CTR), found by dividing the UCA SNR by the linear scatterer SNR, showed CTR enhancements of 13 dB, 15 dB and 18 dB for the 2-, 4- and 8-chip GPIAM sequences, compared with 7 dB for the PI sequence and 11 dB for AM. Envelopes of the UCA in the flow cell demonstrated that the axial resolution was not significantly degraded following compression, regardless of the GPIAM code length. M-mode acquisitions showed that agent disruption was minimal during insonation. The results indicate that GPIAM can be used to detect the nonlinear components of the UCA response in the minimally-attenuating transmission band of the transducer, while enhancing the SNR and CTR and preserving imaging resolution.

**References**

Borsboom JMG, Chin CT, Bouakaz A, Versluis M, de Jong N. Harmonic chirp imaging method for ultrasound contrast agent. IEEE Trans Ultrason Ferroelect Freq Contr 2005; 52: 241-249.

Eckersley RJ, Chin CT, Burns PN. Optimising multi-pulse imaging schemes for microbubble contrast agents at low acoustic power. Ultrasound Med Biol. 2005; 31: 213-219

Haider B, Chiao RY. Higher order nonlinear ultrasonic imaging. IEEE Ultrason Symp 1999; 1527-1531.

Hope Simpson D, Chin CT, Burns PN. Pulse inversion Doppler: a new method for detecting nonlinear echoes from microbubble contrast agents. IEEE Trans Ultrason Ferroelect Freq Contr 1999; 46: 372-382.

*The use of contrast enhanced ultrasound in liver patients' clinical care*

Yuko Kono, MD, PhD
Assistant Clinical Professor
Department of Medicine, Gastroenterology Division,
University of California, San Diego

Ultrasound (US) is a very useful diagnostic tool in hepatology practice world wide. For example, hepatocellular carcinoma (HCC) surveillance in high risk cirrhotic patients, has been performed by a combination of serum tumor marker, alpha fetoprotein (AFP) and US every 6 months, recommended by EASL (European Association of Study of the Liver) [1], and guideline for HCC surveillance from AASLD (American Association of the Study of Liver Diseases) even eliminated AFP and recommends US every 6 to 12 months [2].

US contrast media and contrast specific imaging technology has greatly changed liver ultrasound. Contrast media is now as critical in clinical practice for US as it is for CT and MRI, in many countries where US contrast agents are available. With contrast agents, US has become competitive with CT and MRI in lesion detection and studies suggest that US may even be superior in lesion characterization and assessment of tumor viability following focal therapy. Moreover, ultrasound imaging maintains its advantage of being portable, inexpensive and real-time.

Contrast-enhanced ultrasound (CEUS) has been shown to be useful in many clinical radiological applications. Important applications of CEUS in liver imaging are 1) liver tumor imaging including tumor characterization [3], lesion detection [4], monitoring local tumor treatment [5, 6], 2) vascular imaging such as TIPS patency [7], thrombosis of vessels of the liver, most importantly post liver transplantation and 3) liver trauma diagnosis [8].

**1) Liver tumor imaging**

The most useful and widely used application in liver US imaging is liver tumor characterization. CEUS has been used for liver tumor characterization and is proven to be very useful [3, 9]. The characteristics of the dynamic enhancement pattern of hepatic tumors such as HCC, metastatic liver tumors, hemangioma, focal nodular hyperplasia (FNH), hepatic adenoma (HA), are very similar to those with contrast enhanced CT (CECT) and MRI. This is despite the fundamental difference between CT/MRI agents, with small molecules that leak into interstitial space very quickly, and US microbubbles that are in the micron range and stay intravascular.

In clinical practice, there are two important applications in liver tumor characterization. One is to diagnose incidental lesions encountered in screening ultrasounds in both the normal and cirrhotic liver. Prior to the introduction of CEUS, these cases were routinely sent to CECT or CEMRI for characterization. While CECT/CEMRI are still necessary in some cases, many of these lesions are easily characterized with CEUS and do not need more expensive tests or radiation. The other important application is indeterminate lesions in both normal and cirrhotic liver. In normal liver a fairly common problem is the differentiation of benign vs. malignant tumors when the appearance is not typical or lesions are too small to characterize with CECT/CEMRI. Among benign lesions, hemangiomas are usually easy to characterize with any contrast study, but the differentiation of HA vs. FNH remains difficult on many occasions. HA and FNH are both benign but the management for each is different, as HA has risk of bleeding diameter and also has a potential risk of malignant transformation, thus surgical resection is recommended when it is larger than 5cm, while FNH does not have these risks and therefore no intervention is necessary. The pathognomonic feature of

FNH, its central feeding artery spoke wheel appearance, is not often seen by CECT/CEMRI, but easily seen by CEUS due to its higher temporal and spatial resolutions. On the other hand, HA is supplied by arteries from the periphery and enhancement is seen from outside-in. The high spatial, and more importantly, temporal resolution of CEUS can differentiate these features of HA and FNH. Recently, maximum intensity hold technique, microflow imaging (MFI) or microvascular imaging (MVI), have been implemented in some ultrasound machines and have made this differentiation even easier.

Small hepatic arterial phase enhancing lesions are frequently observed with CECT/CEMRI in cirrhotic patients being screened for HCC. These lesions are difficult to characterize, are a major source of diagnostic confusion, and may lead to errors in patient management and prognosis. In fact, 43 to 93% of these small arterially enhancing lesions are reported to be benign. CEUS is helpful in diagnosing those indeterminate small liver lesions as we previously showed in 42 patients. Small indeterminate early enhancing lesions, which had been detected by CECT and/or CEMRI were studied with CEUS. CEUS detected all true lesions with 3 false positive foci and correctly recognized all malignant from benign lesions with 2 false positive diagnoses [10].

Another important application in liver tumor imaging is to evaluate the efficacy of local treatment, such as transarterial chemoembolization (TACE), focal tumor ablation (radiofrequency, ethanol, microwave, hot saline, etc.), radioembolization with Yttrium90 and gene therapy. CECT, CEMRI and PET have been used to evaluate tumor viability and the role of ultrasound was limited before the introduction of contrast agents. CEUS has been shown to be very useful in the guidance and monitoring of radiofrequency ablation of liver tumors [5]. CECT is limited, especially post TACE, due to dense Lipiodol in the tumor that hides subtle enhancement. CEMRI can detect residual tumor blood flow and is currently accepted as the most sensitive technique. However, because all current MR contrast agents have a small molecular weight and are water-soluble, confusion between granulation tissue and residual tumor persists for the first 3 months. PET can detect high metabolic tumors but is limited in spatial resolution. From our study of 42 HCCs post TACE, residual tumor blood flow detected with CEUS performed within 2 weeks after TACE was predictive of tumor outcome that currently requires 3 months to be reliably detected by CECT/CEMRI [6]. For treatments such as radioembolization or gene therapy, quantification of tumor blood flow and blood volume to predict the efficacy may be helpful as it takes more time to take effect than ablative therapy. We are quantifying blood flow and blood volume by applying the quantification model with bubble destruction in these patients. Our preliminary results are encouraging.

Screening and staging liver metastasis is a good application for CEUS. It was shown that CEUS is not only significantly better than conventional US in detecting liver metastasis, and comparable to CT, but US can also be better than CEMRI/CECT in a multi center study [4] that was performed with Levovist. Levovist is a unique agent with a liver specific phase, but metastasis detection is feasible with other second generation agents without significant liver uptake. Metastasis screening can be performed during portal venous phase or late phase as metastatic liver tumors wash out contrast very quickly and become hypoechoic compared to surrounding liver. The contrast between metastatic lesions and the liver is very high in most cases and the portal venous phase lasts for a few minutes, thus scanning the entire liver to detect lesions as hypoechoic lesion is fairly easy. Sonazoid, a contrast agent recently approved in Japan, seems to be promising as it has both a good vascular phase and a late liver specific phase.

The role of CEUS in HCC surveillance, however, is debatable. While CEUS is good at differentiating nodules that were already detected without contrast, finding HCC in the cirrhotic

liver is not very easy. There are several reasons for this; 1) in the cirrhotic liver, there are innumerable regenerative nodules that make the liver very heterogeneous, 2) early, small HCC may not be hypervascular, and may have a normal portal venous supply, 3) and well differentiated HCC may maintain functioning Kupffer cells. Even when HCC is hypervascular and enhances in the arterial phase the arterial phase is fairly short, in the order of around 10 seconds, and unlike metastasis, many HCCs do not washout significantly and are hard to detect during the portal venous phase. HCC surveillance is still a challenge for CEUS and CECT/CEMRI.

**2) Vascular imaging**

Color and power Doppler ultrasound have been improved and are sufficient to diagnose many vascular problems [11]. However, when the lesion is deep or there is not enough blood flow, it is still difficult to obtain a confident diagnosis. Contrast agents enhance Doppler signals significantly and the second harmonic technique has improved Doppler imaging by decreasing flash artifacts generated from non-contrast-containing pulsatile perivascular tissues and by limiting color to regions filled with bubbles. However, these techniques do not overcome the limitations of Doppler, such as unreliable filling of vessels, poor spatial resolution of color, and poor temporal resolution of power Doppler. Harmonic imaging with gray-scale improves upon standard gray-scale imaging by increasing contrast between the lumen and surrounding tissues. Gray-scale filling of vessels is more powerful than filling the vessel with Doppler signal because the latter relies on flow to fill vessels and to provide anatomical detail.

In liver imaging, contrast-enhanced ultrasound is useful in evaluating the patency of transjugular intrahepatic porto-systemic shunt (TIPS) [7], vascular complications post orthotopic liver transplantation (OLT), and many other applications. Hepatic arterial thrombosis (HAT) that follows OLT is potentially a life threatening complication. Although the incidence has decreased significantly it is still not a rare complication as it is seen in 3 to 9% of all the OLT cases. Doppler US is the first screening test, but when HAT is suspected, CEUS can provide more specific and accurate information. CEUS can directly visualize the hepatic artery with high spatial resolution. CEUS also enhances Doppler signal and therefore it is easier to obtain arterial waveform. Intermittent imaging is helpful, especially in evaluating slower flow system, such as portal vein/TIPS patency.

The other important liver vascular application is to differentiate benign vs. malignant portal venous thrombosis in cirrhotic patients, as both conditions are not uncommon, and differentiation is not easy in many occasions. Currently percutaneous biopsy is performed when non-invasive imaging is inconclusive and if it is crucial for patient management. CEUS can easily differentiate these conditions as it is very sensitive and provides accurate vascularity information in the thrombus. A malignant thrombus, mainly from HCC, has arterial blood supply, while a benign thrombus is a blood clot and has no enhancement after contrast injection.

**3) Trauma diagnosis**

In trauma cases, the focused abdominal sonography in trauma (FAST) examination is the first line triage [12] and is performed to look for any free fluid in the abdominal cavity, but is limited in diagnosing solid organ injury. With contrast injection, which takes only a few more minutes, we can actually diagnose solid organ injury [8, 13].

In summary, CEUS is very important in liver ultrasound imaging. In liver tumor characterization, it eliminates unnecessary CECT/CEMRI and also helps differentiate

indeterminate lesions. Evaluation of therapeutic efficacy on liver tumors is another crucial application. CEUS is accurate and can be done at an earlier time point than conventional CECT/CEMRI at bedside. CEUS is also very useful in many vascular applications when Doppler US is not conclusive. When hepatic arterial thrombosis or other vascular complication is suspected post liver transplantation, CEUS can provide accurate information, facilitate necessary treatment or eliminate an unnecessary invasive procedure.

In the USA, not a single US contrast agent has been approved for radiological applications. At our institution, we have been conducting contrast ultrasound in highly selected cases for clinical need. In a previous series of 95 CEUS cases studied for clinical reasons, we found that CEUS added valuable information in 75% of the cases and changed management in 20% of the cases without adding any risk to the patients. The number of these clinical cases, however, is increasing and hopefully we can obtain approval from the FDA in the near future.

References:


1. Bruix J, Sherman M, Llovet JM, et al. Clinical management of hepatocellular carcinoma. Conclusions of the Barcelona-2000 EASL conference. European Association for the Study of the Liver. J Hepatol 2001; 35:421-430.
2. Bruix J, Sherman M. Management of hepatocellular carcinoma. Hepatology 2005; 42:1208-1236.
3. Wilson SR, Burns PN, Muradali D, Wilson JA, Lai X. Harmonic hepatic US with microbubble contrast agent: initial experience showing improved characterization of hemangioma, hepatocellular carcinoma, and metastasis. Radiology 2000; 215:153-161.
4. Albrecht T, Blomley MJ, Burns PN, et al. Improved detection of hepatic metastases with pulse-inversion US during the liver-specific phase of SHU 508A: multicenter study. Radiology 2003; 227:361-370.
5. Solbiati L, Ierace T, Tonolini M, Cova L. Guidance and monitoring of radiofrequency liver tumor ablation with contrast-enhanced ultrasound. Eur J Radiol 2004; 51 Suppl:S19-23.
6. Kono Y, Lucidarme O, Choi SH, et al. Contrast-Enhanced Ultrasound as a Predictor of Treatment Efficacy within two weeks after Transarterial Chemoembolization of Hepatocellular Carcinoma. J Vasc Interv Radiol 2007; In Print.
7. Kono Y, Mattrey RF, Sirlin CB, S.C. R, Hassanein IT. Usefulness of Gray-scale Ultrasound Contrast Enhancement for Evaluation of TIPS Stenosis. Hepatology 1999.
8. Mattrey RF, Kono Y, Pinnell S, Sirlin C. Diagnosing Solid Organ Injury with Ultrasound Contrast Media. J Ultrasound Med 2000; 19:S64.
9. Bryant TH, Blomley MJ, Albrecht T, et al. Improved characterization of liver lesions with liver-phase uptake of liver-specific microbubbles: prospective multicenter study. Radiology 2004; 232:799-809.
10. Kono Y, French J, Alton K, Alpert E, Hassanein TI, Mattrey RF. Role of contrast enhanced ultrasound in diagnosing indeterminate small liver lesions. J Ultrasound Med 2006; 25:S48.
11. Kruskal JB, Newman PA, Sammons LG, Kane RA. Optimizing Doppler and color flow US: application to hepatic sonography. Radiographics 2004; 24:657-675.
12. Rose JS. Ultrasound in abdominal trauma. Emerg Med Clin North Am 2004; 22:581-599, vii.
13. Blaivas M, Lyon M, Brannam L, Schwartz R, Duggal S. Feasibility of FAST examination performance with ultrasound contrast. J Emerg Med 2005; 29:307-311.

# Dynamic Contrast Enhanced-ultrasonography (DCE-US) with Quantification of Tumour Perfusion. Interest to evaluate the Efficacy of Anti-angiogenic Treatments.

Nathalie Lassau MD, PhD
Ultrasonography Unit, Imaging department
UPRES EA 4040
Institut Gustave-Roussy. France

New treatments based on antiangiogenic substances are developed in order to destroy tumor vessels and are the object of promising clinical research for cancer treatment. Considering the large number of new targeted drugs under development, there is a great need for early reliable imaging indicators of tumour responses, and identification of a recommanded modality of drug administration to guide further steps in the clinical development. The response rate remains the best objective parameter of efficacy of the treatments tested in Phase 1 2, or 3 but this parameter is obtained very late in the clinical development, while the effect on the tumour must be determined as soon as possible in order to optimise the schedule. The early functional evaluation of new treatments is a main goal.

At present, technical advances in DCE-ultrasonography using contrast agent (SonoVue®, Bracco) and perfusion software (Aplio, CHI-Q, Toshiba) allow the detection of microvascularization and perfusion for superficial and deep malignant tumors. Thus, it becomes possible to early evaluate the efficiency of antiangiogenic or anti-vascular molecules in pre-clinical and clinical studies. Treatment response can be early predicted according to modifications of this vascularization before any volume modification. The acquisition of raw linear data affords the precise quantification ( peak intensity, time to peak intensity, slop of wash-in, area under the curve) of the perfusion, in particularly using time tracking of region of interest. Our results are focused on metastasis of RCC , melanoma and GIST and GIST, with different molecules at different doses and with different schedules.

# CONTRAST APPLICATIONS IN BRAIN ULTRASOUND

Thilo Hölscher, M.D.

Department of Radiology, University of California San Diego, USA

## TRANSCRANIAL ULTRASOUND ANGIOGRAPHY (TUSA)

Transcranial vascular imaging in color or power Doppler mode, the dominant transcranial ultrasound methods, have improved significantly since the introduction of ultrasound contrast agents (UCA). However, UCA specific artifacts like 'blooming' occur, limiting the diagnostic impact of contrast-enhanced color or power Doppler ultrasound studies. UCA specific imaging techniques, such as tUSA, offer an angiography-like view of the intracranial arteries. Based on B-mode phase inversion tUSA provides detailed anatomical display at native B-mode spatial resolution with less artifacts, yielding improved delineation of intracranial vessels in the 1 to 2mm range (Figure 1).

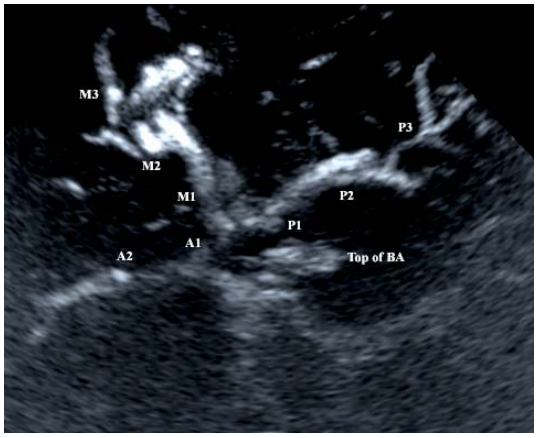


Figure 1
tUSA image of the Circle of Willis.
M1,M2,M3: middle cerebral artery segments, A1,A2: anterior cerebral artery segments, P1,P2,P3: posterior cerebral artery segments, Top of BA: top of the basilar artery

Early clinical data demonstrate that tUSA provides high anatomical resolution and high inter-rater reliability amongst inexperienced and seasoned readers.

## FLOW DYNAMIC ASSESSMENT USING DPIV

To evaluate the potential of contrast-enhanced ultrasound to visualize the hemodynamics in intracranial aneuryms and to quantify the ultrasound data, using Digital Particle Image Velocimetry (DPIV) technique. Spatial and temporal distribution of the velocity in the aneurysm and in the parent vessel can be measured with DPIV using the backscattered signals from microbubbles. Subsequently, the fluid stresses, vorticity, circulation, etc. can be calculated from the velocity fields (Figure 2).

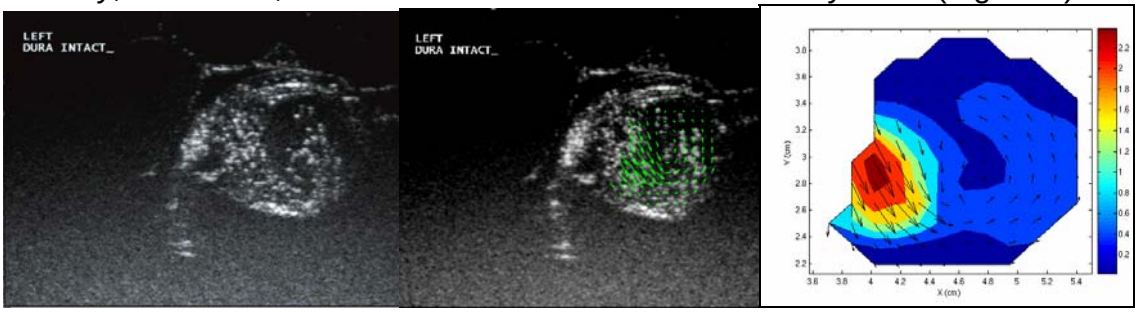


Figure 2: Left – visualization of single UCA microbubbles within the aneurysm sac, Middle – microbubble tracking and generation of corresponding flow vectors using DPIV, Right – parameter based animation of the flow velocity field inside the aneurysm.

Contrast-enhanced ultrasound can be used to quantify the flow dynamics within an aneurysm, using DPIV.

## INTRAOPERATIVE APPLICATIONS

PIHI provides anatomically detailed information of intracranial pathologies during neurosurgical intervention (Figure 3). In combination with an UCA, angiography-like views of the vascular pathologies, including their surrounding vessels, can be obtained. Flow velocities in afferent and downstream vascular segments, as well as inside the pathology, can be assessed. Flow dynamics inside the aneurysm sac or the AVM can be studied in real-time (Figure 4). Postintervention, contrast-enhanced PIHI enables immediate monitoring of the success of the surgical procedure.

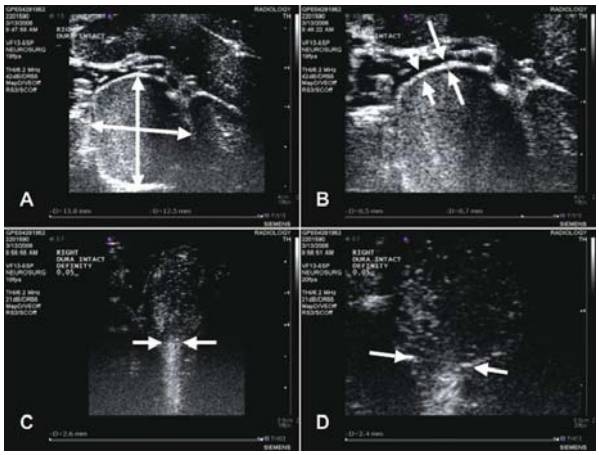


Figure 3
Pre-contrast PIHI: A – white arrows represent the inner diameter of an aneurysm (vertical 13.8 mm, horizontal 12.5 mm). B – measurements of the wall thickness at two different locations (short arrows 0.5 mm, long arrows 0.7 mm).
Post-contrast PIHI: C – arrows mark the width of the aneurysm neck (2.6 mm). D – corrected measurement of the same aneurysm neck after zooming (2.4 mm).

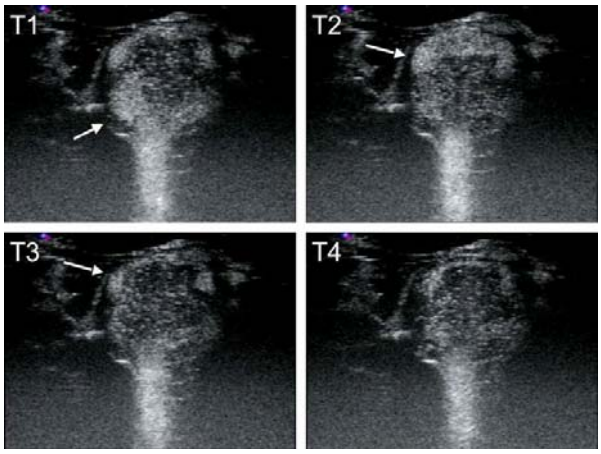


Figure 4
Postcontrast, sequence of snapshots during a cardiac cycle (T1: early systolic, T2: late diastolic). Arrows mark areas of high bubble concentration, due to turbulent flow. This can be seen best at the aneurysm entrance (T1: early systole) and the aneurysm dome (T2: mid systole)

Phase inversion harmonic imaging enables intraoperative visualization and morphologic assessment of neurovascular pathologies, such as MCA aneurysms or AVMs. In combination with an ultrasound contrast agent, the flow dynamics of these lesions can be displayed in real-time.

References

Hölscher T, Wilkening W, Lyden P, Mattrey R: Transcranial Ultrasound Angiography (tUSA): A New Approach for Contrast Specific Imaging of Intracranial Arteries. *Ultrasound in Medicine and Biology 2005. 31 (8): 1001-06.*

Hölscher T, Rodriguez J, Wilkening W, Lasheras J, U H: Intra-Operative Brain Ultrasound: A New Approach to Study Flow Dynamics in Intracranial Aneurysms. *Ultrasound in Medicine and Biology 2006. 32 (9): 1307-13.*

Hölscher T, Burak O, Singel S, Wilkening W, Mattrey R, U H: Intraoperative Ultrasound Using Phase Inversion Harmonic Imaging: First Experiences. *Neurosurgery 2006 (accepted).*

**Targeted binding of microbubble contrast agents to αVβ3 integrin expressing prostate cells**

Simone Mader, Alexander L. Klibanov, Radu Rogojanu, Georg Bartsch, Helmut Klocker, Iris E. Eder(*)
Dept of Urology, Innsbruck Medical University, Austria, Cardiovascular Division, University of Virginia, Charlottesville, VI, TissueGnostics GmbH, Vienna, Austria

**Introduction and Objective:** We have shown previously that microbubble (MB) enhanced ultrasound can be used to deliver short antisense molecules into prostate tumors in vivo. In the present study we investigated the possibility to further improve this delivery system by modifying the MB surface with antibodies against αVβ3 integrin, a cell surface receptor that is assumed to be overexpressed in prostate cancer. We therefore evaluated expression of αVß3 integrin in the vasculature of human prostate and then tested the adhesion of αVb3-modified MB to different prostate cells in vitro.
**Methods:** Immunofluorescent double staining of αVß3 integrin and von Willebrand factor (vWF) was performed on frozen tissue specimens obtained from 13 different patients after radical prostatectomy. Fluorescent staining was quantified using computer-assisted image analysis. A biotinylated anti human αVß3 antibody was conjugated to fluorescent biotinylated MBs via streptavidin (αVß3-MB). αVß3 integrin expression in different prostate cell lines was confirmed by Western blot and flow cytometry. Adhesion of αVß3-MB to cells was measured in binding assays and flow-through experiments by counting the number of bound αVß3-MB in comparison to unmodified MB.
**Results:** αVb3 integrin was detected in all prostate tissue specimens (n=13) tested. Expression in blood vessels was heterogeneous with an average of 40% αVß3 and vWF-positive cells (range 3-98%). Among the cell lines, strongest expression of αVß3 was found in benign prostate stromal cells (PrSCs). DU-145 and PC-3 prostate tumor epithelial cells also expressed αVß3 but to a lower extend than PrSCs. LNCaP cells were found to be negative. Binding assays as well as flow-through experiments showed that adhesion of αVß3-MB to PrSCs, DU-145, and PC-3 was signficantly higher than adhesion of unmodified MB. By contrast, there was no increase in binding of αVß3-MB to LNCaP cells as compared with unmodified MB.
**Conclusion:** Our results demonstrate that αVb3-targeted MB have an increased ability to attach to αVß3-expressing cells. Since αVß3 integrin expression was confirmed in the vasculature of human prostate tissue, αVß3 may represent a good candidate for targeted delivery of drugs to prostate tumors.

Financial support by the Tiroler Wissenschaftsfonds and the Austrian Resarch Foundation (FWF P17352-B13).

**Infused microbubbles to facilitate sonothrombolysis in patients with acute ST-elevation myocardial infarction**

O. Kamp, MD, PhD
Department of Cardiology and Institute of Cardiovascular Research, VU University Medical Center, Amsterdam and Interuniversity Cardiology Institute of the Netherlands

Thrombo-occlusive cardiovascular diseases are the leading cause of death in the Western world. Among these, ST-elevation acute myocardial infarction (AMI) is an important contributor of mortality. Reperfusion therapies, such as thrombolysis and percutaneous coronary intervention (PCI) have strongly improved the outcome of patients suffering from AMI. When applied early in the disease process, these therapies can prevent myocardial damage by timely restoration of coronary blood flow.
Intravenous infused microbubbles have been introduced in the late nineties and have improved the diagnostic yield of echocardiography. Acoustic properties of these agents, especially resonance and cavitation under influence of ultrasound, are used to generate a contrast-enhanced image. Additionally, ultrasound has been shown to enhance dissolution of thrombi in vitro and in vivo (sonothrombolysis). Infusion of microbubbles augments this effect significantly. As this technique is simple, safe, and readily available, it may have additional value for reperfusion therapy in patients with AMI. The rationale and study design of a prospective randomized study will be discussed.

**Case Report: Neovascularisation of Carotid Plaque**

**David Cosgrove**
**Imperial College, Hammersmith Hospital, London**

The evolution of atheromatous plaque is a multistage process. One critical late phase is the development of neovascularisation. Because this renders the plaque soft, friable and unstable with an increased liability to ulcerate and attract platelet and red cell thrombi, both of which may detach and embolise, this phase is critical at a clinical level. If it could be predicated and appropriate intervention (surgical or pharmaceutical) effected, the clinical benefit could be major.

The process of plaque neovascularisation is similar to malignant neovascularisation. As well as lipids, the enlarging plaque contain living cells (smooth muscle, phagocytes), which can survive by diffusion of oxygen, nutriments and waste products when they lie close to the lumen and the arteries supplying the arterial wall (vasa vasorum). Beyond this, they become hypoxic and respond by secreting vasculogenic messengers including vascular endothelial growth factor (VEGf), which stimulate capillary budding from nearby vasa vsorum. These neovascular buds grow into the hypoxic regions and restore the local oxygen (and nutriment) deficit. Especially when newly formed, they are thin-walled and weak and so liable to fracture and bleed. This leads to further ischaemic regions and perpetuation of the process.

Ultrasound with microbubble contrast agents seems to be able to detect these neovessels by virtue of the fact that multipulse bubble detection methods can detect their non-linear responses regardless of the size of vessels they lie in or of whether they are moving or stationary. The carotid arteries are clinically important (they supply the brain and are subject to atheroma, especially at branching points, typically the carotid bifurcation) and, conveniently, the extracranial portion in the neck is readily accessible to ultrasound.

Thus, detection of carotid plaque neovascularisation became a natural goal once the appropriate software was implemented on vascular probes. We have observed intraplaque signals of two types that appear a few seconds after contrast arrives in the lumen of the carotid artery itself. The first consists of a blush of signal that is somewhat irregularly distributed in the plaque. The second takes the form of fine, discrete lines sometimes against the background blush, sometimes against a black background. We suggest that the fine lines are individual neo-vessels while the blush may represent a vascular network that is too fine toe be anatomically resolved or possibly intra-plaque haemorrhage.

Comparison with histology of endarterectomy specimens with specific stains for neovascularity are obvious next steps.

1. Vascular case:
Mr. LD is a 60 year old man with a recent history of left hand numbness (TIA). He was referred for a second opinion and **contrast-enhanced carotid ultrasound examination.**
Previous history was unremarkable for cardiovascular events. He denied a history of diabetes, hypertension or MI/CVA. His family history was unremarkable for premature cardiac events. He did not smoke and occasionally drank wine.
His diet and exercise were typical of a Westerner. He ate large portions and exercised very little.
On exam:
Blood pressure 140/88mmHg, pulse 84bts/min, weight 210lbs height 5'10"
General: Mr. LD appeared his stated age and appeared to have a "pasty" appearance
Lungs: clear to auscultation, Carotid: bruit present on the left, not on the right; Cor: regular rate and rhythm, peripheral pulses were intact throughout.
Labs: ECG
HgbA1C 6.4 (3.9-6.2)
Cholesterol fractionated (NMR) to be shown
Carotid ultrasound exam: to be shown
Treatment: TLC, medical and surgical (to be discussed)
Follow up

2. Cardiac case:
Mr. RS is a 58 year old bald, man with an endomorphic body habitus
He was referred for Primary Prevention. His life style, diet and exercise were typical of the general population. He did not smoke; he drank alcohol occasionally and worked as an accountant. There was some history of early cardiac events.
On exam:
Blood pressure 135/85mmHg, pulse 88bts/min, weight 200, height 5'8"
General: Anxious middle aged man appearing older than his stated age.
Carotid: normal upstroke, without bruits. Lungs: clear to auscultation. Cor: regular rate and rhythm. Ext: peripheral pulses intact throughout, no edema.
Labs: to be shown
**Contrast-enhanced, stress echo** and ECG: to be shown
Heart scan (EBCT): to be shown
CT-Angiogram: to be shown
Medical/Surgical therapy: to be discussed
Follow up

**Steven B. Feinstein, M.D., FACC, Professor of Medicine**

# Left Ventricular Function In Patients Treated With Skeletal Myoblasts: Results Of A 4-Year Follow-Up

C. E. Veltman, O. I. Soliman, W. B. Vletter, M. L. Geleijnse, A. Nemes, P. C. Smits, F. J. ten Cate, W.J. van der Giessen
*Department of Cardiology, Erasmus MC, Rotterdam, the Netherlands*

**Background:** Initial clinical studies suggest improvement of left ventricular (LV) function after intramyocardial injection of skeletal myoblasts in patients with ischemic cardiomyopathy. The follow-up in these studies, however, does not extend over 12 months.

**Objectives:** We set out to compare the long-term effect on LV function between patients treated with autologous myoblasts and a matched control group. Primary end-points were difference in left ventricular ejection fraction (LV-EF) and end-diastolic volume (LV-EDV).

**Methods:** The study comprised 18 patients with ischemic cardiomyopathy who underwent percutaneous injection of autologous myoblasts during 2001-2003 (M group) and 38 control patients matched for age, sex, localisation and time of the myocardial infarction (C group). After a mean follow-up period of 4 years resting 2D contrast echocardiography and tissue Doppler imaging (TDI) were used to compare global and regional LV function between the groups. Tracings were analysed by two observers.

**Results:** At 4-year follow-up 6 patients (33%) had died in the treated group and 15 patients (40%) in the control group ($p = 0.66$). The remaining 35 patients (12 M and 23 C) underwent 2D contrast echocardiography and tissue Doppler imaging. LV-EF was 36 ± 10% in M and 38 ± 9% in C ($p = 0.53$) The LV-EDV was 210 ± 74 ml in M vs. 213 ± 74 ml in C ($p = 0.92$). LV-ESV was 138 ± 59 ml M and 135 ± 56 ml in C ($p = 0.90$). The inter-observer variability 1.7%, 3.9%, and 4.4% for LV-EDV, LV-ESV and LV-EF, respectively. The mean systolic TDI velocity in the anterior wall was 6.0 ± 1.8 m/s in M and 5.9 ± 1.7 m/s in C ($p = 0.85$). For all other walls a higher systolic TDI velocity was measured in the treated patients compared with the control patients, but this difference was not statistically significant. The inter-observer agreement for the systolic tissue Doppler velocity measurements of the anterior wall was 98%.

**Conclusion:** Intramyocardial skeletal myoblast injection in heart failure patients has no effect on resting global and regional LV function as compared to age-, sex- and infarction-matched controls at a period of 4-year follow up.